



CAGE - Centre for Arctic Gas Hydrate Environment and Climate Report Series, Volume 1 (2013)

To be cited as: Andreassen, K. (2023). CAGE13-5 Cruise Report: Investigation of glacial geomorphology in the Storfjordrenna. *CAGE - Centre for Arctic Gas Hydrate Environment and Climate Report Series, Volume 1*.

DOI: <https://doi.org/10.7557/cage.6845>

Additional info at: <https://septentrio.uit.no/index.php/cage/database>

© The authors. This report is licensed under the Creative Commons Attribution 4.0 International License (<https://creativecommons.org/licenses/by/4.0/>)

ISSN: 2703-9625

Publisher: Septentrio Academic Publishing Tromsø Norway



Cruise Report GEO-8144/3144

## INVESTIGATION OF GLACIAL GEOMORPHOLOGY IN THE STORFJORDRENNA



**Participants:** Anastasia Fokina (Master student, MSU), Andrea Barbolla (PhD student, UiT), Dina Gillazetdinova (Master student, MSU), Mariana Esteves (PhD student, UiT), Robert Virs (Master student, UiT), Sunil Vadakkepuliambatta (PhD student, UiT), Trude Hansen (Master student, UiT)

**Teachers:** Karin Andreassen and Steffen Aagaard Sørensen

**Staff:** Anna Yurchenko, Eythor Gudlaugsson, Katharina Streuff

**Engineers:** Steinar Iversen and Anoop Nair

**21-07-2013 to 28-07-2013**

**Longyearbyen-Storfjordrenna -Longyearbyen**

**R/V Helmer Hanssen**

## CONTENTS

1. INTRODUCTION (F, B) .....	3
2. BACKGROUND INFORMATION ON THE STUDY AREA.....	5
2.1 Oceanographic Setting (G).....	5
2.2 Topographic Setting (E) .....	9
2.3 Geological Setting and Environment (C, A & F (Figure 2.3.3)).....	11
2.4 Glacial History (D).....	16
3. METHODS.....	21
3.1 Subbottom Profiler (Chirp) (B) .....	21
3.2 Multibeam Echosounder (B) .....	22
3.3 CTD (F) .....	23
3.4 2D Reflection Seismic (F).....	25
3.5 Coring (F) .....	27
3.6 Single Beam Echo sounder (F).....	28
3.7 Gas Sampling (C&A) .....	29
4. RESULTS, INTERPRETATION AND DISCUSSION .....	31
4.1 Bottom Sampling (C&A) .....	31
4.2 Lineations and elongated features (G&E) .....	41
4.3 Iceberg plough marks (D) .....	45
4.4 Melt water features (C&A) .....	51
4.5 Grounding Zone Wedges and glacier retreat through Storfjordrenna (G&B) .....	55
4.6 Pockmarks (F) .....	60
4.7 Gas Flares (F) .....	66
5. SUMMARY .....	71
6. REFERENCES.....	73
APPENDIX TO THE CRUISE REPORT .....	79

## 1. INTRODUCTION (F, B)

The course GEO-8144/3144 Marine geology and geophysics cruise, taught at the University of Tromsø, is part of the obligatory courses to be completed by PhD students affiliated with the AMGG research school and yields 5 credits (ECTS). Participants include scientific staff and students.

This cruise was conducted within the framework of 1) the Norwegian Science Council (NFR) project Glaciations in the Barents Sea area (GlaciBar) and 2) the trainee school in Arctic Marine Geology and Geophysics (AMGG) financed by the University of Tromsø. The cruise was funded by AMGG.

The main target areas are the Storfjordbanken and Storfjordrenna south of Svalbard. The cruise addressed marine glacial processes of the areas, with a focus on the last glacial-interglacial cycle in order to reconstruct in a more detail way the retreat of the Barents Sea – Svalbard Ice Sheet.

To collect data have been used different methods and instruments, which will be described in a more detailed way in chapter 3. Below here there is only an overview:

- Multibeam echo sounder: Sound-wave beams are transmitted in a fan perpendicular to the ship track from a hull-mounted echo sounder. Produces high-resolution seafloor bathymetry.
- Chirp: High-resolution acoustic profiling.
- CTD (Conductivity, Temperature, Depth): Sensors installed in a frame measure CTD properties of the water column. Generally used for oceanographic studies, but here mainly to calibrate the multibeam data from calculated velocities.
- 2D seismic: GI airguns and hydrophone cable (streamer).
- Sediment coring: Gravity coring.
- Gas sample collection

The targeted study area is under-explored compared to similar areas (Bjørnøyrenna) in the SW Barents Sea. The study areas in the Storfjordrenna and Storfjordbanken are shown in figure 1.1. Several different features have been identified on the seafloor, like MSGs,

grounding zone wedges, flares, pockmarks and ploughmarks. All these features will be described in detail in chapter 4.

In addition, 9 gravity cores were acquired in areas likely to provide information on the timing of the formation of the sediment accumulation. The specific core locations were chosen based on information from multibeam swath bathymetry and chirp data. Furthermore, gas samples were collected from the cores from pockmarks and will be analyzed later.

The new results add new detailed data regarding the deglaciation of the Storfjorden trough. Glacial geomorphologic features similar to the ones in Bjørnøyrenna were discovered. The observation of gas flares were the first such discovery in the northern Barents Sea. The discovery of flares and pockmarks might have a big impact on future petroleum exploration activities in the region.

The locations of data collected and ship sail tracks are shown in figures 1.1 and 1.2

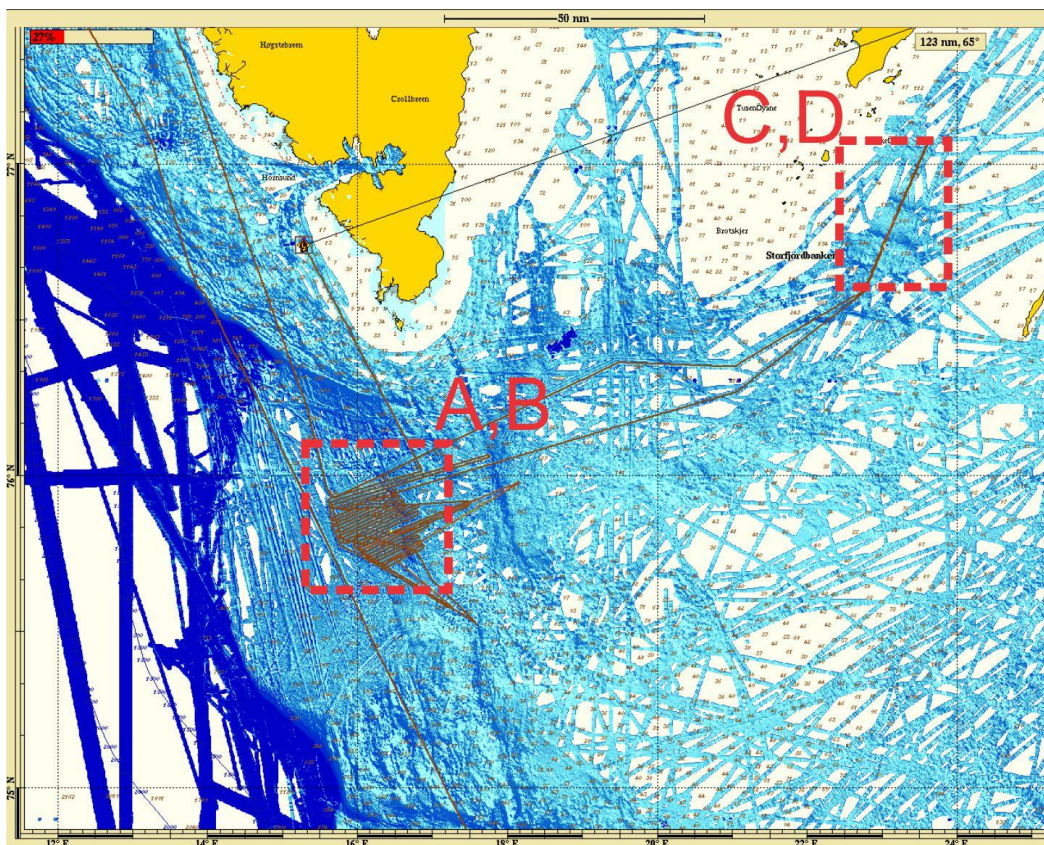


**Figure 1.1** Map showing the sail lines in the study area and Olex bathymetry

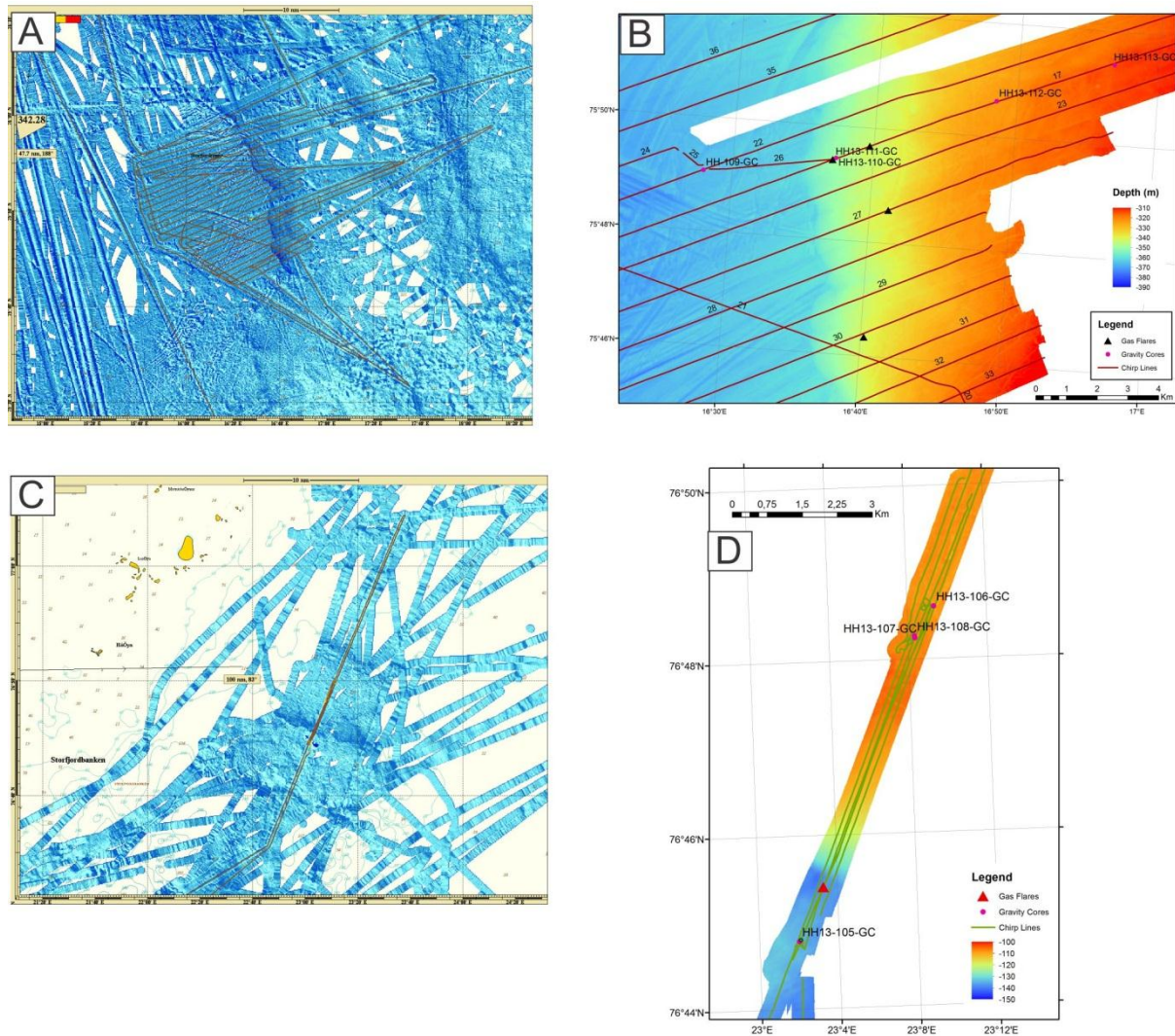


**Figure 1.2** Location of data collected during the cruise

## 2. BACKGROUND INFORMATION ON THE STUDY AREA

### 2.1 Oceanographic Setting (G)

The North Atlantic Current (NAC) is a surface current that transports warm ( $>3^{\circ}\text{C}$ ) and salty ( $>35$ ) Atlantic water into the North Atlantic and further into the Arctic Ocean (Aagaard-Sørensen *et al.* 2010). The major inflow of Atlantic water into the Nordic Seas occurs through the Faeroe-Shetland Channel, where it follows the Norwegian slope as the Norwegian Atlantic Current (NwAC). The NwAC splits in the SW Barents Sea into the West Spitsbergen Current (WSC) and eastward via the North Cape Current (NCaC). WSC follows the western Spitsbergen shelf and continues into the Arctic Ocean through the Fram Strait. The WSC submerges at about  $78^{\circ}\text{N}$  below the colder and less saline Beaufort Gyre

circulation. The presence of Atlantic Water keeps the western Spitsbergen more or less sea ice free year-round, while sea ice regularly form both south, east and north of Svalbard

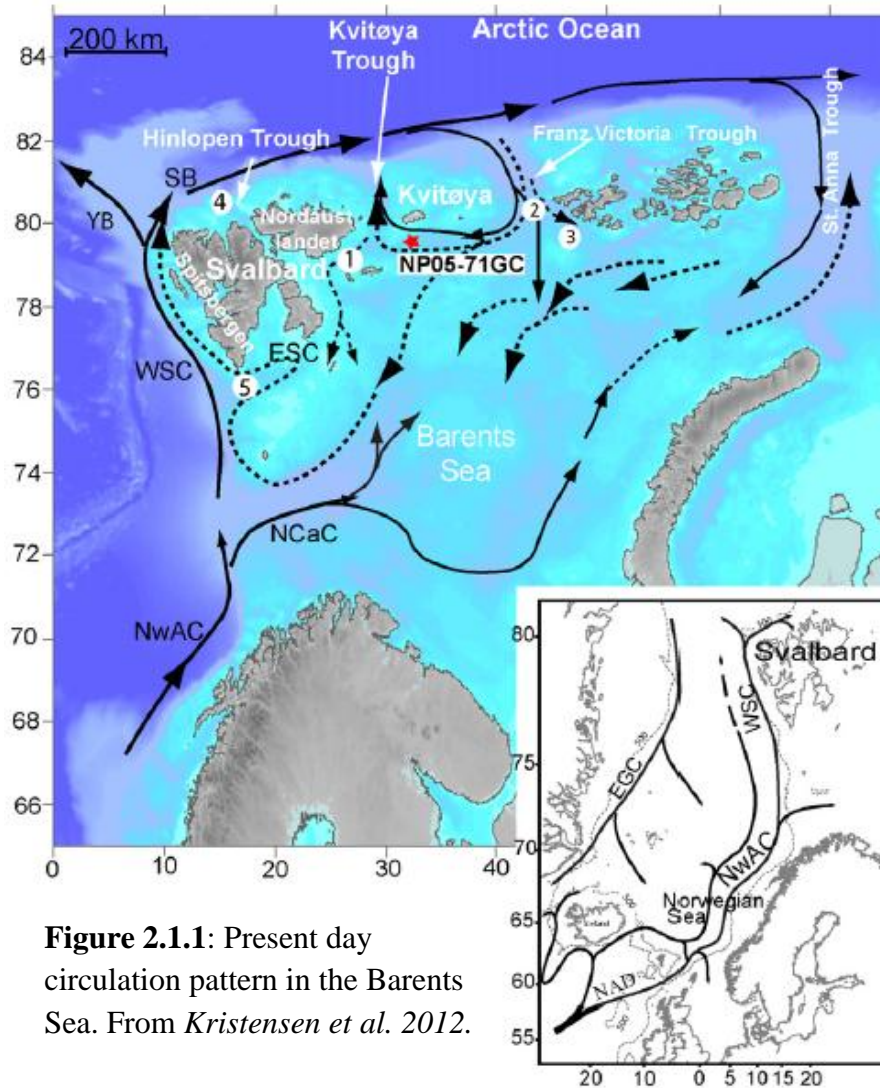


**Figure 2.1.1:** Present day circulation pattern in the Barents Sea. From *Kristensen et al. 2012*.

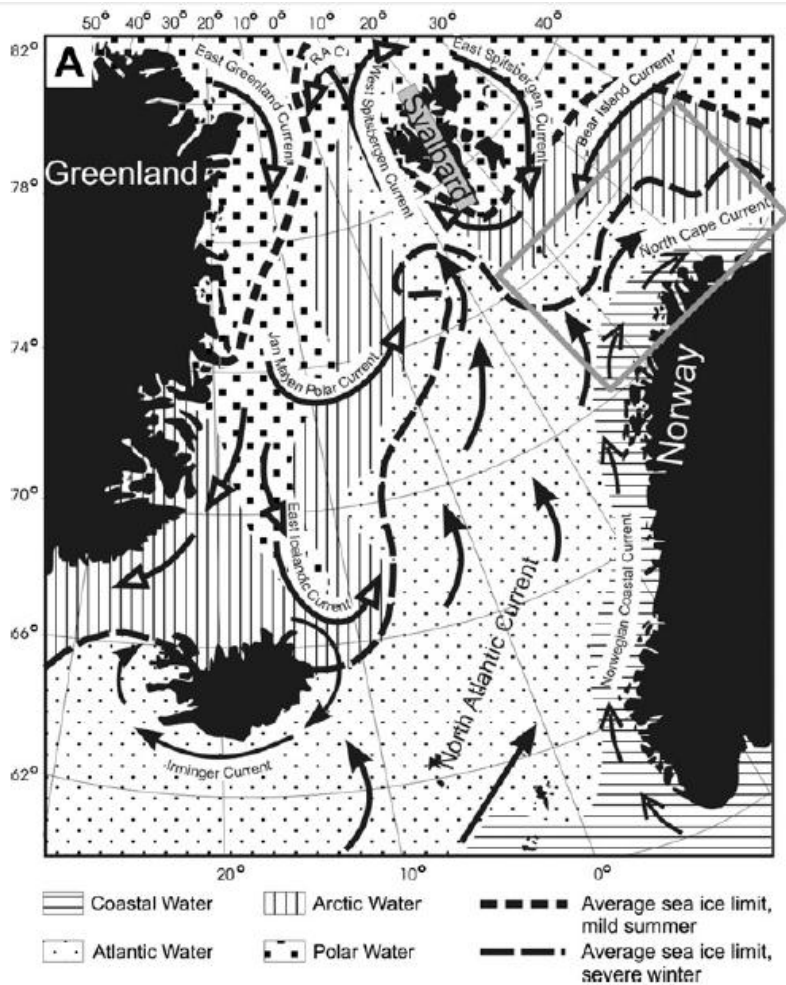


**Figure 2.1.2:** Water mass distribution on the Nordic and Barents Seas. From *Aagaard-Sørensen et al. 2010*.

At present, the Atlantic Water occupies the water column between approximately 50-500 m on the western and northern Svalbard shelf, and between 120-200 m in the northern Barents Sea (*Slubowska-Woldengen et al. 2008; Rasmussen et al. 2007*).

A cold Arctic surface current enters the Barents Sea from the north east of Spitsbergen. Arctic Water, formed by mixing of Polar and Atlantic Water, dominates the northern Barents Sea, and is colder and less saline than the other water masses and enters via the East Spitsbergen Current (ESC) and the Bear Island Current (BIC). The northern Barents Sea is seasonally

covered by sea ice. The southern Barents Sea is dominated by Atlantic water masses. In addition to these two there is the Norwegian Coastal Current (NCC) that transports Norwegian Coastal Water into the southernmost Barents Sea as a wedge above the Atlantic Water, thinning seawards. This water is diluted by runoff water from the mainland Norway and is therefore less saline (34) and has temperatures from 3-9 °C (*Aagaard-Sørensen et al. 2010*).

The surface circulation is important for heat exchange and moisture with the atmosphere and heating of adjacent landmasses, as well as a part of the driving force in the formation of North Atlantic Deep Water (NADW). Any changes in the surface currents affect both sea ice distribution and extent of glaciers and ice caps. The boundary between the Atlantic Water and Arctic Water masses is termed the Arctic Front and forms strong climatic gradients with regard to salinity, temperature and sea ice cover. Svalbard has strong precipitation and temperature gradients from west to east, which affect the extent and volume of glaciers on the archipelago (*Kiltgaard-Kristensen et al. 2012*).



Figure 2.1.3 A) below show the position of two of the CTD stations we took during the cruise; 349 in the north and 351 further south. Figure 2.1.3B) Show the conductivity, temperature and depth plot of station 349. This plot is quite different from the plot of station 351. In station 349 the surface temperature is only around 4°C, whereas at 351 (figure 2.1.3C) it was more than 7 °C. Temperature then decreases with depth. For both stations salinity is low in the topmost 20-50 meters, and then salinity increases drastically. The difference in temperature of the two stations can be explained by the water mass distribution in the two areas. Station 351 is closer to the shelf margin where warm Atlantic water is present. Station 349 is closer to the eastern Svalbard margin and is likely influenced more by the cold ESC bringing Arctic water into the eastern Barents Sea. The salinity stratification can be explained by a surface layer of fresher runoff coastal water from the Svalbard archipelago.

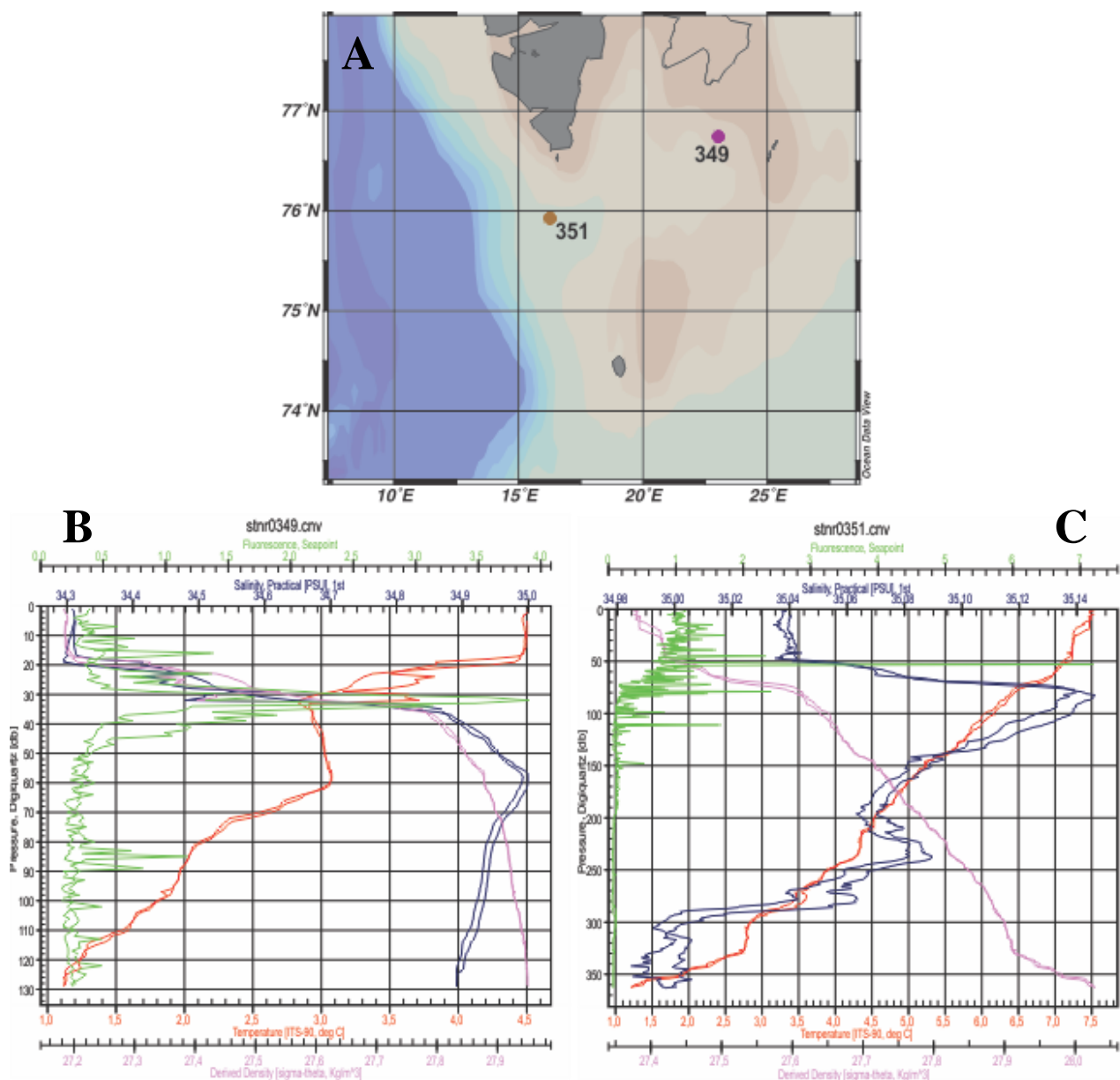


**Figure 2.1.3** – A) Map position of the CTD-stations. B) CTD plot from station 349. C) CTD plot from station 351.

## 2.2 Topographic Setting (E)

The Barents Sea covers one of the widest continental shelves in the world (Fig. 2.2.1) (Andreassen & Winsborrow, 2009). It is bordered by the island archipelagos of Svalbard and Franz Josef Land to the north and Novaya Zemlya to the east. Otherwise we can say that it is bounded to the north and west by Tertiary rift and shear margins and to the south by the Norwegian and Russian coasts (Faleide et al. 1993).

The Barents Sea is a shallow epicontinental sea north of Scandinavia and NW Russia that covers  $1.2 \times 10^6$  km<sup>2</sup> (Faleide et al. 1993). The sea-floor bathymetry is characterized by relatively shallow banks of 100–200 m, separated by troughs opening towards the Norwegian Sea and Arctic Ocean (Fig.2.2.1). The south-western Barents Sea margin is cut by a series of troughs (i.e. Bear Island and Storfjorden Troughs). Water depths within the troughs range typically from 300 to 500 m, but an average water depth of about 230 m, is dominated by the Bear Island Trough, which is oriented E-W and reaches a depth of about 500 m at the shelf break (Laberg & Vorren, 1995) (Andreassen & Winsborrow, 2009).

The main troughs in the west Barents Sea are the Storfjorden Trough (200-500 m deep) where our study area is located, and the Bear Island Trough (Fig.2.2.2). The largest and most prominent trough is Bjørnøyrenna (Bear Island Trough), extending 750 km from Sentralbanken in the east to the shelf edge in the west. It has a width of 150–200 km and spans water depths of 300–500 m (Winsborrow et al. 2010).

At the western and northern Barents Sea there are large trough mouth fans at the margins (Fig.2.2.1) which appear as seawards-convex bulges in the bathymetry at the mouths of the troughs that extend to the shelf edge (Fig.2.2.1) (Andreassen & Winsborrow, 2009). Bear Island Trough is flanked by shallow bank areas Sentralbanken and Spitsbergenbanken to the east and north, and Tromsøflaket and Nordkappbanken to the south. The southernmost Barents Sea shelf is transected by two south-east to north-west trending troughs (Ingøydjupet and Djuprenna), which reach water depths of 450 m. To the south-east, the shelf area is generally shallower, with water depths of less than 200 m. An exception is the over-deepened Kandalaksha Gulf south of Kola Peninsula, which has water depths of 250 m (Winsborrow et al. 2010).

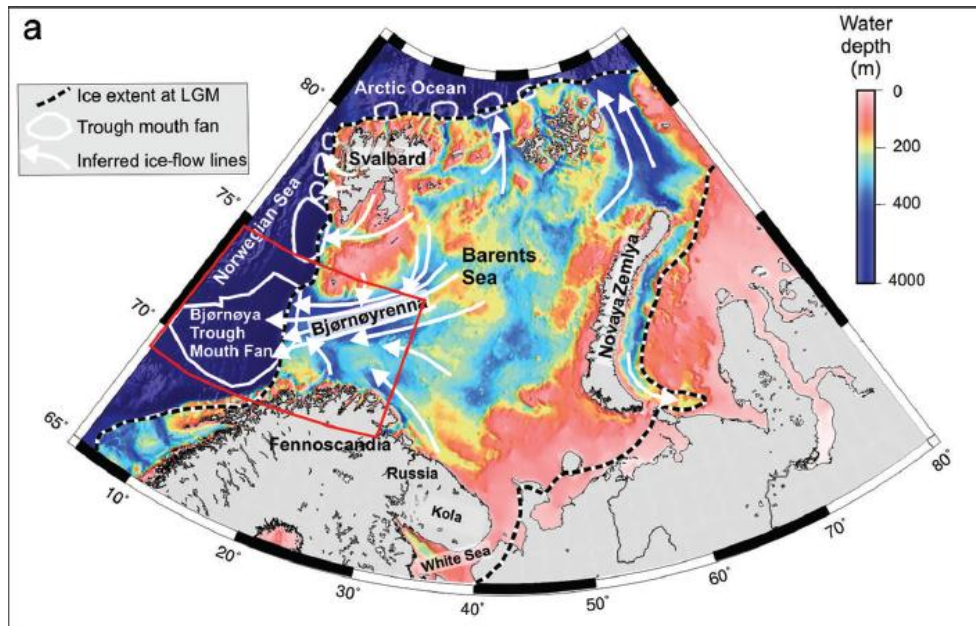


Figure 2.2.1. Shaded relief bathymetry of the Barents Sea (Andreassen,&Winsborrow, 2009).

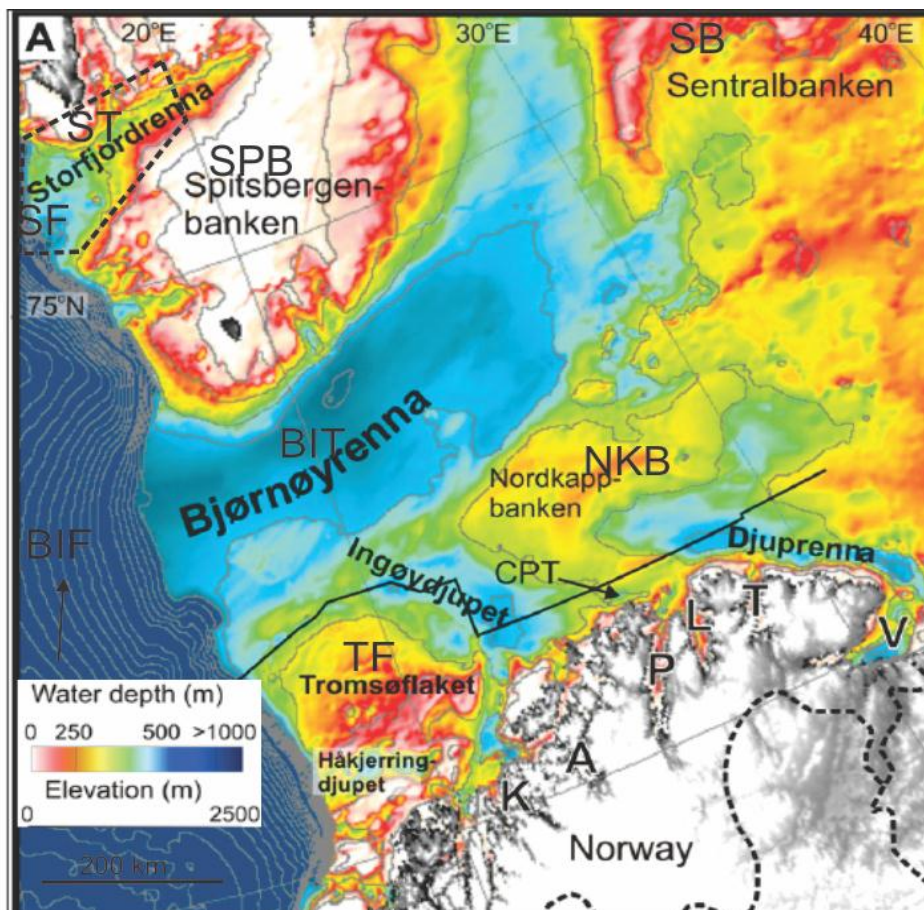


Figure 2.2.2. Color shaded relief map of Svalbard and the Barents Sea (modified from Winsborrow et al. 2010). Abbreviation key: Black dotted are – study area. TF-Tromsøflaket; BIT- Bear Island Trough; BIF- Bjørnøya; SF-Storfjorden trough mouth fan; ST-Storfjorden trough; SPB-Spitsbergenbanken; NKB-Nordkappbanken; SB-Sentralbanken.

### **2.3 Geological Setting and Environment (C, A & F (Figure 2.3.3))**

The Barents Sea today is a shallow epicontinental sea with an average water depth of around 230 m and an area of about  $1.2 \times 10^6$  km<sup>2</sup>. It is bound in the north and west by Tertiary rift and shear margins. The Novaya Zemlya region forms the eastern boundary whereas the Norwegian coast and the Kola Peninsula mark the southern boundary. The bathymetry is characterized by banks and troughs. The western Svalbard–Barents Sea Margin is characterized by large accumulations of sediments on the continental slope, believed to have resulted from late Cenozoic glaciations.

The present-day climate at high northern latitudes is regulated by the advection of warm North Atlantic waters into the Nordic Seas and the water-mass transformations that take place therein. The Barents Sea receives about 40% of these northward flowing waters and is thus an important part of the system (Butt et al, 2002).

The Barents Sea region has an intracratonic setting and has been affected by several phases of tectonism since the Caledonian orogenic movements terminated in early Devonian times. The Barents Sea continental shelf is dominated by ENE-WSW to NE-SW and NNE-SSW to NNW-SSE trends with local influence of WNW-ESE striking elements (Fig.2.3.1). In the southern part, a zone dominated by ENE-WSW trends is defined by the major fault complexes bordering the Hammerfest and Nordkapp Basins. This trend is sub parallel to another major zone to the North defined by the Veslemøy High and the fault complexes separating the Loppa High from the Bjørnøya Basin. N-S trends prevail to the west and northwest (the Tromsø basin, Knolegga Fault and Hornsund Fault Complex).

The western part of the Barents Sea has been the tectonically most active sector through Mesozoic and Cenozoic times. In contrast, eastern and northeastern parts have been dominated since late Carboniferous times by relatively stable platforms with less pronounced tectonic activity. Few data exist on the pre-Carboniferous structure history of the Barents shelf. However, data from Svalbard, unpublished reflection seismic data and data from northern Scandinavia indicate that most of the known major structural trends may have been established by Devonian times and some important features may even be related to structures formed during the Caledonian Orogeny.

In Svalbard and northern Norway deformation activated N-S to NNW-SSE and WNW-ESE to NW-SE trends, respectively whereas Caledonian deformation in northern Scandinavia mainly involved ENE-WSW to NE-SW trending faults, and reactivation of WNW-ESE lineaments like the Trollfjord-Komagelv fault. Lineament analysis has demonstrated the regional importance of these trends.

It is regarded as likely that the older fracture systems are preserved in the basement under lying the sediments of the continental shelf, and that they have influenced the late Paleozoic to Cenozoic structural development in the Barents Sea. Thus, the Devonian sedimentation may have taken place in fault-bounded basins following older structural trends.

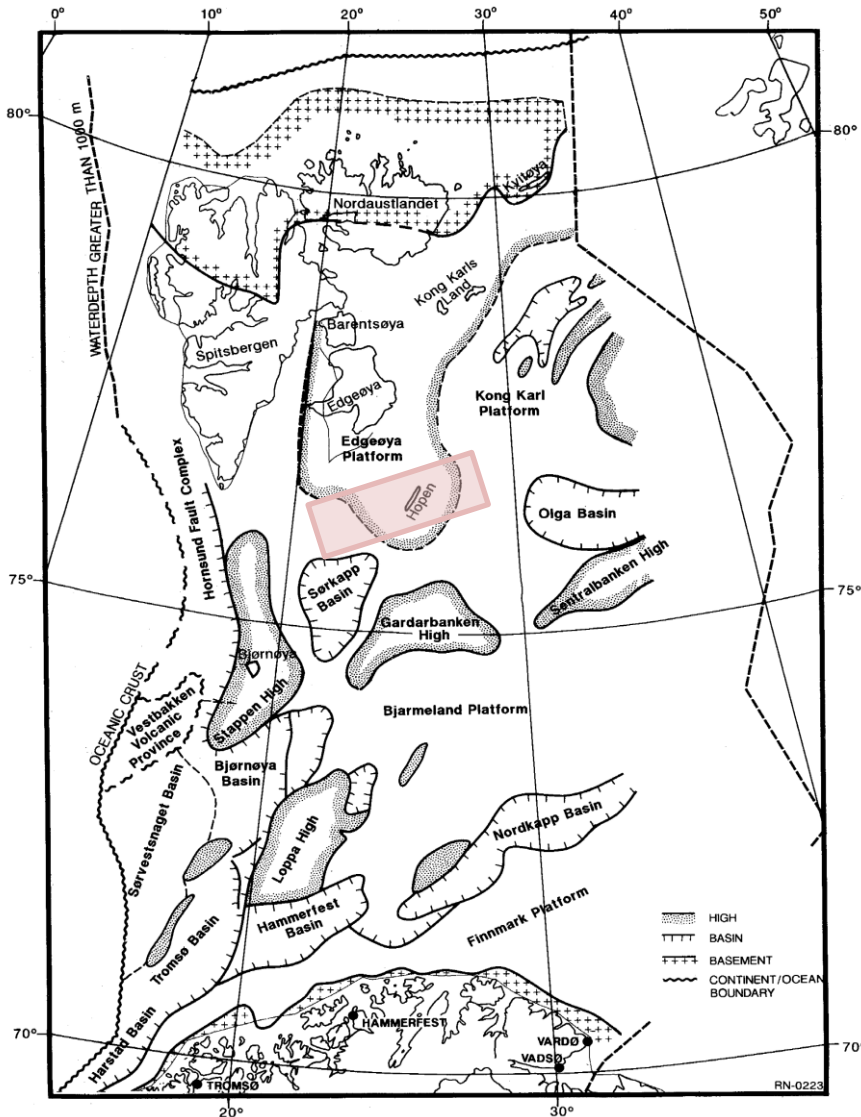


**Figure 2.3.1.** Tectonic framework of the Barents sea region and study area within (Gabrielsen et al, 1990).

Paleocene epeiric sea sedimentation was sourced by erosion at the Stappen High. Earliest Eocene extension associated with volcanism was followed by rapid subsidence of the Vestbakken volcanic province, which became filled by sediments from an uplifted Stappen High. By the Middle Eocene, siliciclastic shelf sediments were deposited and the infill had reached a balance with subsidence. Tectonic movements at this time may have caused local uplift, which restricted the ventilation of local basins west of the Stappen High, but marine

conditions existed in the area until Early Oligocene times, when sub aerial exposure was caused by tectonic uplift and probably also a fall in eustatic sea-level.

Pronounced Oligocene and Pliocene unconformities reflect major events of uplift and erosion at the margin, and abundant fossil reworking indicates erosion of the uplifted Cretaceous and Tertiary strata. The Oligocene erosion had its associated depocentre to the south and west of the study area, and was less important regionally than the Pliocene-Pleistocene phase. The Pliocene uplift first led to local erosion along the margin. Subsequent subsidence may initially have had a thermal component. This was followed by extensive downwarping under the load of large-scale deposition sourced by regional erosion in the Barents Shelf region (Fig 2.3.2).

An Eocene volcanic phase was probably related to the initiation of seafloor spreading. Isotopically dated volcanoclastic intervals in one of the cores give evidence of a Late Pliocene volcanic phase. This event was associated with local tectonic movements, which may be part of a regional uplift in the western northwestern part of the Barents Sea. Glaciations caused by the Neogene climatic deterioration became enhanced by uplift, and this led to extensive regional glacial erosion. The main depocentre was offset to the south by ice flow curving around the uplifted area. (Saettem et al, 1994)

Geological exploration of the Norwegian Barents Shelf started with seismic surveys in the 1970s, resulting in the first differentiation of the province into a series of major sub provinces with a complex structural and sedimentological development. Hydrocarbon exploration drilling started in 1980 and this ongoing exploration activity has resulted in a series of papers integrating regional well information with the steadily expanding seismic grid and pointing out the regional similarities of the geological development of Svalbard and both the Norwegian and Russian sectors of the Barents Shelf. A total of 59 exploration wells have been drilled in the Norwegian Barents Sea, with more than half of these located in a relatively small area either in, or in close proximity to the Hammerfest Basin. The remaining wells are spread across the shelf and have tested a variety of plays - 14 wells have drilled in-situ Upper Paleozoic strata, but only 6 of these had the Upper Paleozoic succession as a primary or additional target (Larssen et al, 2002)

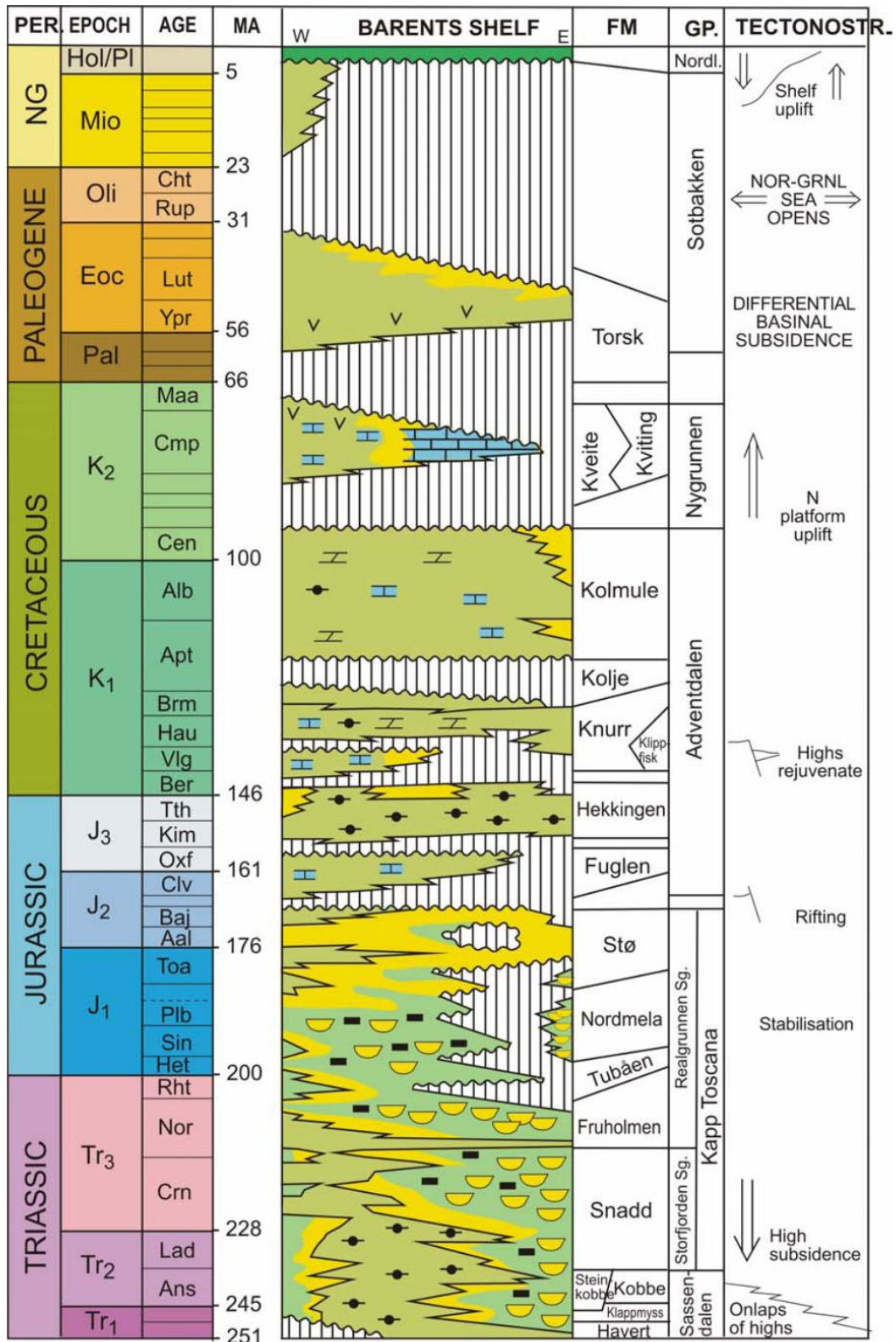


**Figure 2.3.2.** The Mesozoic and Cenozoic development of the southwestern Barents Sea, modified from Nøttvedt et al. (1993), with geological time scale based on Gradstein et al. (2004).

Northern part of the Barents Sea is covered by Quaternary sediments over the Mesozoic sedimentary bedrock (Solheim et al., 1990) (Fig.2.3.3). There are Upper Regional

Unconformity (URU) between the pre-glacial bedrock and the thin cover of glacial deposits on the continental shelf (Solheim and Kristoffersen, 1984). The Quaternary succession is believed to consist of till, overlain by softer sediments and a thin cover of postglacial mud. The till might be continuous over large areas, but is often irregular and may fill depressions in the bedrock surface.

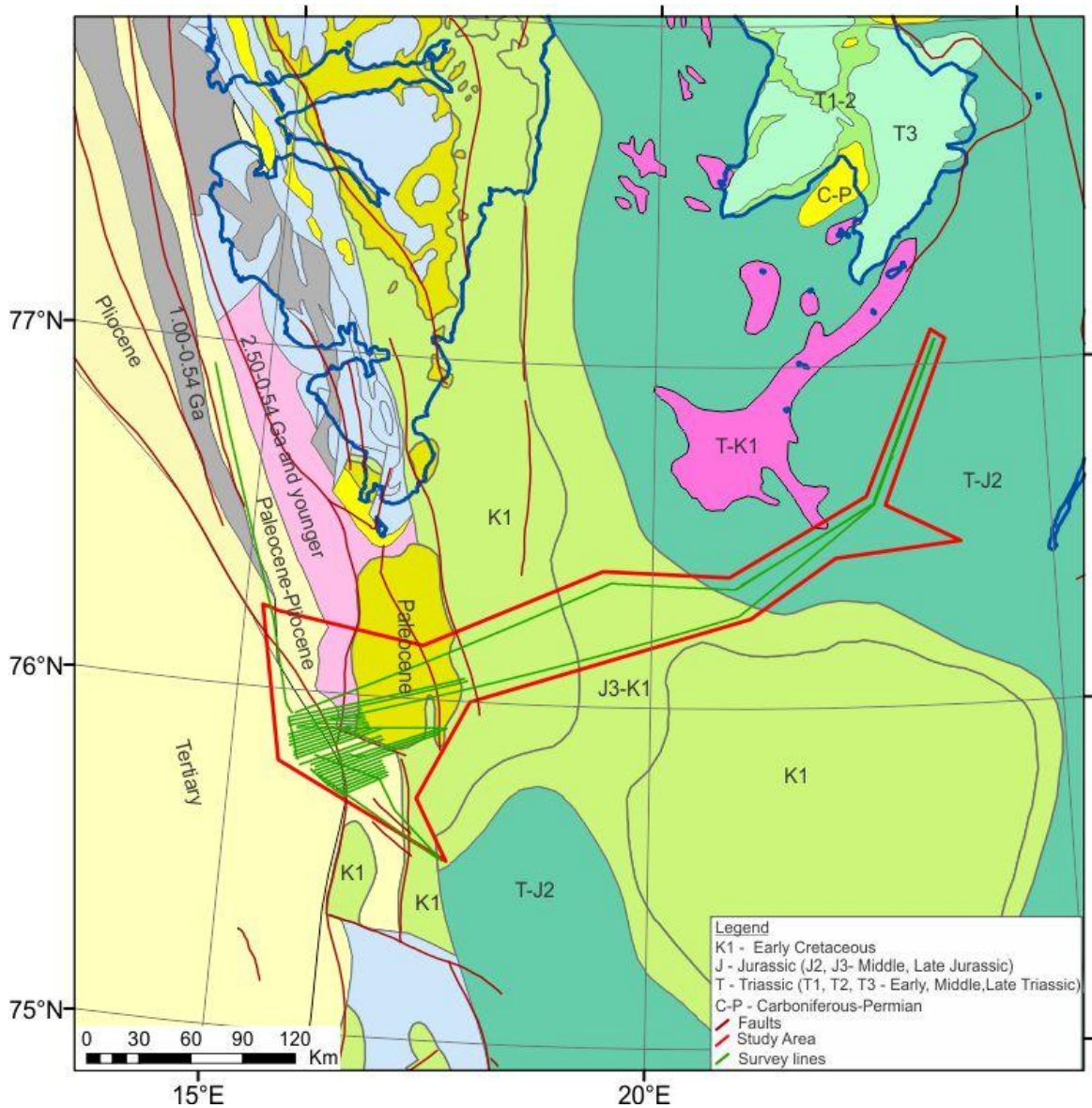


Fig. 2.3.3. Geological map of bedrock distribution within the study area.



## 2.4 Glacial History (D)

Throughout the past two decades there has been a significant increase in the amount of studies attempting to reconstruct the size and extent of the Barents Sea Ice Sheet (BSIS). However, despite the growing amounts of research in this area there still remains a large uncertainty regarding the ice sheet dynamics and margin extents during and post the Last Glacial Maximum (LGM; Landvik et al., 2005). In particular, there is a large ambiguity in regards to the patterns and processes, as well as the timing, of the deglaciation in this region (Landvik et al., 2005).

Nevertheless, numerous studies (e.g. Svendsen et al 2004; Knies et al., 2009) have noted that the Barents Sea must have undergone several glaciations and deglaciation cycles during the last ~3.5 million years ago (Ma; figure 2.4.1). Various reconstruction models have been proposed for the development and deglaciation of the Barents Sea. However, the three leading ice sheet reconstructions, and those which will be discussed in this section of the cruise report, will be: Firstly, a three phase model (Figure 2.4.1) proposed by Knies et al., (2009), which covered the late Plio-Pleistocene BSIS extents (Figure 2.4.1). Secondly, a four stage time-slice reconstruction (Figure 2.4.2) proposed by Svendsen et al., (2004), which covered four glaciations in the Barents Sea since the Late Saalian (>140 ka BP; thousands of years ago before present). Lastly, a 5 stage reconstruction of the Late Weichselian deglaciation (Figure 2.4.3) was proposed by Winsborrow et al., (2010).

Between ~3.5 Ma and 2.4 Ma, stage 1, the ice that was present in the Eurasian Arctic, experienced the initial build-up stage, advancing onto the coastlines and the northern shelf edge, covering the mountainous regions in the area (Figure 2.4.1 A; Knies et al., 2009). This build-up stage was likely to have been a result of the onset of the Northern Hemispheric Glaciation, which occurred between ~3.6-2.4 Ma (Mudelsee and Raymo, 2005; Knies et al., 2009). Following the initial build-up, BSIS experienced a transitional growth phase, stage 2, which occurred between ~2.4-1.0 Ma (Figure 2.4.1 B; Knies et al., 2009). This stage was marked by the expansion of the BSIS towards the southern section of the Barents Sea, as well as simultaneously flowing in a northwestern direction towards the Kara Sea (Knies et al., 2009). Post ~1 Ma, stage 3 (Figure 2.4.1 C), there was a large-scale glaciation of the Barents Sea, marked by several meltwater pulses onto the shelf edges, indicative of repeat advances from the BSIS onto the shelf edge (Knies et al., 2009).

Similarly, Svendsen et al., (2004) suggested that during the Late Saalian (160-130 ka BP) the Northern Hemisphere experienced extensive Quaternary glaciations (Figure 2.4.2 A). During this time, the BSIS formed a vast ice sheet complex, covering both the Barents Sea and Kara Sea, where it then extended into the Arctic Ocean forming an ice shelf (Jakobsson et al., 1999; Svendsen et al., 2004). The ice sheet extent during this period was of a much greater size than those present during the Weichselian (Svendsen et al., 2004).

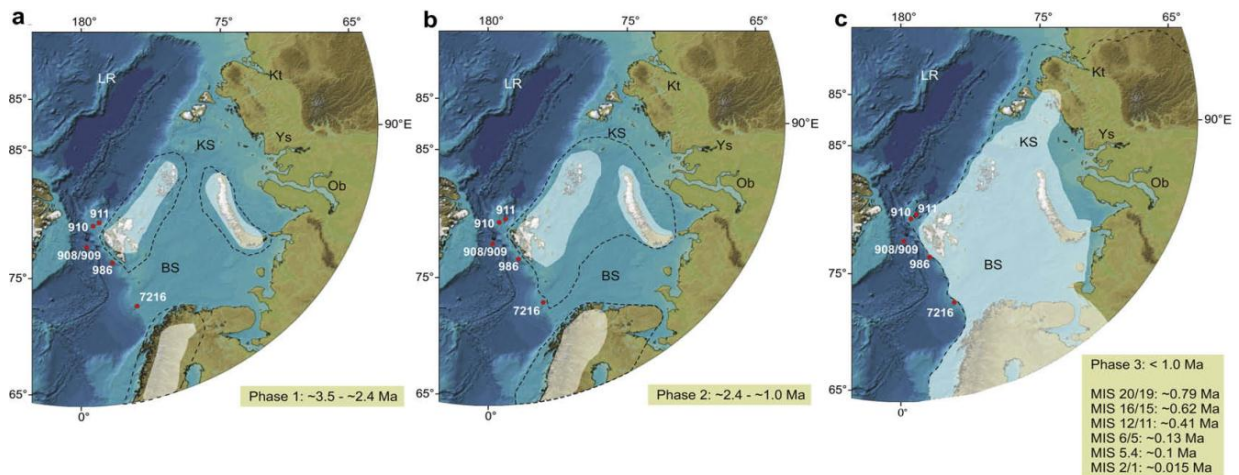


**Figure 2.4.1.** Schematic diagram showing the maximum (black dotted lines) and minimum (white patches) ice extensions in the Barents Sea during the Late Plio-Pleistocene. A) Phase 1; ~3.5-2.4 Ma. B) Phase 2; ~2.4-1.0 Ma. C) Phase 3; <1.0 Ma. Knies et al., 2009.

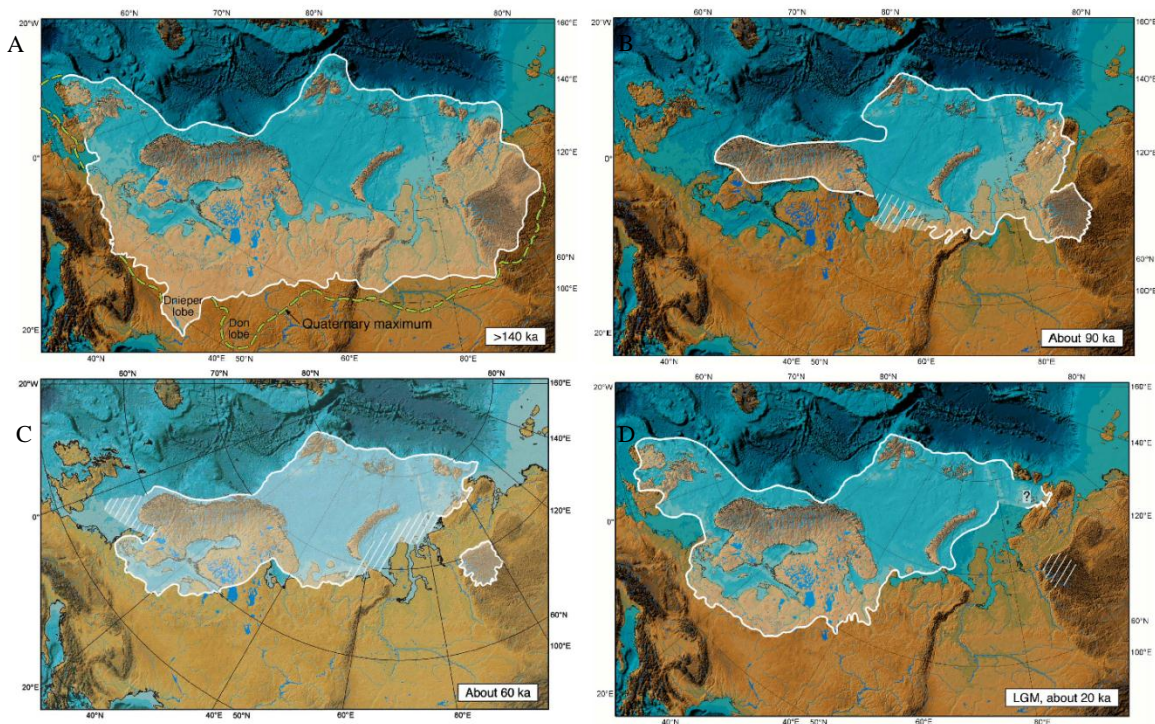


**Figure 2.4.2.** Reconstructions of the maximum ice-sheet extents at several time-slices (Svendsen et al., 2004). A – Late Saalian, ~160-140 ka BP. B – Early Weichselian Glacial Maximum, 90-80 ka BP. C – Middle Weichselian glacial maximum, ~60-50 ka BP. D – Late Weichselian glacial maximum, ~20-10 ka BP.

During the Early Weichselian glacial maximum (~90 ka BP; Figure 2.4.2 B) the Barents-Kara Ice sheet reached its maximum extent, reaching far into the Kara Sea where ice sheet configurations indicate that there was a major ice dome (Svendsen et al., 2004). The margin extent of the western BSIS remains unclear for this period (Svendsen et al., 2004). However, it has been suggested that this glacial maximum corresponds with a ice advance recorded in Svalbard (Mangerud et al., 1998; Svendsen et al., 2004).

Following the Early Weichselian glacial maximum there was a large deglaciation between ~85-75 ka BP, although this was relatively short lived as there was a rapid regrowth of the Barents-Kara Ice Sheet extending into the northeastern margin of the Barents Sea during the early Middle Weichselian (~60-50 ka BP; Figure 2.4.2 C; Mangerud et al., 1998; Knies et al., 2000; Svendsen et al., 2004). Svendsen et al., (2004) and others (e.g. Mangerud et al., 1998), proposed that by the end of the Middle Weichselian (50-30 ka BP) the Barents-Kara sea shelves were almost completely ice free, indicating a major deglaciation during this period.

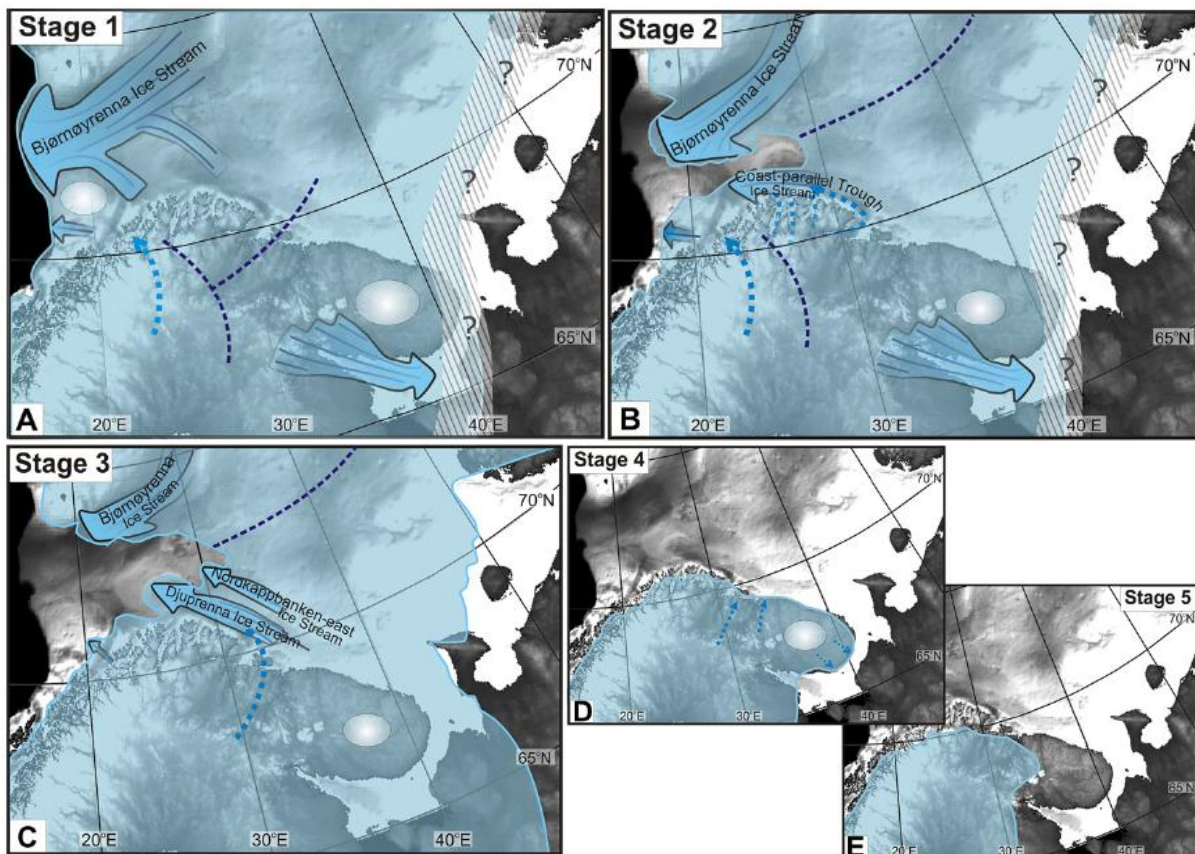


**Figure 2.4.3.** A reconstruction of the Late Weichselian maximum and the subsequent deglaciations of the southern Barents Sea using a five-stage model. A - Late Weichselian maximum (~19 ka BP). B – Early deglaciation (~17 ka BP). C – Ice free period (~16 ka BP). D – Rapid loss of ice in the East (~15 ka BP). E – Possible scenario for the Younger Dryas

(~12-12.5 ka BP). Blue arrows – ice streams. Dashed light blue arrows – warm based ice. White discs – cold based ice. Dark blue lines – possible ice divides. Winsborrow et al., 2010.

Using both onshore and offshore glacial geomorphological data-sets, Winsborrow et al., (2010) was able to formulate a potential five stage model for the maximum extent of the BSIS and the deglaciations that followed during the Late Weichselian (25-10 ka BP). The initiation of the Late Weichselian glaciation was marked by an extensive cooling period in the Northern Hemisphere, known as the Last Glacial Maximum (LGM; ~22-21 ka BP). During this period several of the Northern Hemispheric Ice Sheets reached their Weichselian maximum extent. The BSIS reached its peak in size prior to 22 ka BP during the LGM (Figure 2.4.4) where it covered the whole of the Barents Sea continental shelf (Landvik et al., 1998; Winsborrow et al., 2010; Ingólfson & Landvik, 2013). Although, whilst in the Late Saalian, the maximum extent of the Barents-Kara Ice Sheet was the thickest in the east (Svendsen et al., 2004), during the LGM the ice sheet was thickest in the Northwestern part of the Barents Sea (Winsborrow et al., 2010).

During the Late Weichselian glacial maximum the drainage and ice sheet mass balance was dominated by large ice streams, which flowed from the ice domes present in the BSIS (Winsborrow et al., 2010). The location of these ice domes varied a lot throughout the Barents Sea glacial history. However, during the LGM it was likely to have been positioned over the eastern Spitsbergen and southern Hinlopen Strait (Landvik et al., 1995; Dowdeswell et al., 2010; Ingólfsson and Landvik, 2013). Flowing from this ice dome was one of the most studied ice stream in the Barents Sea, there Bjørnøyrenna Ice Stream. The Bjørnøyrenna Ice Stream played an important role in the stabilisation of the BSIS mass balance and is thought to have reached the continental shelf-edge twice, first prior to 22 ka BP and second ~19 ka BP (Stage 1 in figure 2.4.3 A), indicating the maximum extent of the BSIS (Sættem et al., 1992; Laberg and Vorren, 1995).

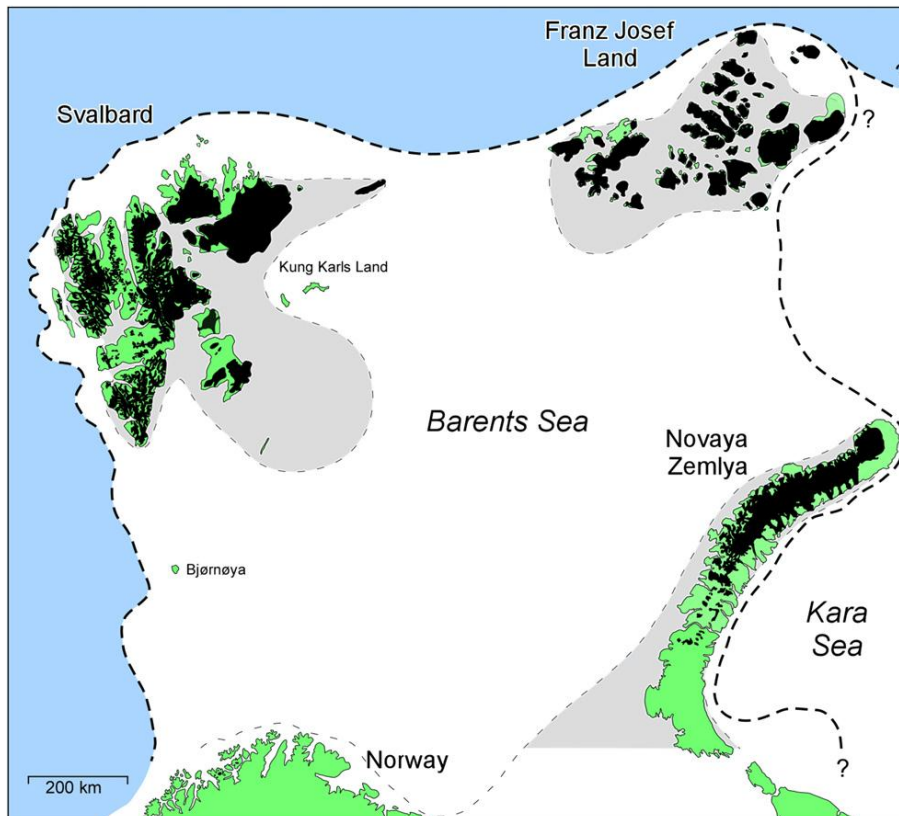


**Figure 2.4.4.** Reconstruction map of the Svalbard-Barents Sea Ice sheet extent during the LGM. White indicates the maximum extent and grey indicates the minimum extent of the ice sheet. Ingólfsson and Landvik, 2013.

The retreat of the BSIS initiated around 19 ka BP and continued until 17 ka BP, during which there was a rapid withdrawal of the Bjørnøyrenna Ice Stream grounding line upstream, leaving the evidence of several rapid readvances with intermediate periods of relatively stable ice margin stability in between (stage 2; figure 2.4.3 B; Andreassen et al., 2008; Winsborrow et al., 2010). Evidence for the BSIS retreat was also recorded in Storfjordrenna, which indicated that it was likely to have been deglaciated by 19 ka BP (Rüther et al., 2011). By 16 ka BP, Bjørnøyrenna trough, as well as the western Barents Sea, was mostly ice free and so, modifying the the dynamics of the BSIS and shifting the mass balance towards the eastern sector of the BSIS (stage 3; Figure 2.4.3 C; Winsborrow et al., 2010). Post ~15 ka BP, the deglaciation of this area began to slow down because the ice margin had retreated far enough onshore for calving to not be possible any more (stage 4 & 5; Figure 2.4.3. D & E respectively; Winsborrow et al., 2010).

### 3. METHODS

#### 3.1 Subbottom Profiler (Chirp) (B)

A X-STAR Full Spectrum Sonar is a versatile wideband FM sub-bottom profiler that generates cross-sectional images of the seabed and collects digital normal incidence reflection data over many frequency ranges. X-STAR transmits an FM pulse that is linearly swept over a full spectrum frequency range (also called “chirp pulse”).

The chirp system comprises a hull-mounted 4 x 4 transducer array operated at an energy level of 4 kW and at a shot rate of 1 s (Fig.1). The signal lasts 40 ms, starts at 1.5 kHz and end at 9 kHz. The system can operate in up to 8000 m of water. The penetration depth depends on the sediment type/thickness, it can be up to 80 m in soft clay.

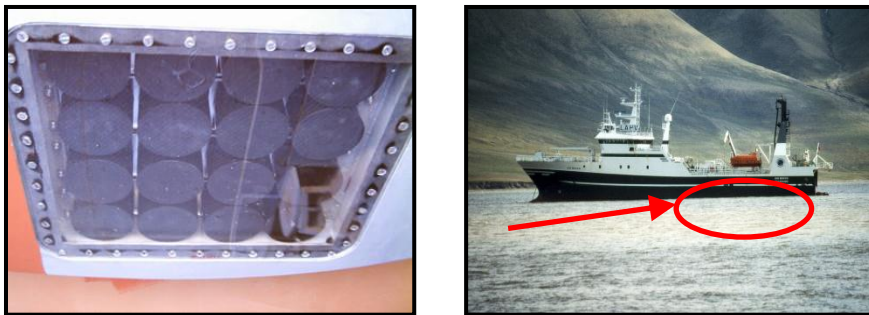


**Fig. 3.1.1** The Chirp system. Photo: M. Forwick, UiT

During this cruise, we image the morphology of the ocean floor and its shallow sub-bottom sedimentary layers and structures (Fig.3.1.2) using the subbottom profiler. This can be important for deciding the location of for example gravity cores.

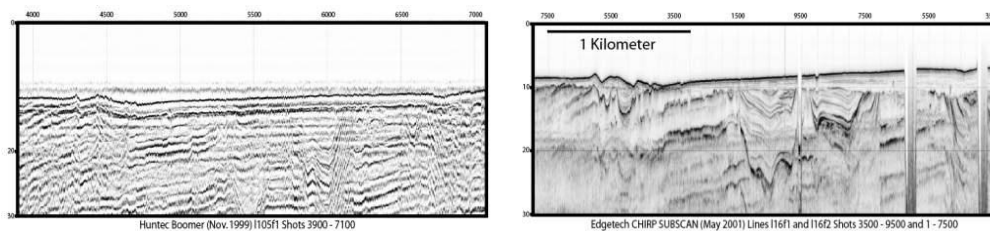


**Fig. 3.1.2** Example of the sub-bottom sedimentary layers and structures.

### 3.2 Multibeam Echosounder (B)

In the hull of R/V Helmer Hansen has been installed a Kongsberg Simrad EM 300 multi-beam echo sounder (Fig. 3.2.1).



Fig. 3.2.1 – The multibeam system: Transmitters mounted in sea box (on the left) and the ice window (receiver) (on the right). Photo: Steinar Iversen, UiT.

The multi-beam system measures the two-way travel time that a sound wave initiated by a transmitter needs to reach the sea floor and come back. These waves have a frequency of 30 kHz, which is too high to penetrate the seafloor sediments, but gives a high resolution for a bathymetric map.

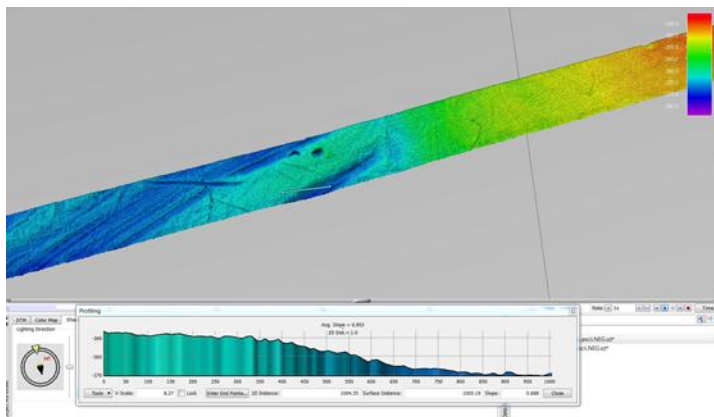
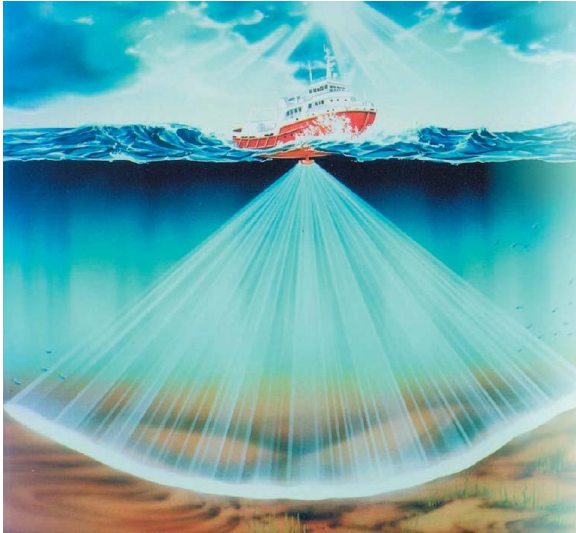


Fig. 3.2.2 Snapshot of one the swaths.

A number of piezo electric transmitters, mounted in the hull, transmit 135 beams producing a fan arc, perpendicular to the ship track. Each beam has a width as narrow as one vertical degree by one horizontal degree (Fig. 3.2.3).



**Fig. 3.2.3** Beams are transmitted in a fan perpendicular to the ship track.

The swath width, dependent on seabed sediments, in shallow water (<500 m) is typically 4 times the water depth. Down to 2000 m, a swath width of 4-5 km is common. The maximum width is 5000 m. The swath width, dependent on seabed sediments, in shallow water (<500 m) is typically 4 times the water depth. Down to 2000 m, a swath width of 4-5 km is common. The maximum width is 5000 m. The multibeam system has been used to map the seafloor morphology and its acoustic backscatter.

We have to take into account that the amplitudes recorded are slightly attenuated (~6 dB) because of protective housing installed around the hardware to avoid damage of ice contact. The outer beams of the EM300 swath can be of low quality, due to speed and signal reception errors because of the great travel distance, large propagation angle and low angle of reflection. That is why we usually have an overlap of 7-25% between the connecting lines. Ship turns also produce unevenly spaced swaths and data logging is normally paused during turns.

Once data have been acquired, we have used the programs Neptune, Fledermaus and ArcGIS to visualize, clean, filter and process them.

### **3.3 CTD (F)**

CTD (Conductivity, Temperature, Depth) sensors measure or evaluate the physical properties of seawater. In addition to measuring the conductivity, temperature and pressure (from which depth is calculated), the CTD sensors can measure or calculate salinity of



seawater, density, P-wave velocity, turbidity, fluorescence/chlorophyll, and oxygen content. Furthermore, it is possible to collect water samples from any depth of choice.

R/V Helmer Hanssen uses SBE 9plus CTD for producing vertical profiles of seawater properties (Fig. 3.3.1). A winch is used to lower the CTD system into the water. The SBE 9plus CTD can measure physical properties of the seawater from up to eight auxiliary sensors, in marine or fresh-water environments at depths up to 6000 meters. However, the winch wire length limits CTD measurements to approximately 3200 meters. The CTD sensors record data at a rate of 24 samples per second. The 9plus system uses the modular SBE 3plus temperature sensor, SBE 4C conductivity sensor, SBE 5T submersible pump, and TC duct (Fig. 3.3.2). The submersible pump pumps water along the sensor to measure the conductivity. The TC duct makes sure that temperature and conductivity are measured on the same parcel of water. 12 water bottles can be attached to the CTD instrument set up shown in figure 3.3.1 to collect the water samples from any depth, if required. A single conductor cable supplies the power to the system and transmits data from and to the CTD system real time.

During our cruise, we used the sound velocity profiles from different CTD stations to calibrate depth calculations in the swath bathymetry data.



**Figure. 3.3.1** CTD sensor set up onboard R/V Helmer Hanssen.



**Figure. 3.3.2** SBE 9plus CTD System

### 3.4 2D Reflection Seismic (F)

Reflection seismic method is widely used to study deeper subsurface which cannot be easily studied by other methods. It uses the acoustic energy reflected by various lithological interfaces to obtain an image of the subsurface from which subsurface geology can be interpreted. A reflection seismic survey typically involves generating seismic events or shots, using various methods, at different locations and recording the reflected waves using sensors or receivers. The sensors convert the ground motion resulting from the seismic event to electric voltage which is recorded.

The major components of a 2D marine reflection survey are the seismic source and the streamer, which houses the receivers/sensors.

*Source:* During our cruise we used mini GI (Generator-Injector) air gun as the seismic source (Fig. 3.4.2). It is especially suited for high resolution surveys. The air gun generates seismic waves by releasing compressed air in to the water. The working principle of a GI gun is detailed in figure 3.4.1. The total volume of the gun is 30 in<sup>3</sup> and is operated in the harmonic mode (e.g., Marine Sources, Sercel), i.e., 15 in<sup>3</sup> each for generator and injector. This generates a high frequency signal which is suited to studying shallow subsurface in detail, which is the region of interest in our studies. A compressor is used to supply air at high pressure (maximum of 210 bars) to the air gun.

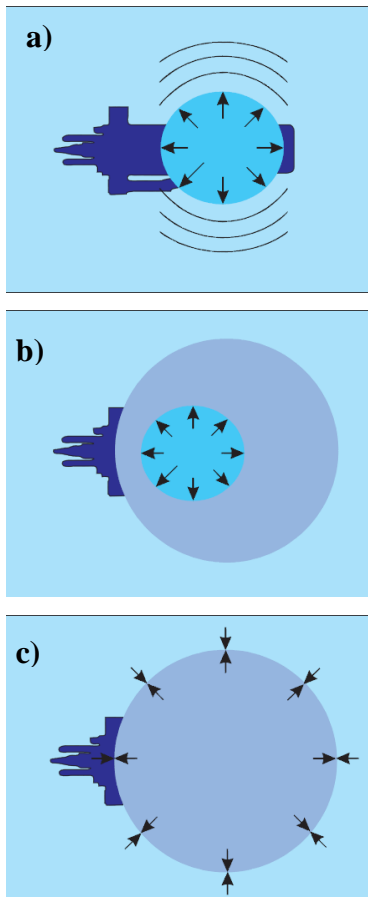


**Figure.3.4.1** a) Phase 1- The Generator is fired. The blast of compressed air produces the primary pulse and the bubble starts to expand.

b) Phase 2- When the bubble approaches its maximum size, it encompasses the INJECTOR ports, and its internal pressure is far below the outside hydrostatic pressure. At this time, the INJECTOR "I" is fired, injecting air directly inside the bubble. Due to the quasi-static state of the bubble, the timing of the INJECTOR is not critical.

c) Phase 3- The volume of air released by the INJECTOR increases the internal pressure of the bubble, and prevents its violent collapse. The oscillations of the bubble and the resulting secondary pressure pulses are reduced and re-shaped.



**Figure 3.4.2** Mini GI gun used for seismic surveys during the cruise.

*Streamer:* In marine surveys, the seismic receivers or hydrophones are enclosed in oil –filled tube known as the streamer. The streamer used during this cruise is 16m long with one channel consisting of 20 sensors (piezoelectric material) spread over 6 meters (active section) (Fig. 3.4.3). The streamer is manufactured by Fjord Instruments.



**Figure.3.4.3** Single-channel streamer used for seismic surveys during the cruise.

*Operation:* The streamer is towed at a distance of 64 meters behind the ship. The mini-GI gun is towed at a distance of 32 meters behind the ship, at a depth of 2 meters below mean sea level and is fired every 3 seconds at 160 bar air pressure (Fig. 3.4.4). The ship speed is maintained at 4 knots per hour. The data collected in the streamer is analog and converted to digital by the Fjord Instruments system and the software Delphseismic, which also provides a real-time display of acquired data.

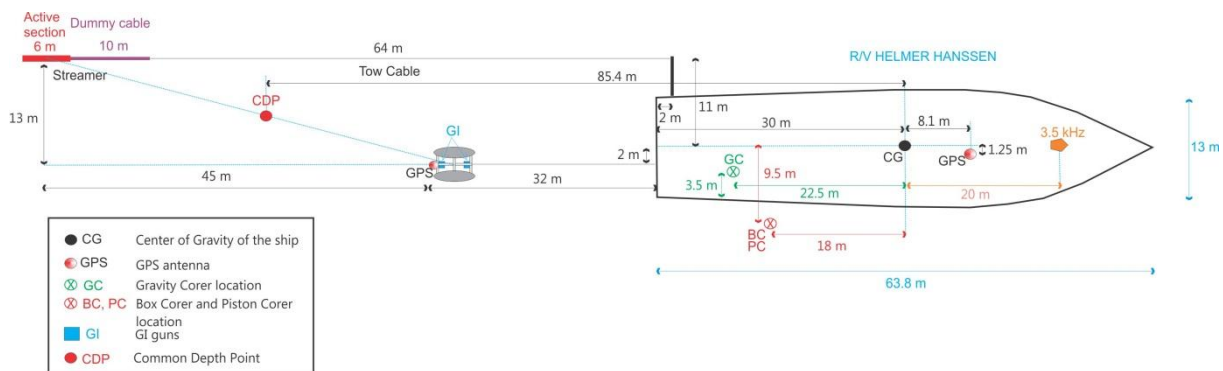


**Figure. 3.4.4** Operational layout of seismic system onboard R/V Helmer Hanssen.

We occasionally used seismic system during the cruise to acquire seismic data over interesting features such as pockmarks, gas flares.

### 3.5 Coring (F)

Coring is the primary tool for ground truthing, studying sediment types, paleontology, and paleo-climate. R/V Helmer Hanssen has a piston corer, box corer, multi corer and a gravity corer. During our cruise we used only gravity corer for sampling sediments. The gravity corer onboard Helmer Hanssen consists of a 6m long iron barrel with iron weights attached on top of it (Fig. 3.5.1). The whole apparatus weigh close to 2 tonnes. The gravity corer has an inner diameter of 11cm. A plastic liner with outer diameter of 11cm and inner

diameter of 10.2 cm is inserted in to the iron barrel. During the coring operation, a core catcher and core cutter is attached to the lower end of the gravity corer. Core catcher keeps the sediments from falling out of the core, whereas core cutter helps the penetration of the core in to the sediments.

The gravity corer lies on a rail, which, during operation, is lifted vertically and the gravity corer is lowered to the seabed using a winch. The winch has a wire length of 2900 meters. When the gravity corer is lifted from the seabed and is brought to deck, the core catcher and core cutter are sampled first, if there are sediments present in them. Then, the plastic liner is taken out, cleaned, cut to 1 meter sections, labeled and stored in a cold room (Fig.3.5.2).



**Figure.3.5.1** Gravity corer on Helmer Hanssen without core catcher and cutter.



**Figure.3.5.2** A 1 meter, labeled section from a gravity core

Some of the cores were split in the lab onboard and sediment samples were taken for extracting gas. Core logs are also prepared. These samples can be used for various types of gas analysis and various other sedimentological analyses.

### **3.6 Single Beam Echo sounder (F)**

Single beam echo sounders are common among all types of ships. Their primary purpose is to estimate the depth of the seafloor. In a single beam echo sounder, a properly designed transducer projects a sound pulse through water in a controlled direction and the reflected wave is received. The depth is calculated from the travel time of the sound pulse. R/V Helmer Hanssen has a keel-mounted Simrad EK 60 single beam echo sounder with transducers at three different frequencies, 18 KHz, 38 KHz and 120 KHz (Fig. 3.6.1). The 18

KHz transducer can be used for depths up to 10 km whereas 38 KHz and 120 KHz can only be used for depths up to 2 km and 500m respectively.

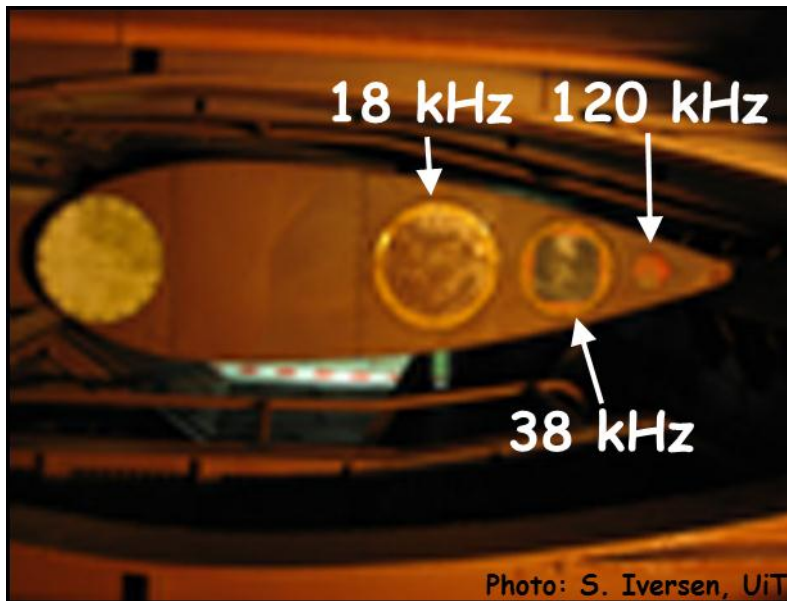


**Figure 3.6.1** Simrad EK60 transducers on the keel of R/V Helmer Hanssen

Other than using it to find the depth of the seafloor, the single beam echosounder is generally used by fishermen to find schools of fishes in the water column. During the cruise, our main aim was to detect gas leakages from the seafloor, since the raising bubbles of gas reflect the sound pulses from echosounder. We used the 18KHz and 38KHz transducers for this purpose.

### 3.7 Gas Sampling (C&A)

Gas from sediments at different depths was collected for further determination of molecular and isotopic composition of hydrocarbon (HC) gases, using “head-space” technique. 40 ml of sediment was taken from each 15-20 cm of the core, according to lithological characteristics, using a syringe. The sediment was put into bottles (120 ml), filled with distilled water (50 ml). Thus, 30 ml of each bottle was left for free gas from the sediment (Fig.3.7.1).

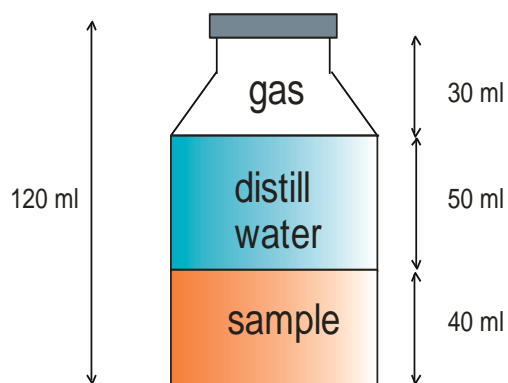


**Figure 3.7.1.** Vial filled with sediment, distilled water and gas

By shaking the bottles, the sediment was mechanically broken to obtain equilibrium in the system “sediment-water-gas”. Afterwards the free gas was collected into 20 ml vials, filled with concentrated salt dissolution (NaCl). The scheme of degassing is shown in Fig. 3.7.2. Collected gas was stored in upturned vials for further analyses in the laboratories of the Department of Petroleum Geology and Geochemistry of the Faculty of Geology of the Moscow State University.

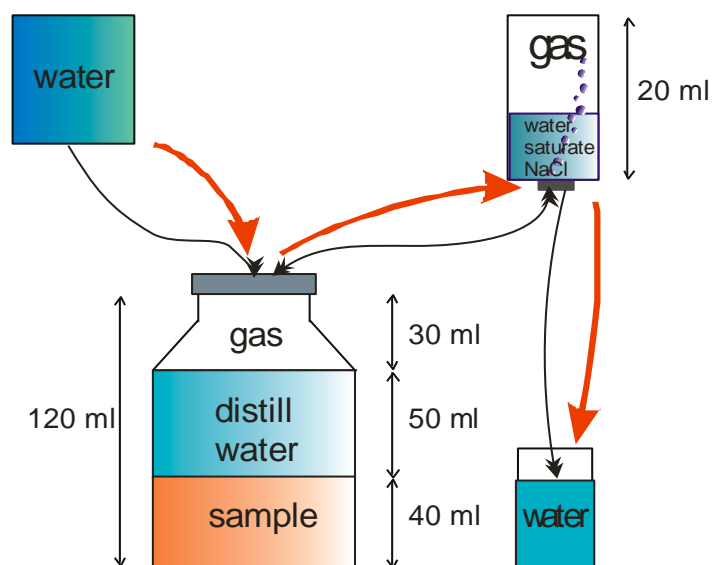


**Figure 3.7.2.** Scheme of sediment degasification and gas conservation

## 4. RESULTS, INTERPRETATION AND DISCUSSION

### 4.1 Bottom Sampling (C&A)

#### *Sampling devices and technique*

Gravity core was used to collect samples of bottom sediments during the cruise HH13KA. Bottom sampling was performed on 9 stations (Fig. 4.1.1). Recovery varied from 256 to 396 cm.

Sediments collected from 5 stations (HH13-105, 106, 109, 110, 112, 113 GC) were cut into 100 cm long sections, packed, labeled, and stored in cool room (5 C °) before transportation to the University of Tromso for further detailed investigations.

Sediments collected from 3 stations (HH13-107, 108, 111 GC) were preliminary studied onboard. Cores were also cut into 100 cm long sections. Each section was split into two halves. One half was used to take photos and for lithological description. The other half of each section was used to collect samples for degasing and more detailed lithological investigations and gas analyses at the Moscow State University.

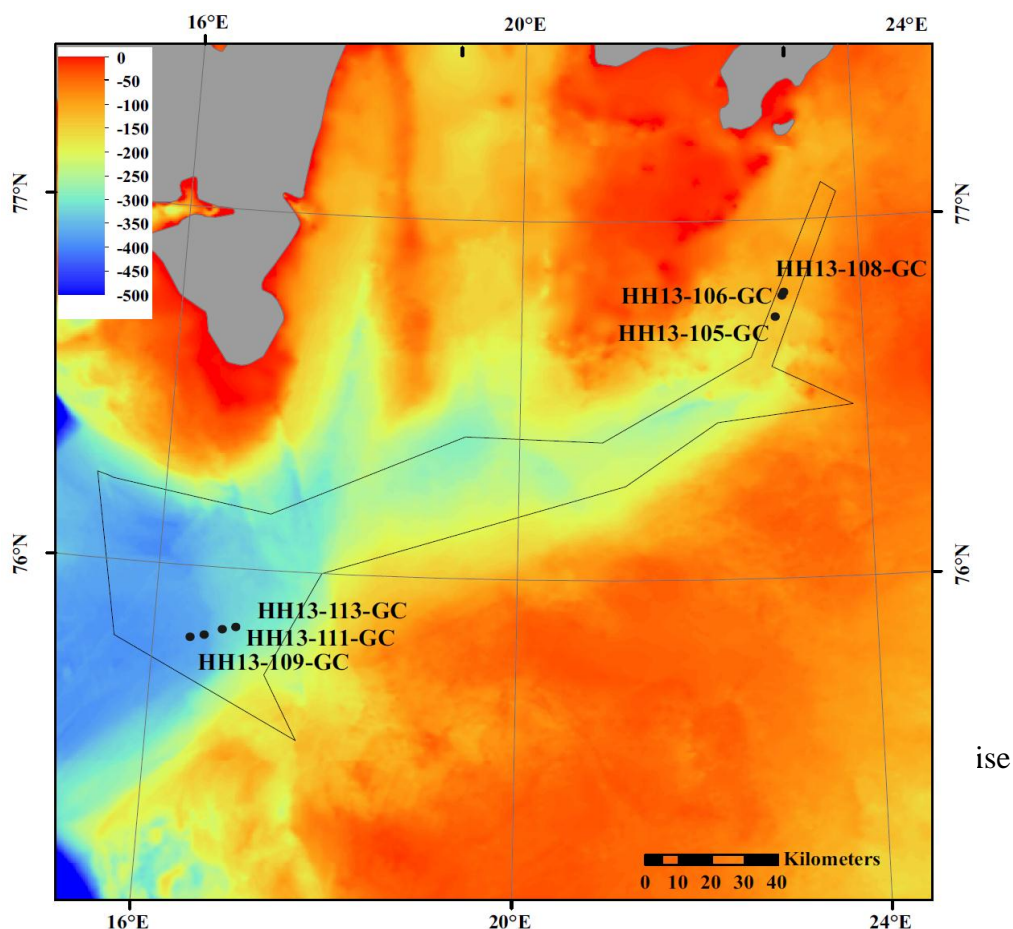


**Figure 4.1.1.** Location of core stations within the study area



Recovery of gravity cores varied slightly from 256 to 364 cm. Cores from stations HH13-105, 106, 109, 110, 112, 113 GC were packed for further analyses at the University of Tromsø.

Cores from HH13-107, 108, 111 stations were opened onboard. Samples for degassing (1 in core logs), grain size analyses (2 in core logs), mCT scanning (3 in core logs). Shells debris and rock clasts were collected (4 and 5 in core logs respectively; table 1).

Samples of sediments (40 ml) for further degassing were collected from each 15-20 cm from different lithological units. Obtained gas is transported to Lomonosov Moscow State University for further investigations, using Gas Chromatography (GC) and Isotope Ratio Mass-Spectrometry (IRMS). From the same intervals sediments for further grain size analyses and determination of mineral composition were collected and put into plastic bags.

From each section undisturbed sediments (10-20 ml) were collected by plastic syringes for further mCT scanning analyses.

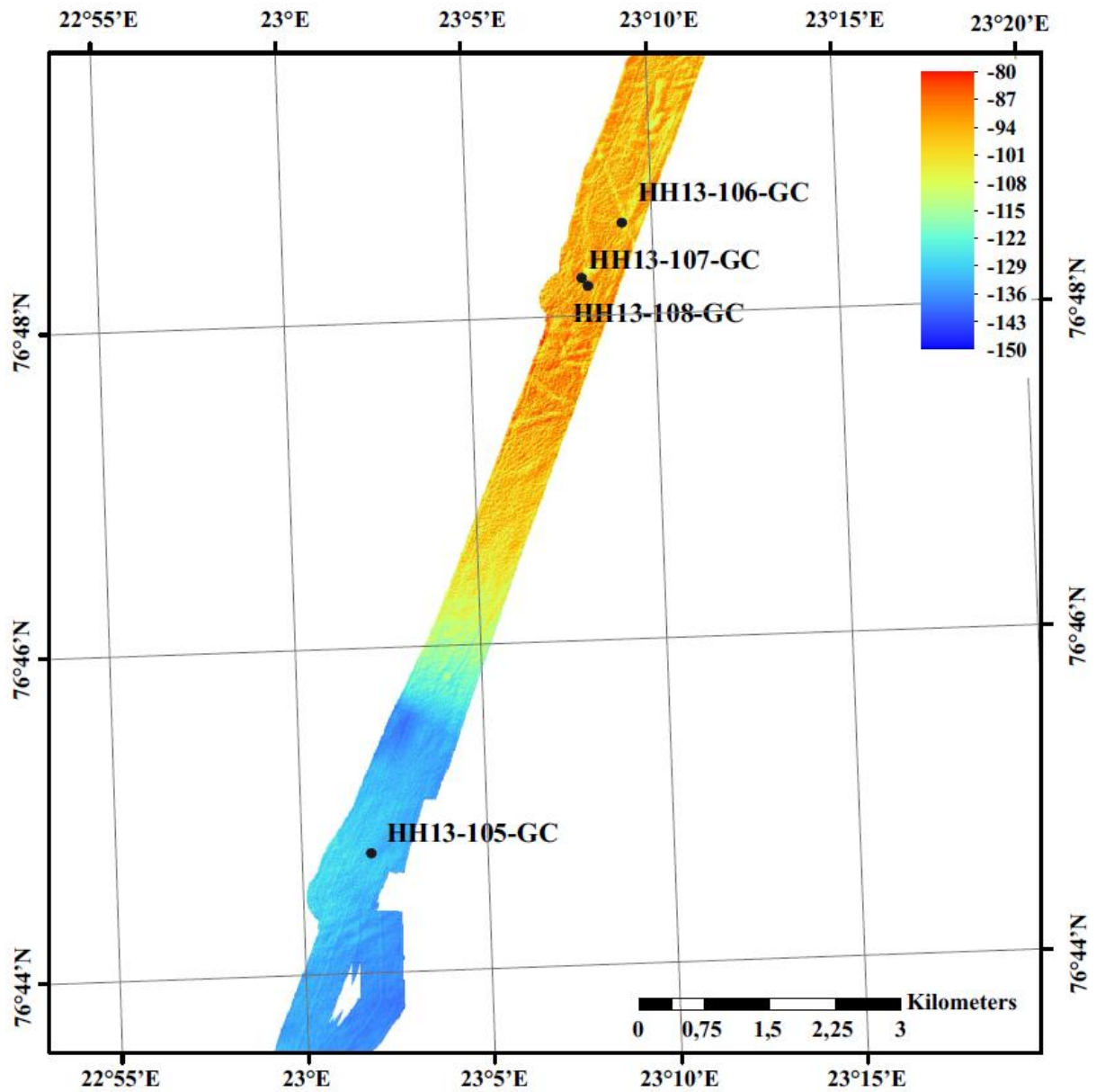
Core station number (recovery)	Section number (length)	Subsampling intervals, cm				
		For degassing	Sediments	For mCT scanning	Rock clasts	Shell debris
HH13-107-GC (256 cm)	1	2-6	2-6	90-100		
		20-24	20-24			
		40	40			
		76	76			
	2	4-8	4-8	61-65		
		27-32	27-32			
		66-70	66-70			
		95-100	95-100			42
	3	7-9	18			
		35-40	45			
HH13-108-GC (297 cm)	1	2-5	2-5	72-75		
		29-34	29-34			
		60-65	60-65			
		94-100	94-100			
	2	4-10	4-10	63-65	9-14	

		42-46	40			40
		88-94	88-94			56
	3	4-8	4-8	51-55		
		26-32	26-32			
		62-68	62-68			
		79-84	79-84			
HH13-111-GC (372 cm)	1	10-18	20	96-100		
		35-40	45			
		51-55	51-55			
		95-90	80			
	2	16-20	16-20			
		37-44	30			45
		65-70	75			
		92-96	92-96			
	3	1-9	1-9	54-59		
		47-54	40			
		72-80	90			100
	4	8-13	20			
		30-36	30-36			
		52-57	60			

**Table 1.** List of subsampling for further analyses at the Moscow State University

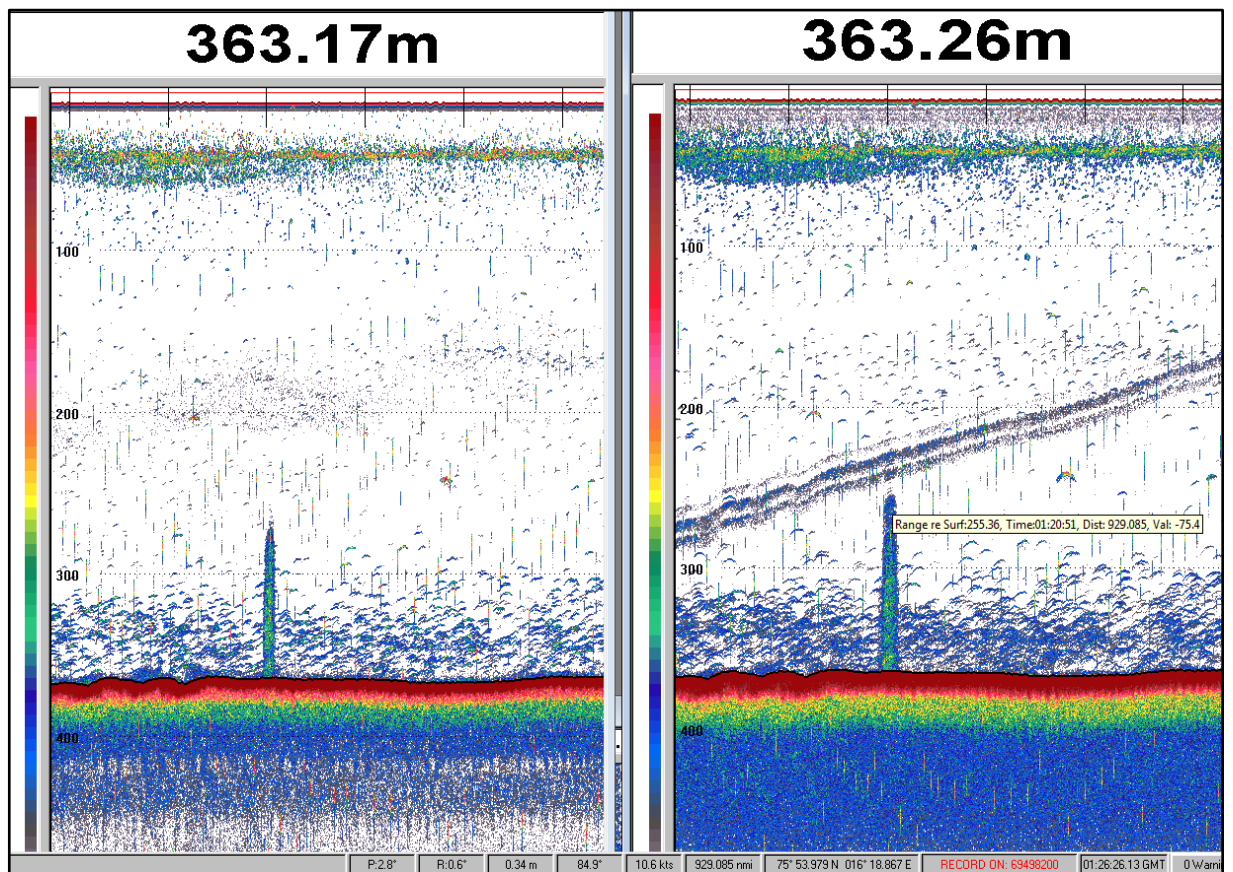
*Preliminary results*Sampling stations HH13-105GC, HH13-106GC, HH13-107GC, HH13-108GC

The gravity cores were taken from the Storfjordbanken area (Fig.4.1.2).





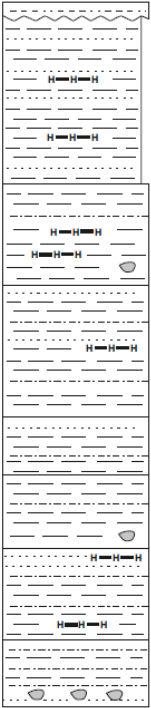
**Figure 4.1.2.** Core stations location within Storfjordbanken area

A ridge was mapped, using multibeam. One station (HH13-105 GC) was taken from the sea plain at the foot of the ridge, another station (HH13-106 GC) collected upper sediments of the ridge. Stations HH13-107 GC and HH13-108 GC are located in the area of gas flares, observed on the echo sounder record (Fig.4.1.3).



**Figure 4.1.3.** Gas flares on echo sounder record (Storfjordbanken area)

Cores from stations *HH13-107 GC*, *HH13-108 GC* were opened and subsampled onboard. Second, undisturbed half of each section was packed and transported to the University of Tromsø for further detailed investigations. Detailed descriptions of core logs *HH13-107 GC* and *HH13-108 GC* are presented on figures 4.1.4 and 4.1.5 respectively.

R/V Helmer Hanssen Cruise HH13 Geo3144-8144 CORE 107 GC							
<b>Location:</b> Storfjordbanken		<b>Date:</b> 23.07.2013					
<b>Latitude:</b> 76°48.246 N	<b>Recovery:</b> 256 cm						
<b>Longitude:</b> 23°08.347 E							
<b>Water Depth:</b> 109 m							
Depth, cm	LITHOLOGY				Colour	Section	Samples
	Photo	Grain size Cl Sil F SM SC S Gr	Description				
0			SILTY CLAY: 0-4.5 cm. Liquefied, soupy, water saturated, structureless, with minor silty admixture. The lower boundary of the interval is sharp and irregular.		olive brown	1	1,2
50			CLAY: 4.5-66 cm. More consolidated than the overlying interval, with interlayers and spots of hydrotroilite, with sandy interlayers from 2 to 10 mm thick at 12, 25 34, 40, 56 cm. Lower boundary of the interval is obscure and planar.		dark olive grey		1,2
100			SILTY CLAY: 66-102 cm. Consolidated, stiff, planar laminated, with interlayers and spots of hydrotroilite. At 95 cm rock clast 0.1-0.2 cm in size was observed. Lower boundary of the interval is gradual and planar.		dark olive grey		1,2
150			SILTY CLAY: 102-150 cm. Consolidated, stiff, planar laminated, with interlayers of sandy clay with hydrotroilite. Interlayers of olive grey colour are observed. Lower boundary of the interval is obscure and planar.		dark olive grey	2	1,2
200			SILTY CLAY: 150-171 cm. Consolidated, stiff, with larger silty admixture, with sandy interlayer at 155 cm. Lower boundary of the interval is sharp and planar.		dark olive grey		1,2
250			SILTY CLAY: 171-200 cm. Consolidated, stiff. At 97 cm rock clast 3x2 cm ion size was found. Lower boundary of the interval is sharp and planar.		dark brownish grey	3	1,2
			SILTY CLAY: 200-230 cm. Consolidated, with sandy admixture, with planar interlayers of hydrotroilite. Upper 5 cm contain sandy interlayer with hydrotroilite Lower boundary of the interval is sharp and planar.		brownish grey		1,2
			SILTY CLAY: 230-256 cm. Consolidated, with sandy admixture (up to 20%). Many rock clasts 0.5 cm in size are observed at lower 10cm.		dark grey		1,2

**Figure 4.1.4.** Core log of HH12-107 CG



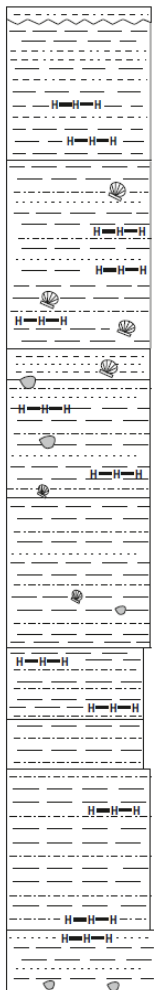
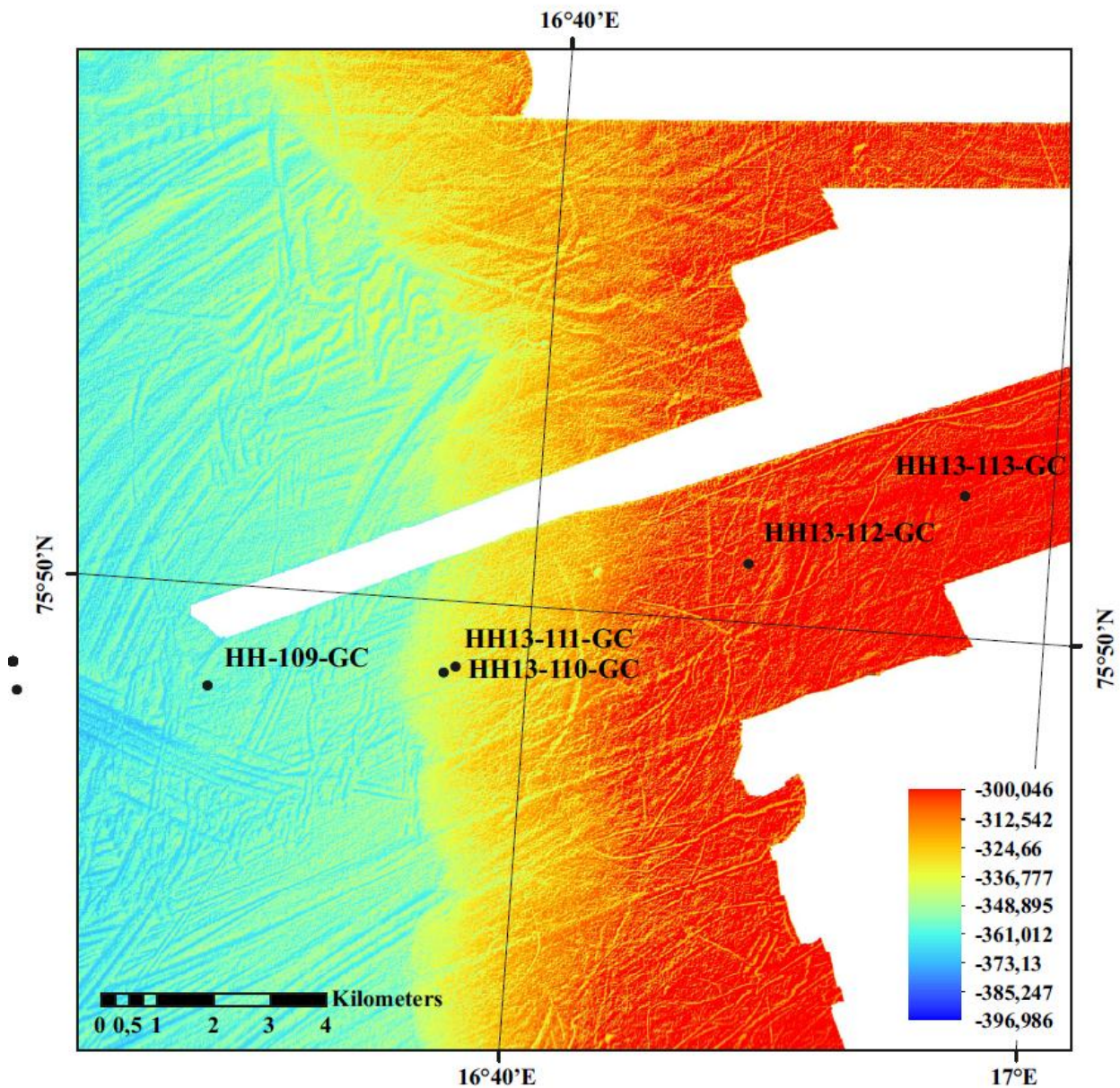
R/V Helmer Hanssen Cruise HH13 Geo3144-8144		CORE 108 GC					
<b>Location:</b> Storfjordbanken <b>Latitude:</b> 76°48.269 N <b>Longitude:</b> 23°08.331 E <b>Water Depth:</b> 109 m		<b>Date:</b> 23.07.2013 <b>Recovery:</b> 297 cm					
Depth, cm	LITHOLOGY				Color	Section	Samples
	Photo	Grain size Cl Silt FMSMSCSGr	Description				
0			SILTY CLAY: 0-4 cm. Liquefied, soupy, water saturated, structureless, oxidized, soft. The lower boundary of the interval is sharp and irregular.	olive brown	1	1,2	
50			SILTY CLAY: 4-45 cm. More consolidated than the overlaying interval, planar laminated, with interlayers and patches of hydrotroilite in the lower part of the interval (25-45cm). In the interval 12-14 soft interlayers with larger amount of silty material (up to 15%) are present. At 5 and 25 cm oxidized brownish tube worms debris (1 mm in size) are present. At 42 cm black tube worms with maximum size of 4 cm were found. Lower boundary of the interval is gradual and planar.	dark olive grey		1,2	
100			SILTY CLAY: 45-100 cm. With sandy admixture (up to 15%) and hydrotroilite interlayers. In the interval 55-56 cm interlayer with larger amount of silty and sandy material is found. Shell debris up to 5 mm in size are spread within interval. Lower boundary of the interval is sharp and planar.	dark olive grey		1,2 3	
150			SILTY CLAY: 100-109 cm. More consolidated, less water saturated than the overlaying interval, with sandy admixture (up to 10%). At 107 cm shell debris were found. Rock clast 5x4 cm size is present in the bottom part of the layer. Lower boundary of the interval is obscure, planar.	dark grey		1,2 5	
200			SILTY CLAY: 109-143 cm. Water saturated, with 10% of sandy and 20% of silt material, with patches of hydrotroilite. At 128 cm a layer with rock clasts up to 2 cm in size is observed. In the lower part of the interval shell debris are present. Lower boundary of the interval is gradual, planar.	olive grey		2	2,4 1 4 3
250			SILTY CLAY: 143-187cm. More consolidated, less water saturated, with sandy admixture (up to 10%). At 175 cm shell debris and tube worms are present. Interval 175-179 cm is characterized by presence of rock clasts up to 4 cm in diameter. Lower boundary of the interval is sharp and planar.	brownish olive grey			1,2
			CLAY: 187-208 cm. Planar laminated with interlayers of hydrotroilite, with silty admixture (about 5%). Lower boundary of the interval is sharp and planar.	brownish grey			1,2
			CLAY: 208-223 cm. Structureless, no hydrotroilite is observed, amount of silty admixture doesn't exceed 5%. Lower boundary of the interval is sharp and planar.	olive grey		3	1,2
			SILTY CLAY: 223-270 cm. With sandy interlayers at 229, 246, 254, 260 and 265 cm, with hydrotroilite patches up to 3 mm in size. In the interval 260-269 cm 2 interlayers of hydrotroilite 1-2 cm thick are present. Lower boundary of the interval is sharp and planar.	brownish grey			1,2 3
			SANDY CLAY: 270-289 cm. More consolidated, than the overlaying interval, massive. In the lower part of interval rock clasts up to 0.5 cm in size are present.	dark olive grey			1,2

Figure 4.1.5. Core log of HH12-108 CG

Sampling stations HH13-109GC, HH13-110GC, HH13-111GC, HH13-112GC, HH13-113GC

The gravity cores were taken from the Storfjordrenna area (Fig. 4.1.6).



**Figure 4.1.6.** Core stations location within Storfjordrenna area

A ridge was mapped using multibeam in the Storfjordrenna area. Core station HH13-109GC is located within the sea plain at the foot of the ridge. Two cores (HH13-112GC, HH13-113GC) collected upper sediments of the ridge. Stations HH13-110 GC, HH13-111GC are located in the area of large gas flares, well observed on the echo sounder record (Fig. 4.1.6).

Core HH13-110 GC was not exactly collected from the gas flare location. So it was not opened onboard. The core was packed for further investigations in the University of Tromsø.

Core HH13-111 GC collected sediments from the gas flare area (Fig.4.1.7). It was opened onboard, described, subsampled (Fig.4.1.8).

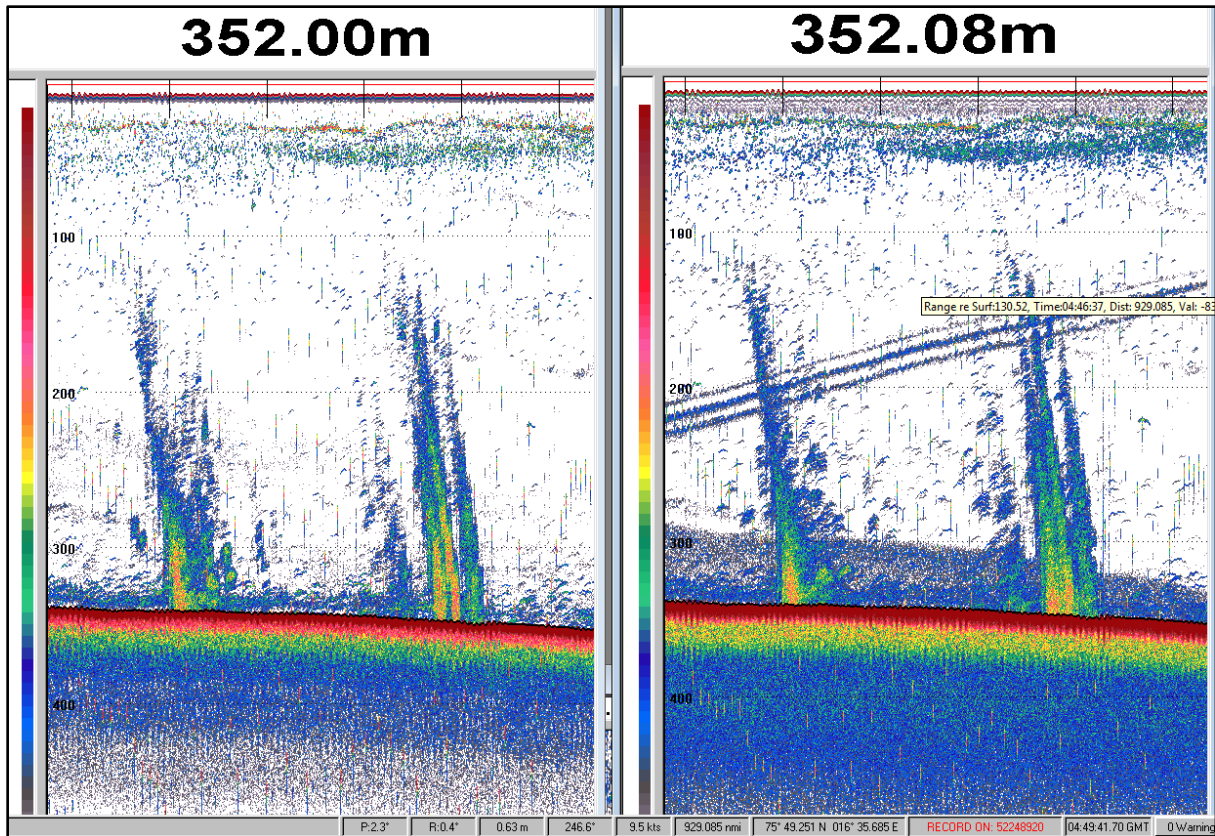


**Figure 4.1.7.** Gas flares on echo sounder record (Storfjordrenna area).





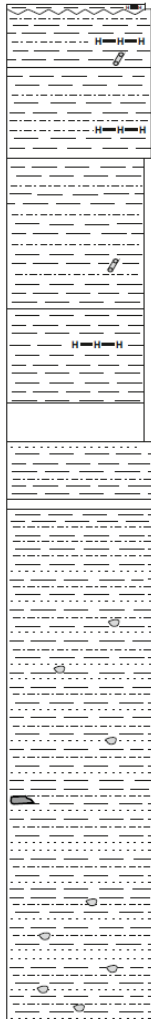
R/V Helmer Hanssen Cruise HH13 Geo3144-8144 CORE 111 GC								
<b>Location:</b> Storfjordbanken <b>Latitude:</b> 75°49.423 N <b>Longitude:</b> 16°37.160 E <b>Water Depth:</b> 349 m		<b>Date:</b> 24.07.2013 <b>Recovery:</b> 372 cm						
LITHOLOGY						Color	Section	Samples
Depth, cm	Photo	Grain size Cl Silt FMSMCSGr	Description					
0			CLAY: 0-2 cm. Soft, creamy, with rare patches of hydrotroilite. Lower boundary of the interval is gradual, irregular.	black	1	1		
50			SILTY CLAY: 2-22 cm. Soft, creamy, with rare patches of hydrotroilite and black tube worms. Silty admixture is about 5%. Lower boundary of the interval is obscure, irregular.	dark olive grey		2		
			SILTY CLAY: 22-55 cm. More consolidated than the overlaying interval, dense, structureless, with larger amount of silty material (about 10%), with rare patches of hydrotroilite. Lower boundary of the interval is sharp, planar.	dark olive grey		1		
			CLAY: 55-111 cm. Soft, creamy, structureless. At 98 cm a tube worm is present. Lower boundary of the interval is gradual, planar.	dark grey		2		
100							3	
			CLAY: 111-145 cm. More consolidated than overlaying interval, with unclear structure, with rare patches of hydrotroilite.	very dark grey	2	1		
150			SILTY SANDY CLAY: 145-160 cm. In this interval sediment is almost absent. According to the material left on the walls, the interval is characterized by larger amount of sandy material.			2		
						1		
						2		
200								1
								1
250							3	2
						1		
						3		
						1		
300							4	2
				4				
				1				
				2				
350						1		
						2		

Figure 4.1.8. Core log of HH13-111 GC

## 4.2 Lineations and elongated features (G&E)

### Results:

#### *Lineations*

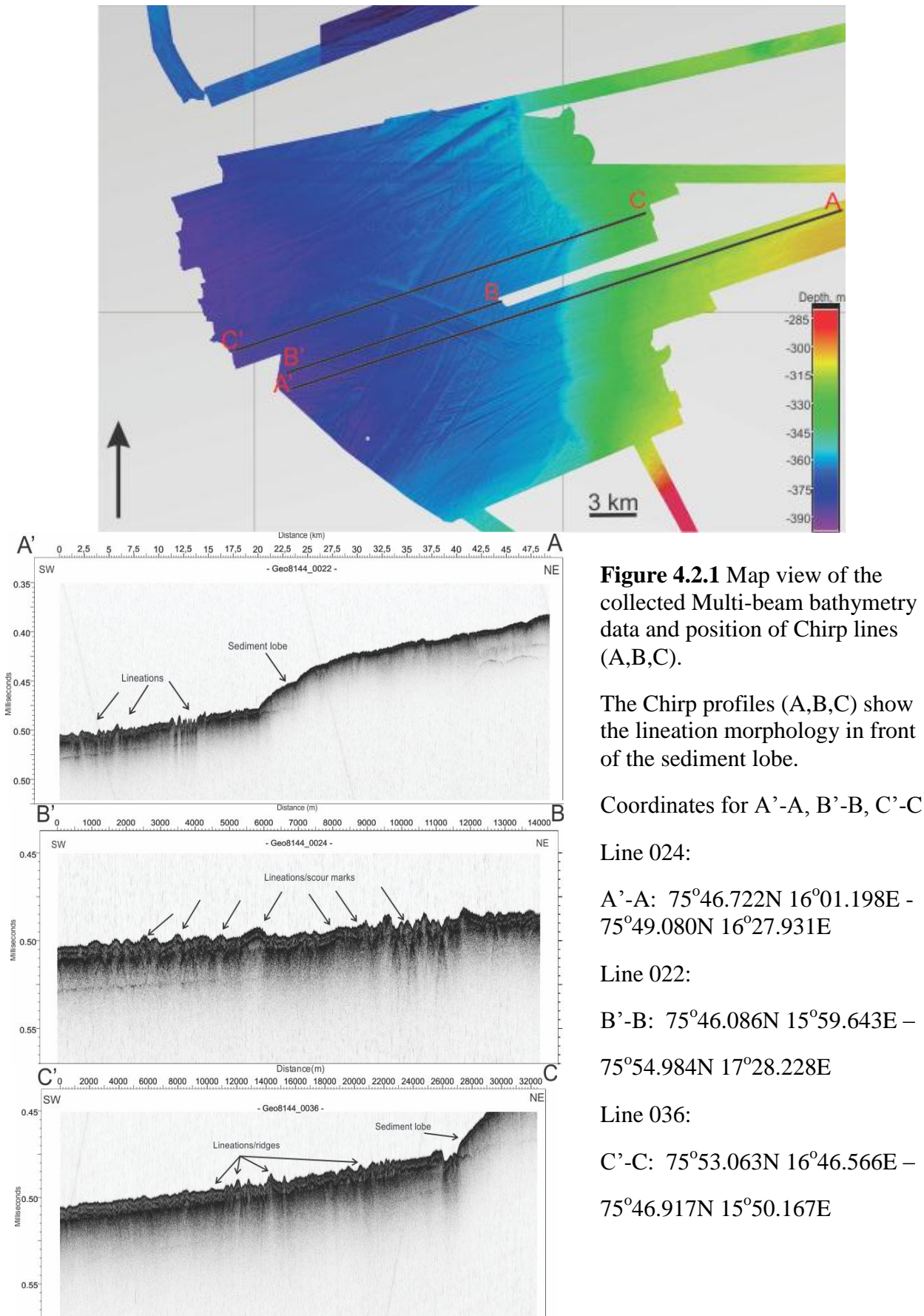
Several lineations and streamlined features were observed on multi-beam swath bathymetry data and on Chirp profiles on the Storfjordrenna seabed. These features produce a relief on the otherwise smooth seabed.

The lineations appear as elongated taper-off parallel to sub-parallel ridges and troughs that varies in width from 30-200 m, 5-10 km in length and heights/depths from 5 to maximum 11 m (see figure 4.2.1). On the Chirp profiles (see figure 4.2.1) the lineations look like single peak- and -trough topography. These large-scale features show several different orientations. We observe mainly four dominant directions: NE-SW, E-W, N/NE-S/SW and W/NW-E/SE (See figure 4.2.2. Arrows represent the different orientations of the lineations). We identify 5 zones that each has a dominant orientation and character of the lineations (see figure 4.2.3):

- Zone 1 – fanning out NE-SW oriented lineations, lengths from 7 to 10 km, depths/heights from 6 m up to 13 m.
- Zone 2 – approximately 6 km wide with N/NE-S/SW oriented lineations. Lateral ridges at the margins of the zone with weaker lineation of 2 to 4 m height/depth. Parallel to this zone are 6 km long lineations that are more pronounced and greater heights (10-15 m).
- Zone 3 – 1.5 km wide zone with W/NW-E/SE oriented lineations that are very sharp and 5-6 m in height/depth. The lineations are very continuous, parallel and approximately the same dimension. This zone also has lateral ridges at the margins.
- Zone 4 – E/W oriented lineations 2-3 m deep/high.
- Zone 5 – NE-SW weaker and high wavelength oriented lineations from 1 up to 4 m high/deep. Some lineations are narrower and deeper (<5 m).

The lineation directions cross each other, suggesting that they were not all formed during the same time. Towards the northeast the lineation structures weaken under a cover of sediment. This unit is interpreted to be sediment lobes which are a part of the proglacial system in front of the grounding zone wedges observed further up in the trough (*ch. 4.5*), and they strongly affected by iceberg ploughing. Ploughmarks also occur below the sediment

lobes in the trough itself. The ploughmarks will be discussed in more detail in *chapter 4.3 – Iceberg plough marks*.



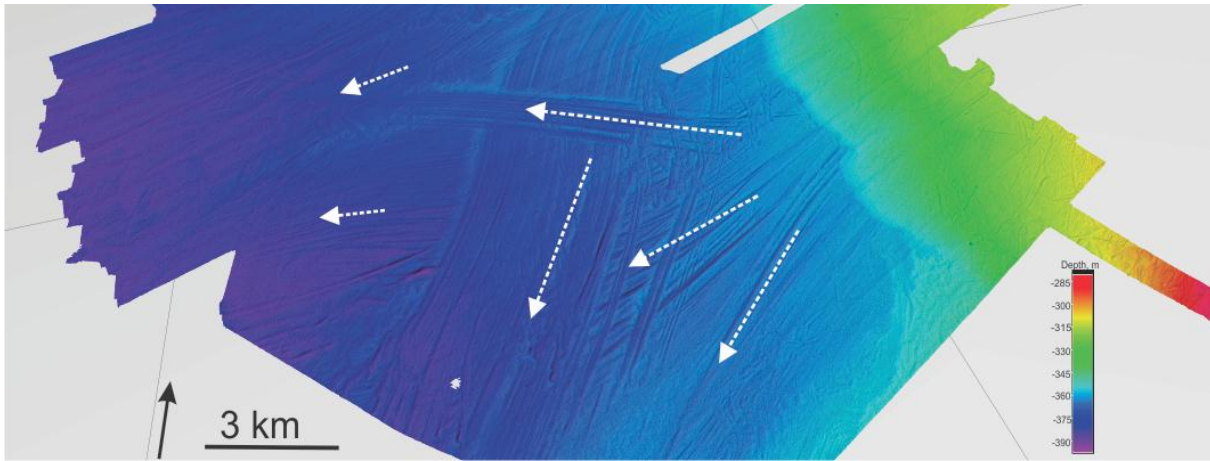


**Figure 4.2.2** Arrows indicating the orientation of the lineations in Storfjordrenna.

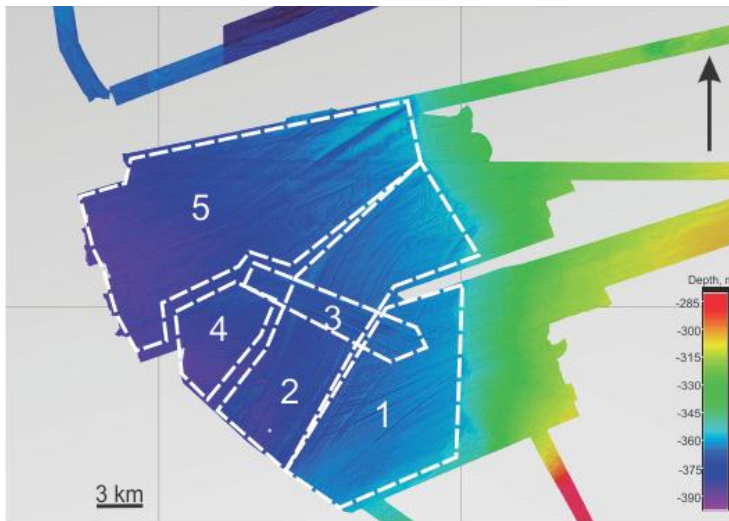


**Figure 4.2.3** The study area divided into Zone 1 to 5.

### *Elongated ridges*

Elongated ridges were also observed on the swath bathymetry and Chirp of line015 (see figure 4.2.4a and b). The ridges were oriented in a NE-SW direction and measured 5-6 m in height, 100-150 km in width and around 2 to 2.5 km in length. A profile (see figure 4.2.4c) across the long axis of one of the ridges revealed a weak asymmetric morphology of these features, with a slightly steeper stoss side towards the NE and a gentle SW-oriented lee side.

### **Interpretation and discussion:**

The glacial lineations have been described by Dowdeswell et al. (2008;2010a) and Andreassen & Winsborrow (2009) as Mega-Scale Glacial Lineations (MSGs); *a series of streamlined curvilinear ridges of length as much as tens of kilometers, amplitudes of a few meters, and wavelengths of tens to a few hundred meters (Dowdeswell et al. 2010a)*. These features form due to deformation of soft sediment at the base of fast-flowing ice streams, and

can be used to indicate palaeo-flow direction (*Ottesen et al. 2005*). Similar features have been found in fjords and cross-shelf troughs in Bjørnøyrenna, on the Norwegian and Svalbard shelf, and the Greenland shelf just to name a few. These evidences suggest the existence of ice streams draining the large ice sheets through the major cross shelf troughs, like Storfjordrenna in our case.

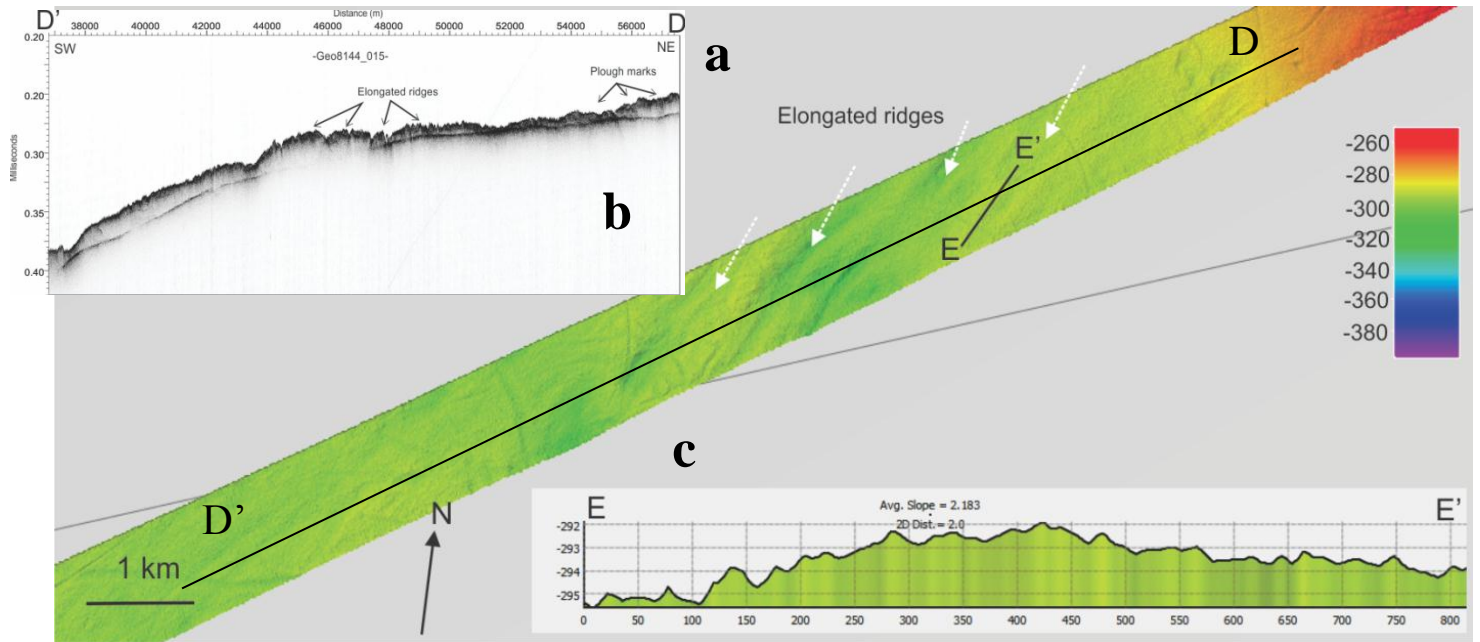


**Figure 4.2.4** a) Multi-beam bathymetry over the elongated ridges (indicated with white arrows). b) Chirp profile (D) over the ridges. c) Fledermaus profile (E) across one of the asymmetric elongated ridges (stoss side on the left and lee side on the right).

As previously mentioned the different orientations of the MSGLs suggest that they were formed during different glacial settings. The character of the lineations is also different. Some are deeper and sharper, whilst others are weaker and shallower. In figure 4.2.2 above, we have indicated the different orientations with arrows. The MSGLs oriented NE-SW and E-W (Zone 1 and 4) seem to be in connection because they spread out towards the mouth of the Storfjordrenna as a fan, and therefore interpreted to be formed under the same ice stream at the same time. These lineations are superimposed by the lineations in Zone 2, 3 and 5 with a different orientation, so we suggest that the NE-SW oriented MSGLs are the oldest. However, the different character of the lineations in zone 2 and 3 cause us to believe that they were not formed under the same setting as the MSGLs in zone 1 and 4. This is due to their sharp and continuous character in a channelized and relatively narrow zone, and the fact that they have eroded into the seabed sediments to a larger degree than the lineations we have interpreted to be MSGLs. Findings from the studies of Jakobsson et al. (2011;2012) from the Pine Island Bay in West-Antarctica, and Dowdeswell et al. (2010b) from Greenland leads us to believe

that the lineations in zone 2 and 3 can have been formed by mega-raft multi-keel icebergs with keels as deep as 300-400 m (*for more details see ch. 4.4*). The lineation features in zone 5 are weaker (long wavelength, small amplitude) and seem to be superimposed on the lineations in the 4 remaining zones, suggesting that they are younger. These lineations are also interpreted to be MSGs, whereas the narrower and deeper lineations in this zone are interpreted to be iceberg ploughmarks.

Since we have no age control in this area so far, we only suggest relative ages of the lineations. The order of formation of the lineations we have suggested is, from oldest to youngest: Zone 1 and 4 (Last Glacial Maximum?), zone 2, zone 3 (Deglaciation?) and zone 5.

The plough marks in Storfjordrenna are observed to disturb the morphology of the lineations, which suggests that they may have formed after the lineations, but from single keel icebergs, not the huge mega-icebergs that we suggested to have produced the plough marks in zone 2 and 3.

Regarding the elongated ridges, it is difficult to say exactly what formed these features due to limited data in the area. However, we believe they are subglacial streamlined landforms which have been observed to be formed under ice sheets where ice is streaming (*Dowdeswell et al. 2010b*). The asymmetric profile over some of the ridges may indicate that they are drumlin or craig-and-tail landforms, but due to the limited data in the area, it is equally plausible that they are MSGs (long wavelength, small amplitude). In the case they are drumlin landforms they support the theory from i.e. Dowdeswell et al. (2010a) of ice draining through Storfjordrenna towards the southwestern shelf margin.

### **4.3 Iceberg plough marks (D)**

Using a combination of multibeam and chirp data-sets we were able to identify a proglacial system, previously unmapped, in the lower section of the Storfjordrenna. Here we note the appearance of several iceberg ploughmarks of varying sizes and patterns (Figure 4.3.1); ranging from single keel ploughmarks and furrows to large multi-keel ploughmarks lineations. We interpreted these features as iceberg ploughmarks and not megascale glacial lineations as they show the 'typical' characteristics of iceberg scouring in this area. The characteristics for iceberg ploughmarks are often that of relatively shallow (1-10m deep) curvilinear furrows and V- or U-shaped cross profiles, showing either a random or a preferred orientation and are often found in shallow bank areas or in water depths up to 450m in the Barents Sea (Polyak, 1997; Andreassen et al., 2008).

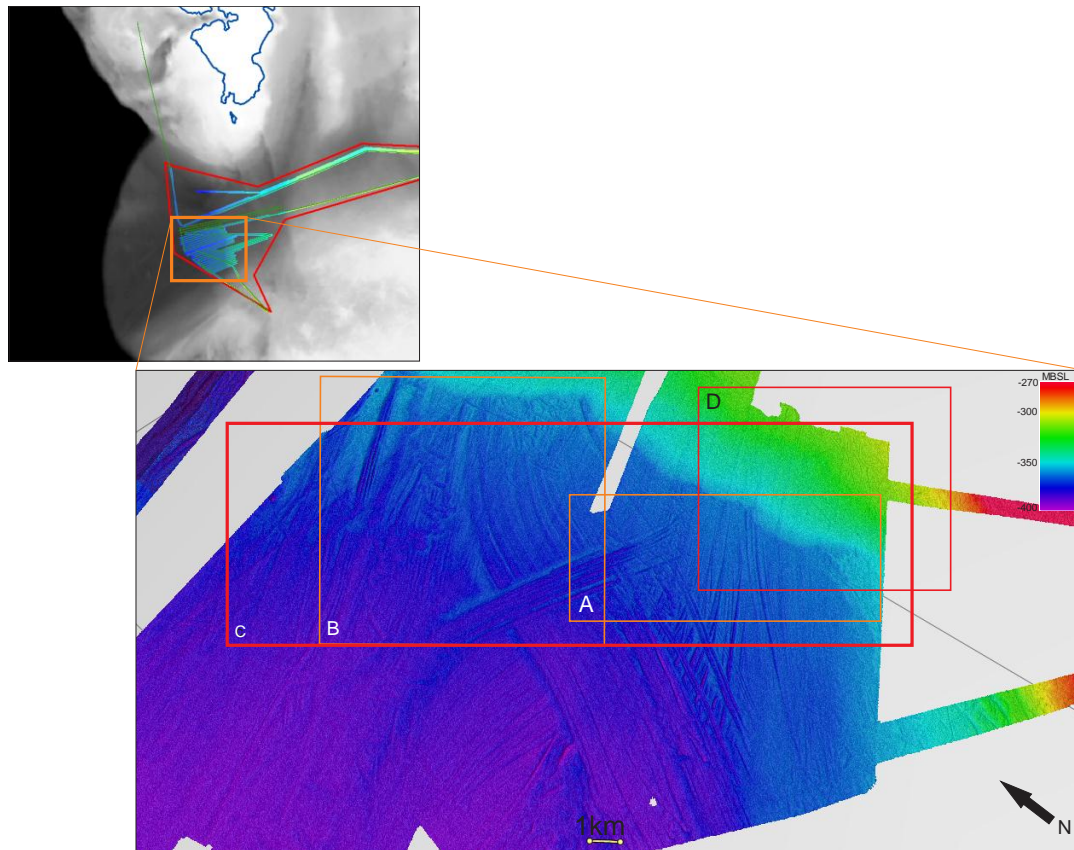


**Figure 4.3.1.** Overview map of study area showing large iceberg ploughmarks. Colour scale represents metres below sea level.

Several previous studies have suggested that following the LGM, Storfjordrenna began to deglaciate and retreat further onshore (Rasmussen et al., 2007; Jessen et al., 2010; R  ther et al., 2011). Thus, it is not surprising to find a vast amount of iceberg ploughmarks at the front of this former grounding zone wedge. In particular, since icebergs are produced at the marine margins of glaciers, ice streams and ice streams (Dowdeswell & Bamber, 2007; Andreassen et al., 2008). The size and depths of the iceberg keels are controlled by several factors, such as ice thickness at the grounding line, creep thinning and rate of melting/freezing at the base of the ice front (Dowdeswell & Bamber, 2007).

In our study site there are two main types of iceberg ploughmarks identified: randomly arranged single keel ploughmarks on the grounding zone wedge and several larger multi-keel ploughmarks on the proglacial section. Also, in figure 4.3.2 C there is clear evidence of cross cutting by the iceberg ploughmarks. This indicates that there must have been several iceberg discharge events into this area, with the youngest discharge event overlaying several of the older iceberg discharge events. The iceberg ploughmarks present in this area show very different orientations, widths and depths, and vary throughout the study area. In particular, there is a large difference between the ploughmarks present in the proglacial section and those

present on the grounding zone wedges. Thus, this study area was subdivided into four smaller zones (Figure 4.3.1).

### **Zone A – Evidence for multi-keel iceberg ploughmarks**

Multi-keel icebergs are characterised by a set of very clear and deep furrows that are subdivided by several levees on the underside of the iceberg. When these large icebergs calve off the ice margin they will leave a large imprint on the sea floor, which can often contain up to 12 scour marks per ploughmark.

In our study area we have found at least three major multi-keel iceberg ploughmark imprints (figure 4.3.2). Imprint 1 show that the icebergs must have flowed in a SE-NW direction. However, the initiation for this feature is a little unclear as the multi-keel ploughmarks only initiate around 4 km from the grounding zone lobe. A possible explanation for this is that there was a slight sea level rise (or an increase in the influence of water between the ice-bed interface). Thus, causing the ice margin to partly float, creating a large instability at the ice front. This could be marked by the irregular iceberg scour marks prior the initiation of imprint 1, which is indicative of a complete iceberg detachment (from the ice margin).

Both multi-keel iceberg ploughmark imprints 2 and 3 show a straight forward and ‘conventional’ initiation. However, due to these features being so linear and following a specific flow orientation it is likely that there may have been some extensive packed sea ice surrounding these large icebergs. Thus, causing them to move in a specific orientation and preventing the iceberg to move in a randomised orientation.

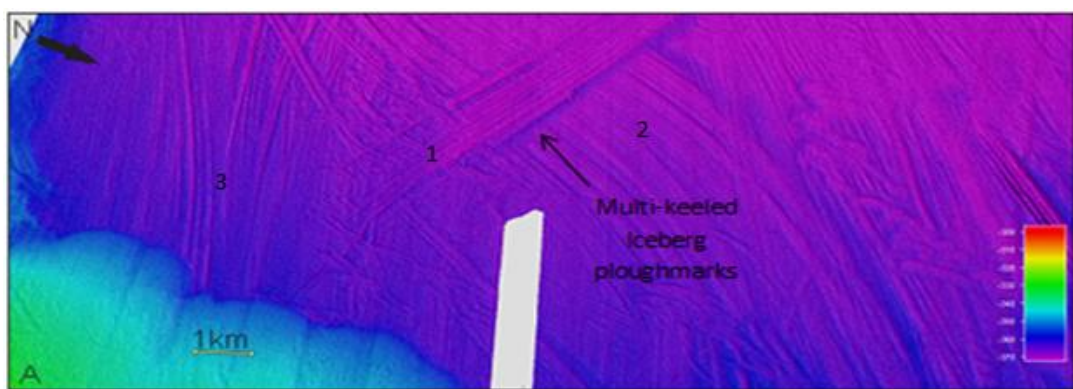


**Figure 4.3.2.** Evidence for multi-keeled iceberg ploughmarks. Colour scale represents metres below sea level.



### **Zone B – Potential corrugated ridges**

During the multibeam data analysis for this study area we noticed that there were some possible corrugated ridges, or washboard ploughmarks (Figure 4.3.3; figure 4.3.4; figure 4.3.5). These features are often associated with both tidal regimes and the presence of an ice shelf (Graham et al., 2013). These features are formed by the movement of the ice when it moves forward and experiences a lifting and lowering effect on the ice mass. Thus, forming several corrugations/washboard ploughmarks imprints on the seafloor. Whilst these features are commonly found in the Antarctic palaeo-ice shelf beds, they are not as commonly found in the Arctic (Graham et al., 2013). In particular there are currently no leading studies supporting the existence of an ice shelf in this region.

The cross profile for these features shows that there are several ridges (figure 4.3.5), indicating the possibility that the ice margin was largely affected by the tidal movements. We decided to not consider the possibility of there being an ice shelf in this region, because if there was a presence of an ice shelf, a larger proportion of this region would be covered in corrugated ridges. It is also important to note that some of the ridges presented in figure 4.3.5 may be artefacts and not actual glacial geomorphological features.

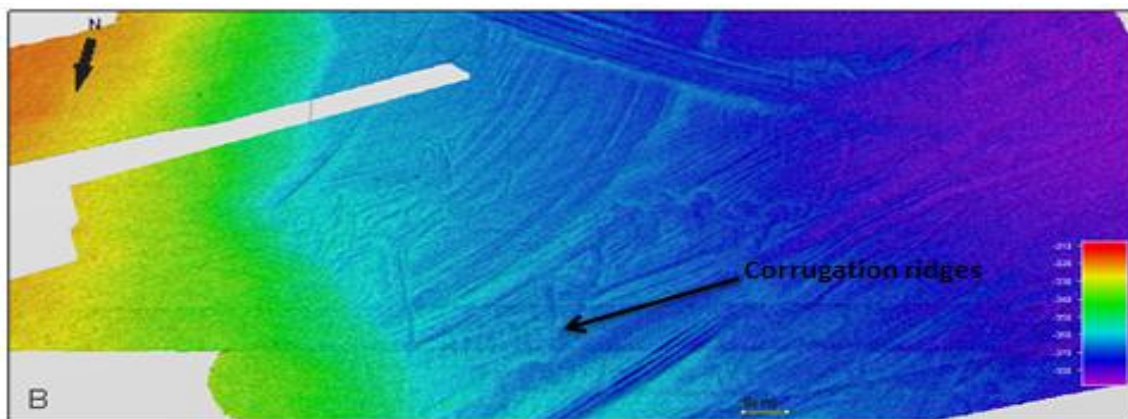


**Figure 4.3.3.** Evidence supporting potential corrugated ridges. Also, see Figure 4.3.5 for cross profile.

### **Zone C – Cross cutting of iceberg ploughmarks/ corrugated ridges**

In this study area, there is clear evidence suggesting that there were several iceberg discharge events (figure 4.3.4). Cross-cutting of the iceberg ploughmarks is quite obvious as the three main events (Figure 4.3.4; D1; D2; D3) all show flowed in different orientations. This can be indicative of three different glacial events, or a rapid switching of the ice stream discharge. It is likely that imprints D1 was the first to be deposited, followed by the D2 event and then most recently by the D3 event (figure 4.3.4).

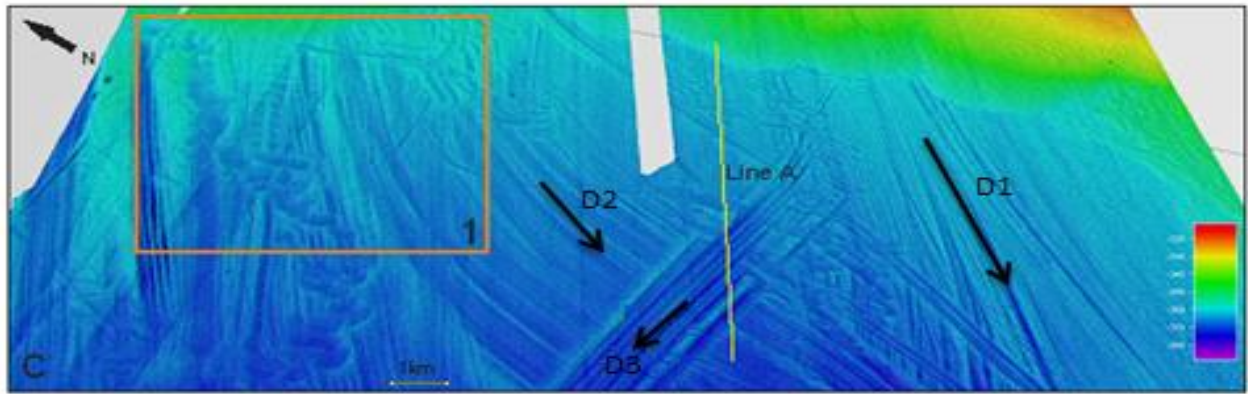


**Figure 4.3.4.** Cross cutting of iceberg ploughmarks. Map C also shows the deposition stages of the iceberg ploughmarks, D1 is the oldest, which is partially buried under D2 and D3 is the youngest. Colour scale represents metres below sea level. For Line A see figure 4.3.6.

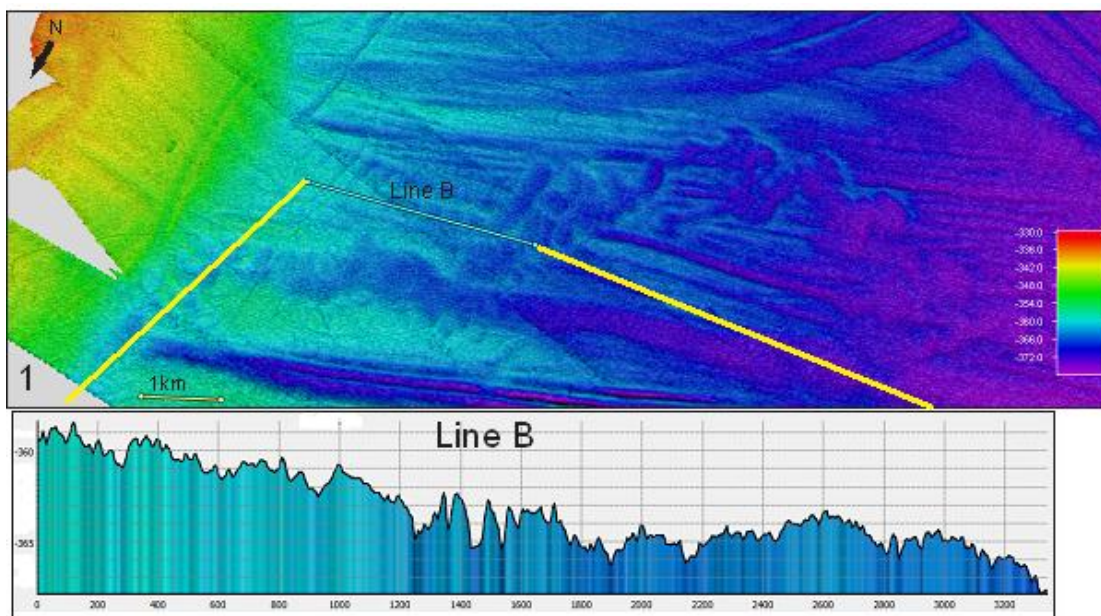


**Figure 4.3.5.** Cross profile of the corrugated ridges made in Fledermaus.

Line A is a chirp profile across the most recent multi-keel iceberg ploughmark and into the grounding zone. The iceberg ploughmarks are clearly visible in this profile suggesting that the icebergs left a deep imprint over this region.

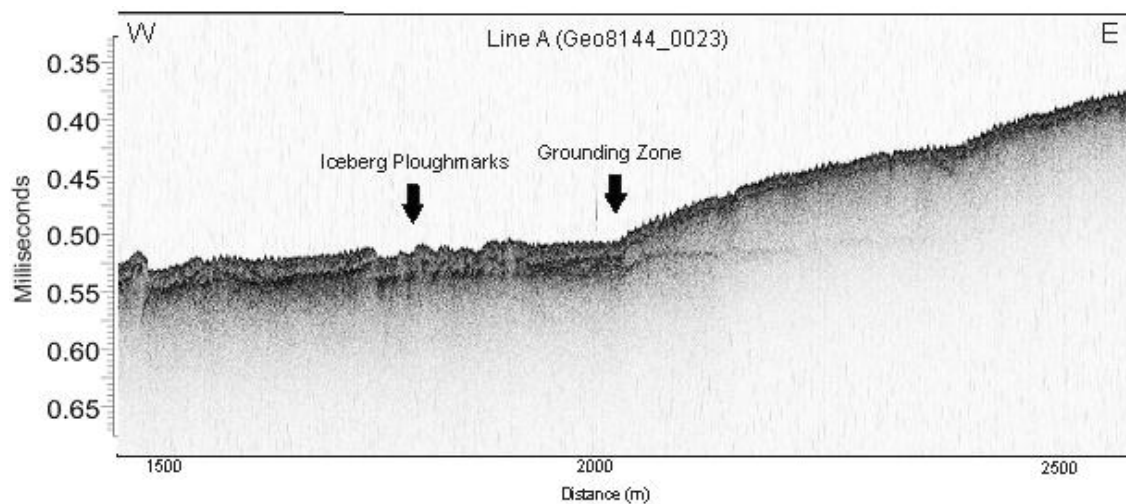


**Figure 4.3.6.** Line A – Chirp profile of the iceberg ploughmarks and grounding zone.

#### **Zone D – Single keel iceberg ploughmarks (figure 4.3.4. D)**

Single keel iceberg ploughmarks often leave ‘relatively’ small and irregular imprints on the sea floor. These icebergs are characterised by their V- or U-shape and often only leave imprints between 2-4 m deep. However, these ploughmarks can leave scours on the sea floor that last for several kilometres (Dowdeswell et al., 2007).

In our study site we found several small irregular ploughmarks, most likely indicative of the single keel iceberg ploughmarks. Many of these ploughmarks ended in an iceberg pit (Figure 4.3.7), which are formed when the iceberg loses energy and as result can become ‘stuck’ on the seafloor. These pits can be identified by a ploughmark line leading into a deeper depression, iceberg pit, which has a thicker berm where the sediment got pushed by the iceberg. It is likely that these icebergs moved into this region post deglaciation as the main evidence for them is located on the grounding zone line. Although, their movement into shallower areas may also be indicative of tidal movements at a later stage.

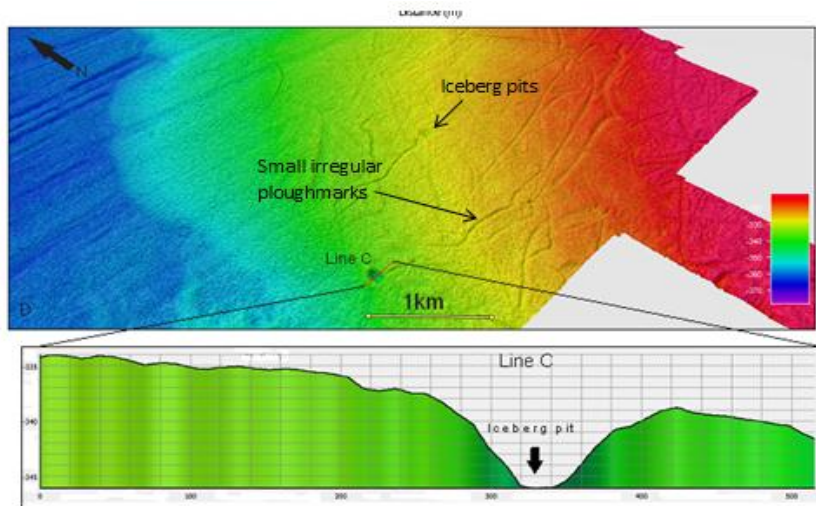


**Figure 4.3.7.** Multibeam image showing the smaller iceberg ploughmarks and their iceberg pits present on the grounding zone wedge, as well as, a profile indicating the depth of the iceberg pit.

#### 4.4 Melt water features (C&A)

Among the most spectacular features of glacial origin are deep, elongated and usually narrow depressions, cut into substratum materials and often completely filled with glacial deposits different from those of the surrounding terrains. Although these depressions in many instances broadly resemble river valleys, they differ from them primarily by greater depths, steeper flanks, inconsistent longitudinal bottom profiles with sections that slope upward in respect to the waterflow direction, and by the infill-sediments which often incorporate tills.

The most plausible origin for these features is subglacial erosion involving channelized outflow of meltwater at the ice/bed interface or direct glacial erosion of substratum strips parallel to the ice flow direction. These two processes can coincide spatially and temporally. They can also substitute one another sequentially, and are often supplemented by glaciotectonic disturbances at the flanks which lead to broadening of the depression. (Piotrowski et al, 1993).

Meltwater channels are erosional products of glacier ablation and meltwater flow close to ice-sheet margins, and consequently their distribution and characteristics may be used to decipher patterns of glacial retreat. Lateral channels flow along the ice margin divided into marginal channels, flowing subaerially, and submarginal channels, which flow at the lateral margin but beneath the ice. Subglacial channels flow at the ice bed.

Orientation of marginal meltwater channels indicates successive positions of palaeomargins, which may thus be drawn parallel to channels. Marginal channels are frequently used to infer cold ice at the margin; under this thermal regime meltwater cannot percolate to englacial or subglacial conduits and is therefore deflected along the lateral ice margins. The orientation of subglacial channels is governed by the disposition of the hydraulic head, which approximates the direction of the steepest ice-surface slope. Subglacial channels can thus indicate ice flow direction close to the terminus, and ice-front margins may therefore be reconstructed orthogonal to these channel systems. Subglacial meltwater channels indicate a warm-based thermal regime. Palaeomargins deduced from the above are reconstructed based on likely configurations with regard to topography and with the assistance (Greenwood et al, 2006).

### **Results, interpretation and discussion**

Melt water channels were identified in the NE part of study area (Fig.4.4.1).

Two types of channels can be subdivided. The first type includes large channels, with depth up to 60 m (fig. 4.4.2 A, B, C) and second – small channels, several meters in depth (fig. 4.4.2A). The small channels are oriented from NE to SW, are characterized by average length of about 2 km, the same orientation is characteristic for large channels, shown on figure 4.4.2 A and B. The length of large channels is about 6 km. These channels form anastomosing networks. Channel, shown on figure 2 C is oriented from E to W.



**Figure 4.4.1.** Research area of melt water channels.

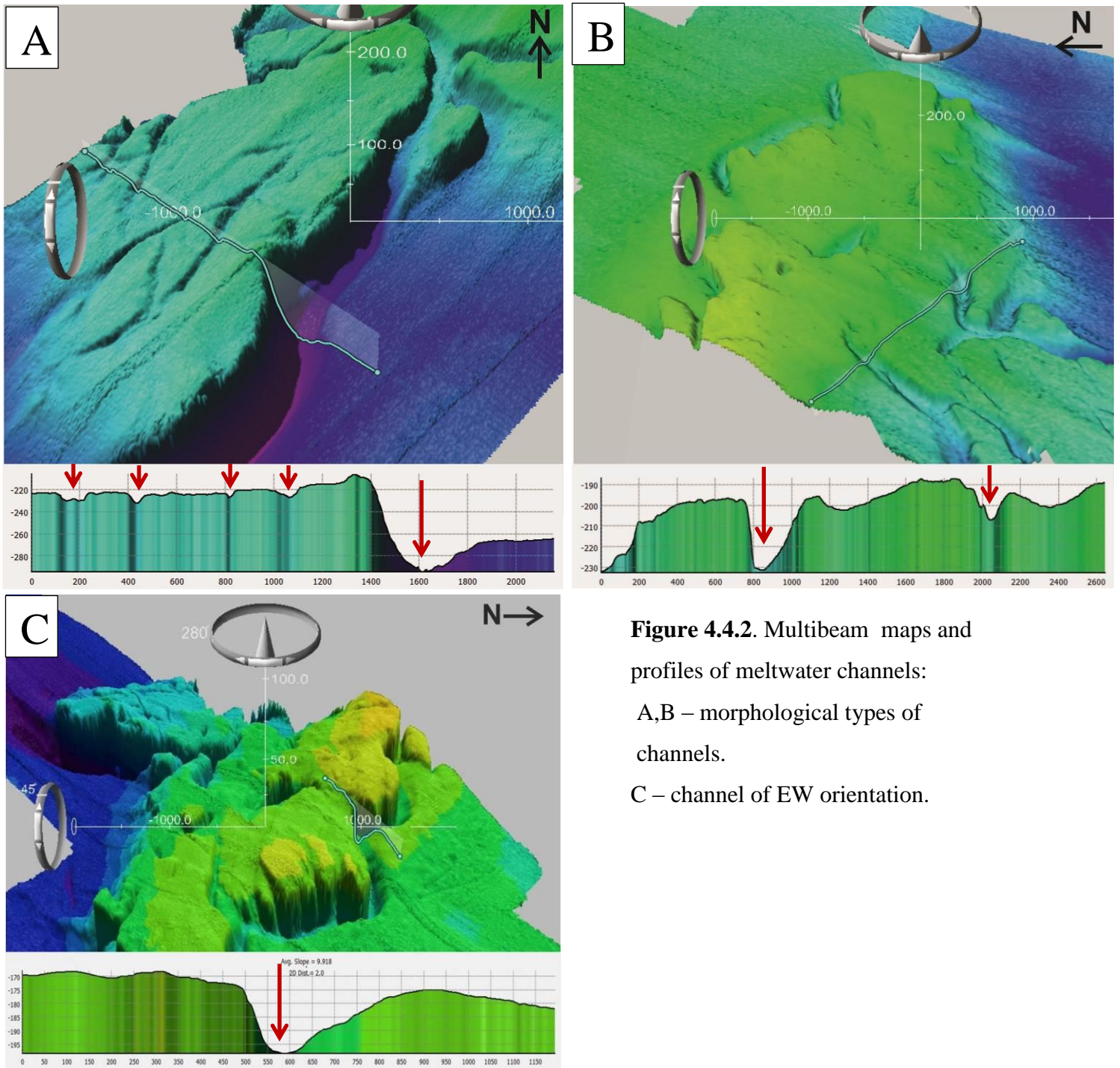


**Figure 4.4.2.** Multibeam maps and profiles of meltwater channels:  
 A,B – morphological types of channels.  
 C – channel of EW orientation.

According to the channels morphology ice sheet moved presumably from NE to SW (Fig.4.4.3). During the surge ice covered stiff sedimentary body. It wasn't completely eroded. Major melt-water flow passed along the sedimentary feature (fig4.4. 3 A). Several channels cut the body. Figure 4 illustrates the channels network and their orientation; channels could cut the stiff sedimentary body due to pressure difference beneath the ice sheet.

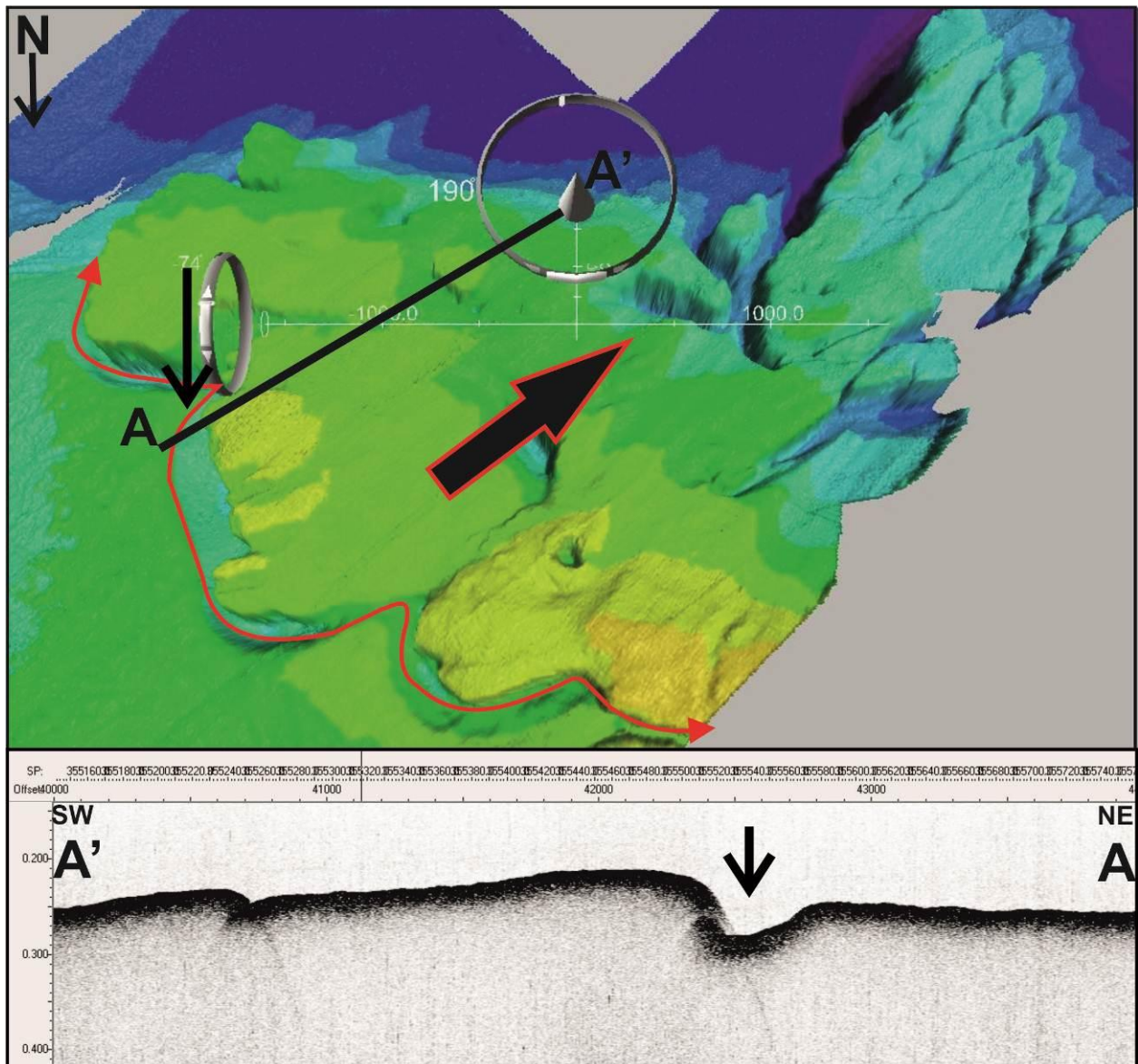


**Figure 4.4.3. A** – Direction of melt water flow (red arrow), direction of ice surge (black arrow).

**B** – Chirp profile along line AA'.

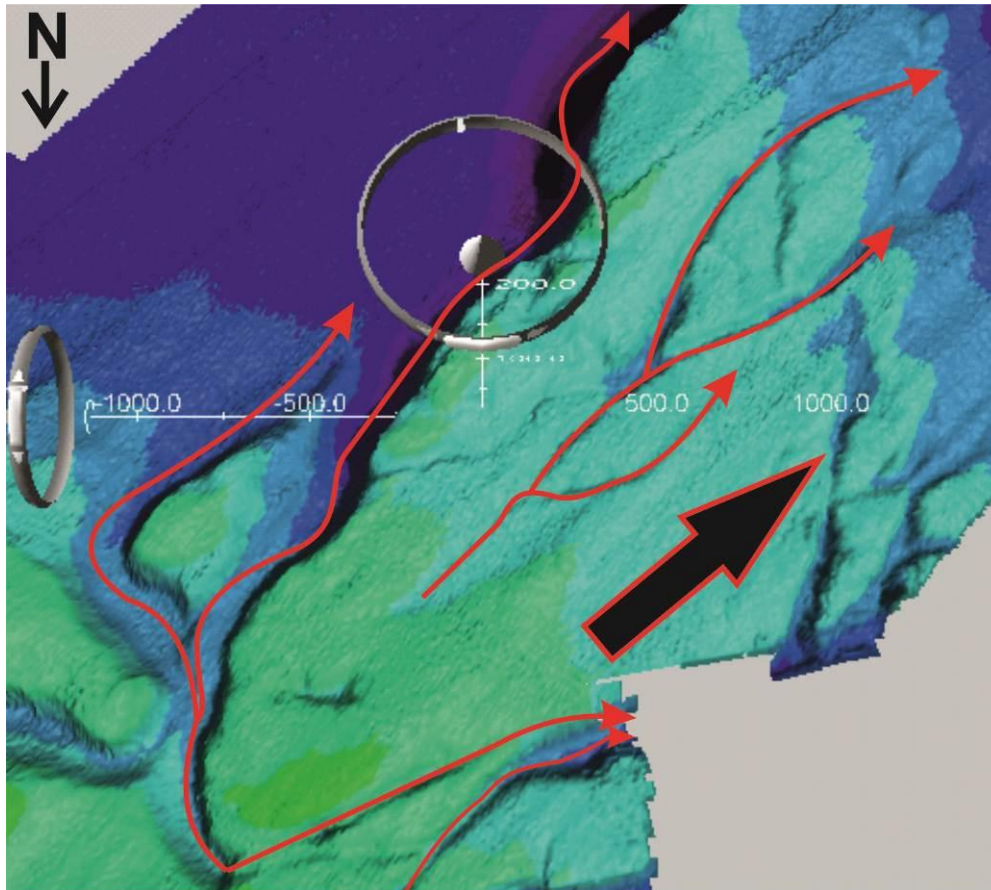


**Figure 4.4.4.** Direction of melt water flow (red arrows), direction of ice surge (black arrow).

#### **4.5 Grounding Zone Wedges and glacier retreat through Storfjordrenna (G&B)**

##### **Results:**

Multi-beam Swath bathymetry data and two seismic lines (10JM-Geo8144-002\_b and 10JM-Geo8144-005, see figure 4.5.1 and 4.5.2) collected during the 2010 cruise reveal a series of large ridge-like features northeast of Storfjordrenna. The ridge features on the two seismic lines show a different character, so we will describe them separately and then do the interpretation together.



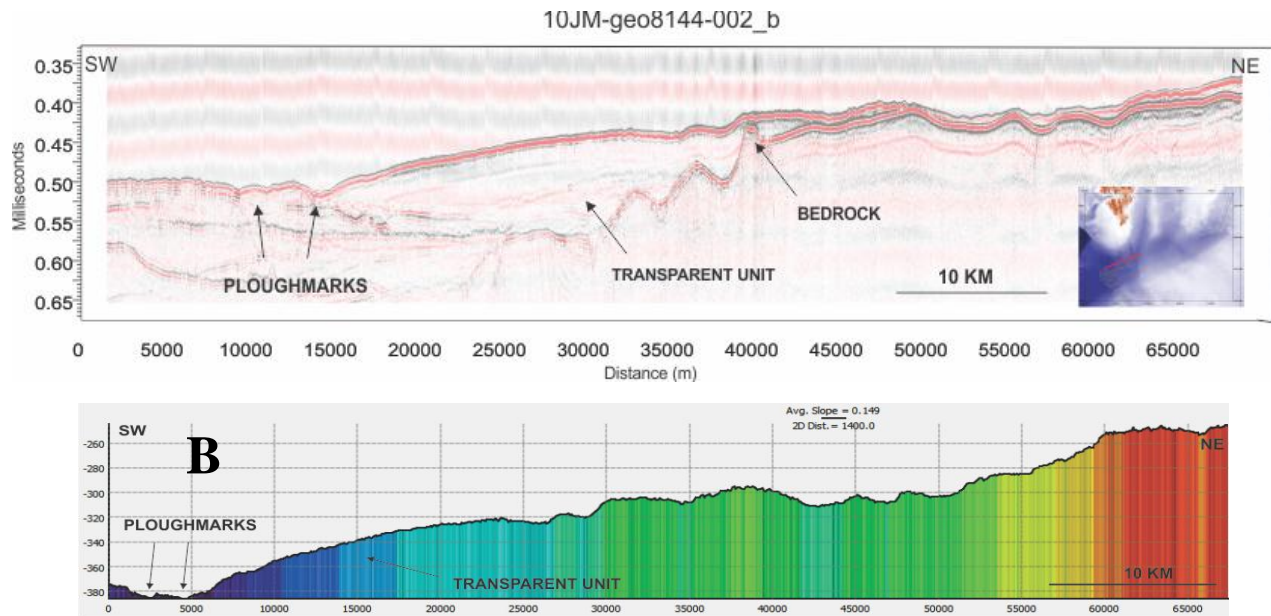


**Figure 4.5.1** A) Seismic line over the mouth of Storfjordrenna. B) Fledermaus profile across the same area in the trough.

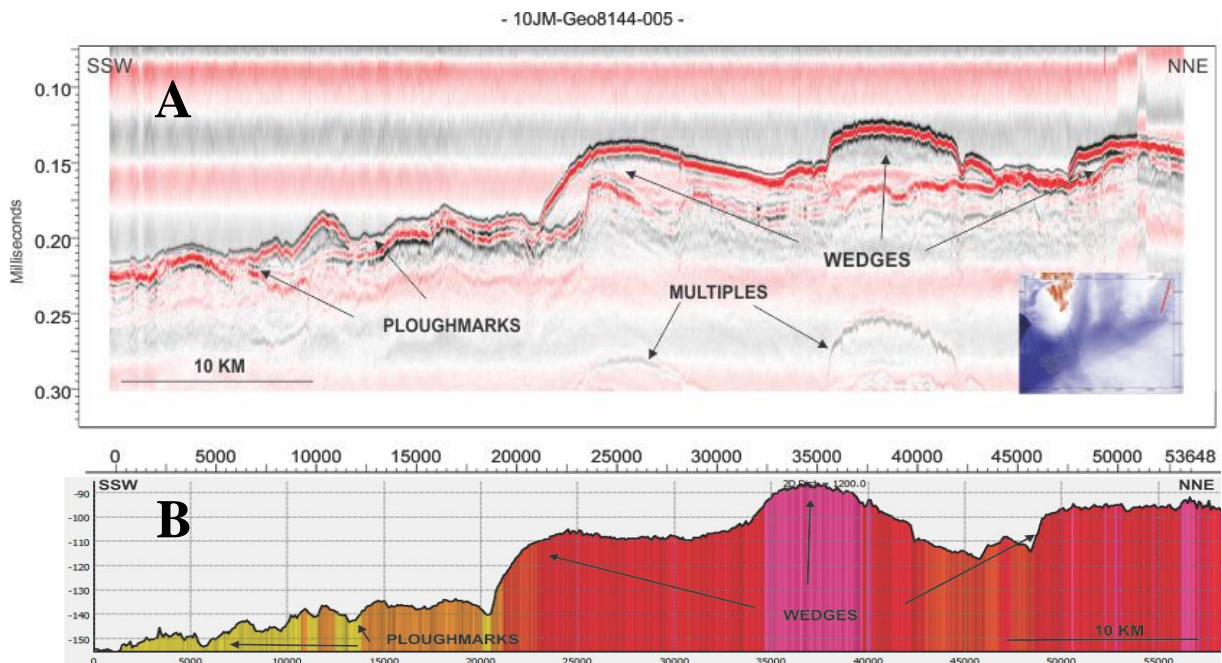


**Figure 4.5.2** A) Seismic line over the northernmost ridges on the Storfjordbanken. B) Fledermaus profile across the same area on Storfjordbanken

*10JM-Geo8144-002\_b*

This seismic line reveals bedrock overlain by an on-lapping lens-shaped transparent sediment unit, approximately 20 km long and 10-15 milliseconds thick (see figure 4.5.1B). The shape of the unit is controlled by the underlying bedrock morphology. On our bathymetric data set and on IBCAO it display like 3 major lobe-shaped sediment packages (see figure 4.5.3 & 4.5.4). However, within the major lobes we also observe a series of smaller lobes. The area in front of the transparent unit is characterized by several small ridges.

*10JM-Geo8144-005*

The seismic show three major ridges that vary in size: lengths from 6-10 km, heights from 15-35 m (see figure). The ridges lie on top of the bedrock below. Also here, the area in front of the ridges shows several smaller ridge structures (see figure 4.5.2 A&B). Both three ridges are similar in morphology, with a steep lee side towards the south/southwest. Due to poor resolution and limited data set in this area, we could not visualize it on the multi-beam swath bathymetry, however, they are visible on the IBCAO bathymetry map (see figure 4.5.4).

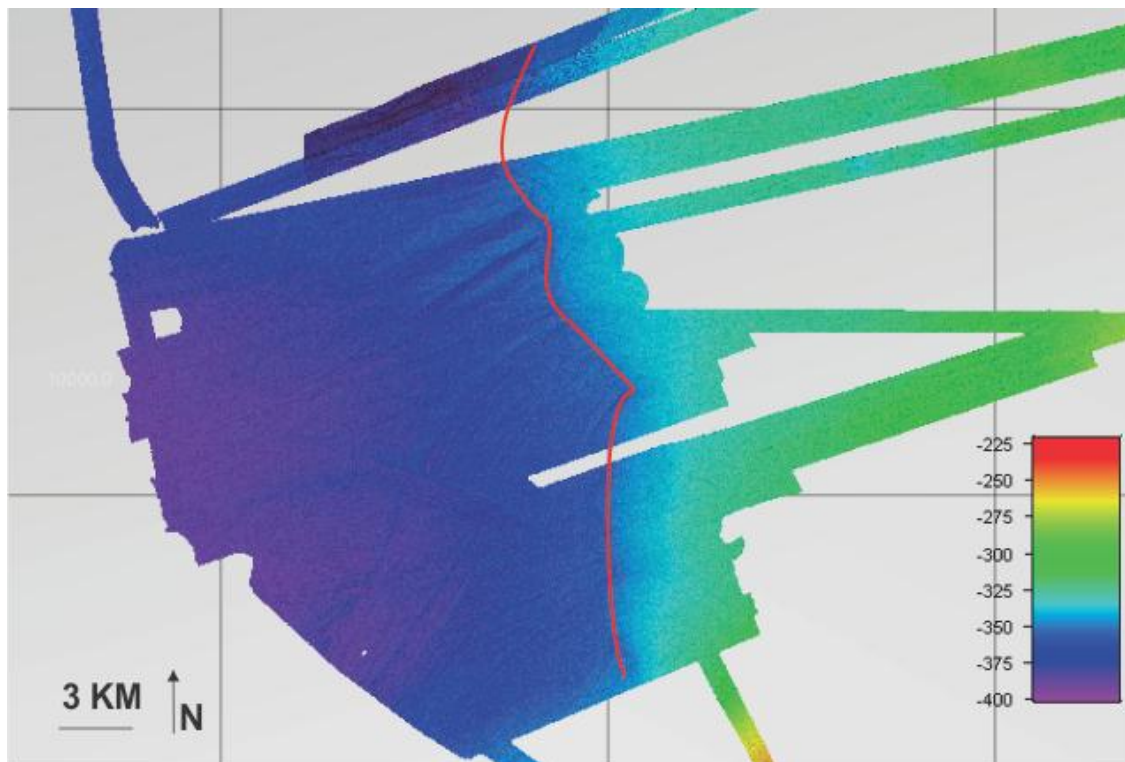


**Figure 4.5.3** Multi-beam Swath Bathymetry of Storfjordrenna. The outline of the lobes is marked with a red line.

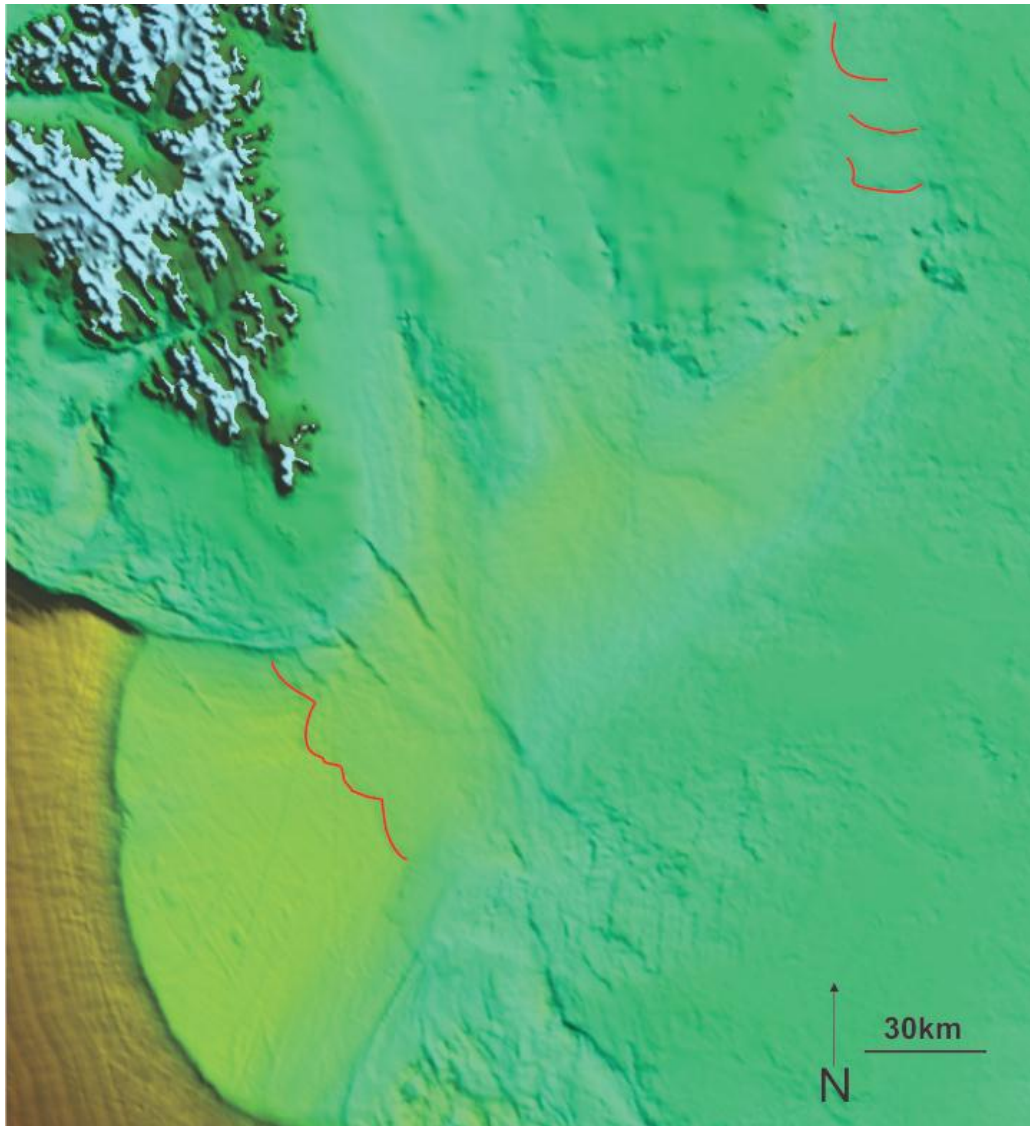


**Figure 4.5.4** IBCAO bathymetry map of Storfjordrenna and Storfjordbanken. Sediment lobes at the trough mouth, and ridges on the bank is marked with a red outline.

#### **Interpretation and discussion:**

The character and morphology of the northernmost ridges (*10JM-Geo8144-005*) suggest that they are Grounding Zone Wedges (GZW) and are often associated with mega-scale glacial lineations (MSGs) (*Dowdeswell et al. 2008*). Similar features have been described from Pine Island Bay, West Antarctica by *Jakobsson et al. (2012)* where they are interpreted to represent grounding line deposits from halts in icestream retreat. *Alley et al. (1989)* also describe modern settings where GZWs occur seaward from icestreams and associated MSGs. Our data set (bathymetry) is not extensive enough to show any possible MSGs in the northernmost area. Large wedges are commonly believed to be formed by subglacial sedimentation and also mass movement deposits in the proglacial part. In our case we have

several smaller ridges in front of, but also on top of the wedges. These are interpreted to be iceberg ploughmarks formed by calved icebergs from the icestream that produced the wedge.

Regarding the sediment unit in the south (*10JM-Geo8144-002\_b*), this is also interpreted to represent a grounding zone wedge, but of a different character than the three northernmost GZWs. The actual wedge shape is difficult for us to visualize with our bathymetric data, but in profile it looks like a lens-shaped, transparent, homogenous deposit of glaciomarine origin. The actual position of the ice front when this wedge was deposited is hard to pin-point. We identified three major lobes on the IBCAO bathymetry map (see figure 4.5.4). This suggests that the icestream depositing this unit most likely had three smaller tributary icestreams converging into the larger one from surrounding smaller troughs on the seafloor. The smaller lobes superimposed on the major ones are interpreted to be mass movement (debris flow) deposits in the distal proglacial setting. The mass movement may have been caused by period of high meltwater-sediment fluxes to the icestream margin (*Streuff, 2012-unpublished*).

As for the glacial retreat through Storfjordrenna, we have used the retreat models from Dowdeswell et al. (2008). This model presents three different types icestream retreat, and compares different submarine features to the retreat rate of the icestream (figure 4.5.5). According to this model retreat of an icestream can be:

- 1) Rapid retreat with formation of MSGLs
- 2) Episodic retreat where GZWs are superimposed on MSGLs
- 3) Slow retreat where retreat moraines are superimposed on MSGLs

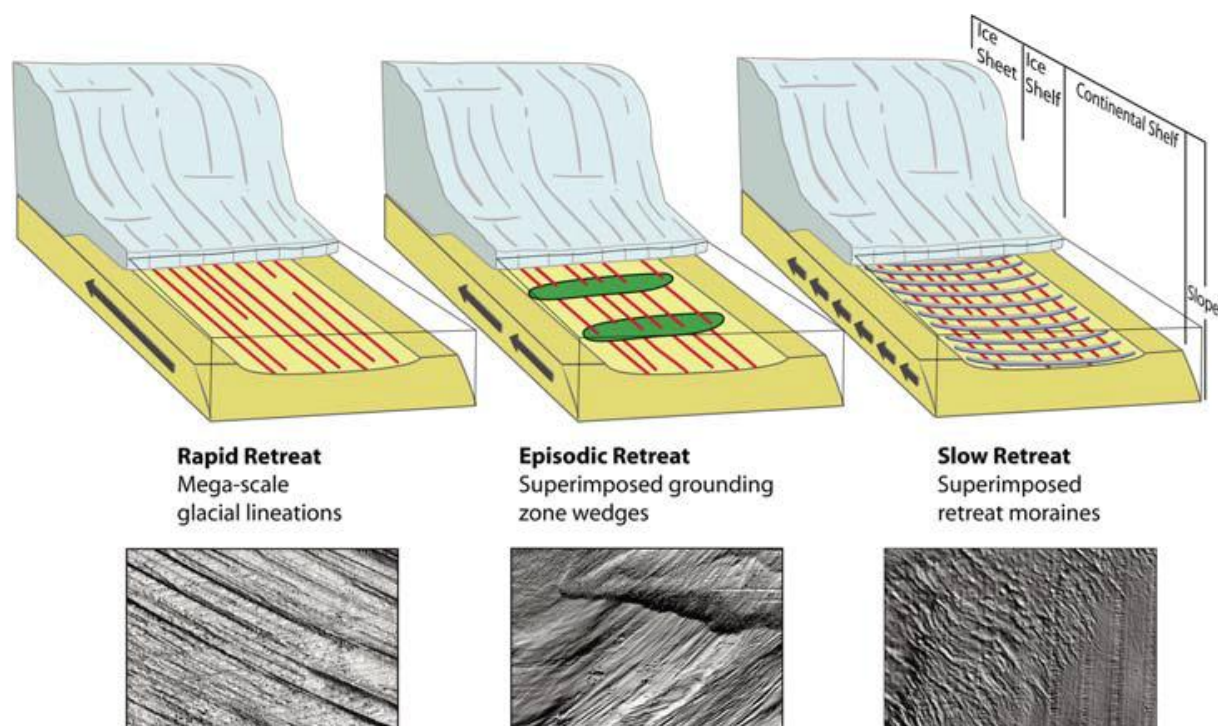


**Figure 4.5.5** Ice stream retreat rate diagram, from Dowdeswell et al. (2008).

Based on the features we have identified in our study area, compared to this model, we suggest that the retreat of the icestream through Storfjordrenna happened *episodically*, because we have formation of GZWs.

During this cruise sediment gravity cores were collected for dating to provide age model for the ice retreat through Storfjordrenna. One of these was taken in front of the northernmost wedges, and will later give us a better perspective on the time frame in which these features were deposited.

#### **4.6 Pockmarks (F)**

Pockmarks are depressions on the seabed resulting from the seepage of gas and pore fluids in soft sediments (King and MacLean, 1970). They are observed in the continental margins of many parts of the world and occur in variety of sizes and shapes (Judd and Hovland, 2007). They are often associated with active gas seepages (e.g., North Sea, NW Svalbard), however pockmarks devoid of active fluid leakage are also observed (e.g., SW Barents Sea). During our cruise, numerous depressions with varying dimensions and shape were detected on the multibeam bathymetry data. Many of these craters are a result of glacier activity, seen by their close association with glacial ploughmarks. Depressions not associated with ploughmarks are also observed and are interpreted as pockmarks. These are described in detail below.

##### *Observations*

Numerous indications of pockmarks are present in the study area (Fig.4.6.1).

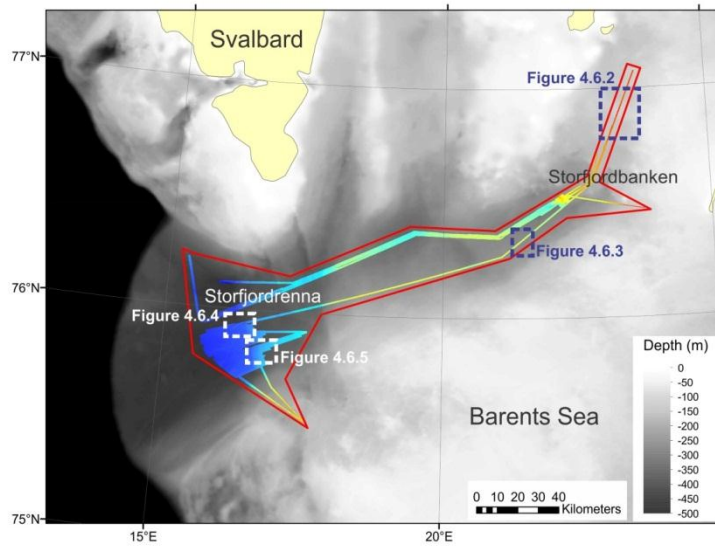


**Figure 4.6.1** Study area (red boundary) with the general bathymetry and acquired swath bathymetry data. Locations of other figures in the chapter are shown.

Storfjordbanken, north eastern part of the study area, show an oval-shaped depression ~200 meter wide and ~4m deep (Fig.4.6.2). Lot of ploughmarks exists in the area and some of them terminate in similar depressions. A chirp line and seismic line was shot across the depression which can be interpreted as a pockmark. Two gravity cores were taken from the pockmark, which is found to be containing gas (Fig.4.6.2B). It was hard to identify any direct indicators of subsurface fluid flow from the seismic or chirp data (Fig.4.6.2C, D). However, the seismic show a wedge of sediments on which the pockmark is located. The penetration of gravity cores (Chapter 4.1) and the samples from it indicate presence of soft sediments in the wedge.

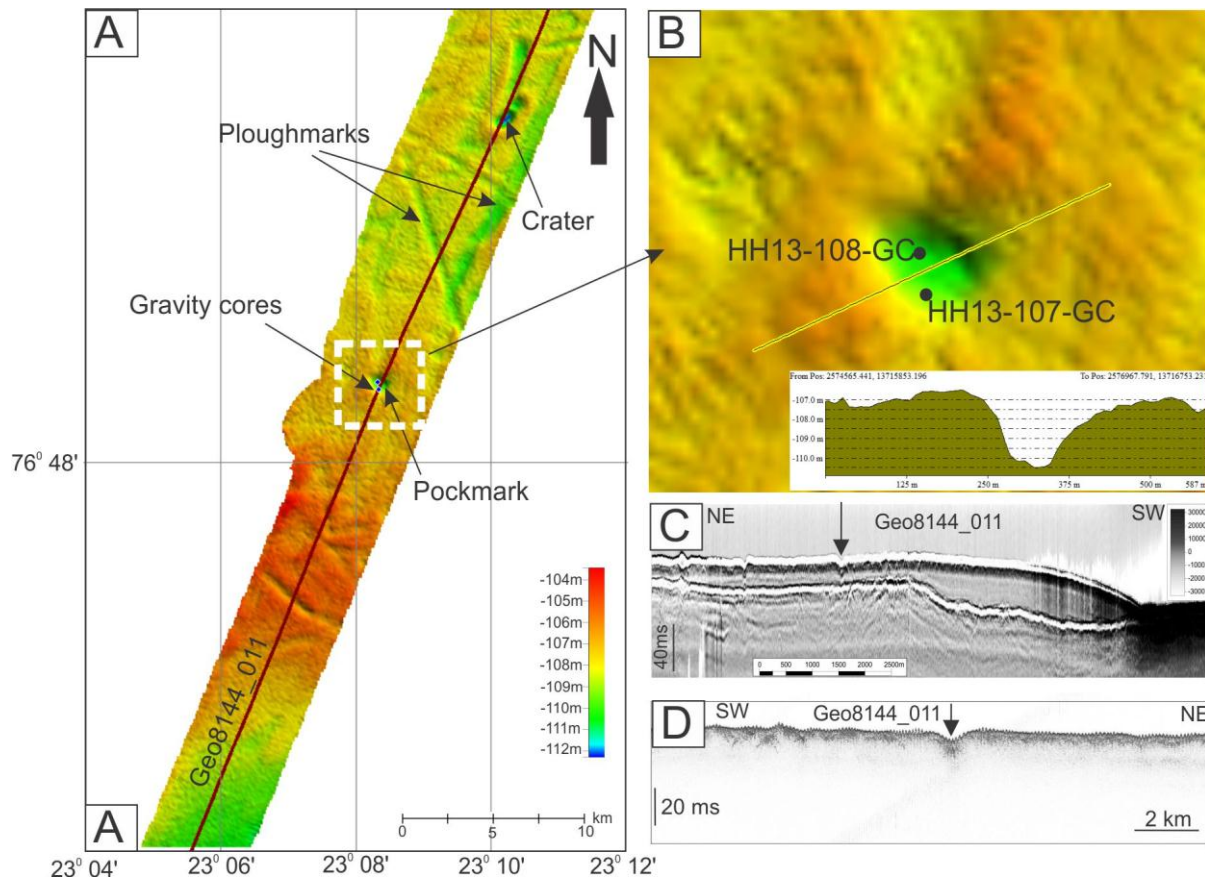


**Figure 4.6.2** A) Pockmark located in the Storfjordbanken area (Fig. 4.6.1) Location of seismic/chirp line Geo3144\_011 and gravity cores are also shown. B) Zoomed in view of the pockmark with a vertical profile across it showing the dimensions. Locations of gravity cores are shown. C) Seismic profile across the pockmark. Location of the pockmark is marked (arrow). D) Chirp profile across the pockmark, with location of the pockmark (arrow).

During the transit from Storfjordbanken to Storfjordrenna (Fig.4.6.1), three pockmarks were observed (Fig.4.6.3A). They varied in shape from elongated to circular. The dimensions of these features are shown in figure 4.6.3B. They were 4-6m deep and 70-130m wide. The chirp line (Fig. 4.6.3C) shows a layer of softer sediments and it forms a ridge-like feature which can be seen on the bathymetry. It is interesting to note that the location of all these pockmarks were on the crest of the ridge feature. The multibeam data also lacked glacial ploughmarks.

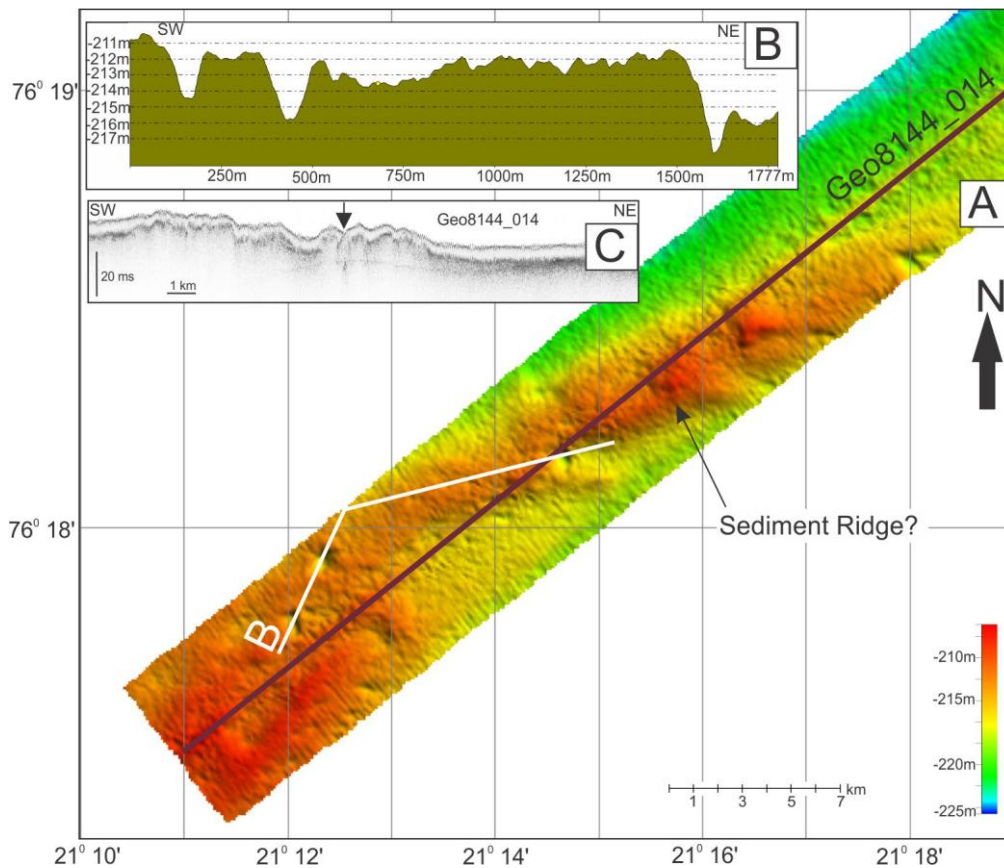


**Figure 4.6.3** A) Pockmark located in between Storfjordbanken and Storfjordrenna area (Fig. 4.6.1) Location of chirp line Geo3144\_014 is also shown. B) A vertical profile across the pockmarks showing the dimensions. C) Chirp profile across the pockmark showing the presence of upper soft sediment section, with location of the pockmark (arrow).

Northern part of the Storfjordrenna study area (Fig.4.6.1) show three large pockmarks (Fig. 4.6.4). They were the largest pockmarks observed during the cruise. They had different shapes and sizes: circular, ~30m deep and ~210m wide (Fig.4.6.4B), oval, ~275m wide, and ~14m deep (Fig.4.6.4C), elongated, ~250m wide longitudinally, ~130m across and ~6m at its deepest (Fig.4.6.4D). The geomorphology of the area was shaped by various glacial periods ploughmarks, lineations and other glacially formed features are visible close to the pockmarks. One of the pockmarks was located on sediment lobe/wedge (Fig.4.6.4A) and the chirp line (Fig.4.6.4E) across it shows thick layer of relatively soft sediments.



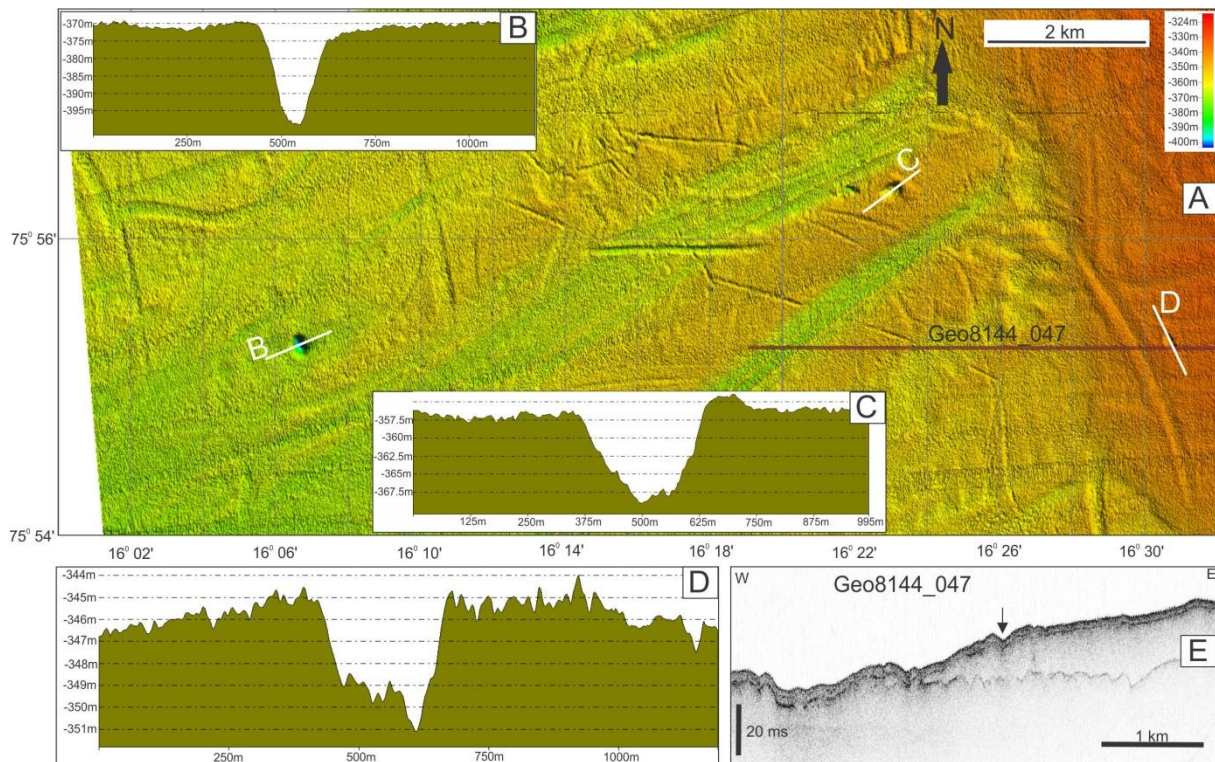


**Figure 4.6.4** A) Pockmarks located in the northern part of Storfjordrenna study area (Fig. 4.6.1) Location of chirp line Geo3144\_047 is also shown. B,C,D) A vertical profile across the pockmarks showing the dimensions. E) Chirp profile across the pockmark showing the presence of upper soft sediment section, with location of the pockmark (arrow).

Numerous depressions are visible on the southern part of the Storfjordrenna study area (Fig. 4.6.1). Due to the presence of high density of glacial geomorphological features, most of these depressions are considered to be formed as part of iceberg movements. However, some of them were not associated with any of the glacially formed features (Fig.4.6.5A). The area considered here showed many gas flares on the single beam echosounder (detailed in next chapter). Most of the depressions were located on the thick sedimentary wedge/lobe. Elongated and circular/oval shaped pockmarks were observed, which were ~ 4-8m deep ~100-190 meters wide (Fig.4.6.5B, C, D, E, F, G). Incidentally, none of the chirp lines cut across any of these pockmarks.

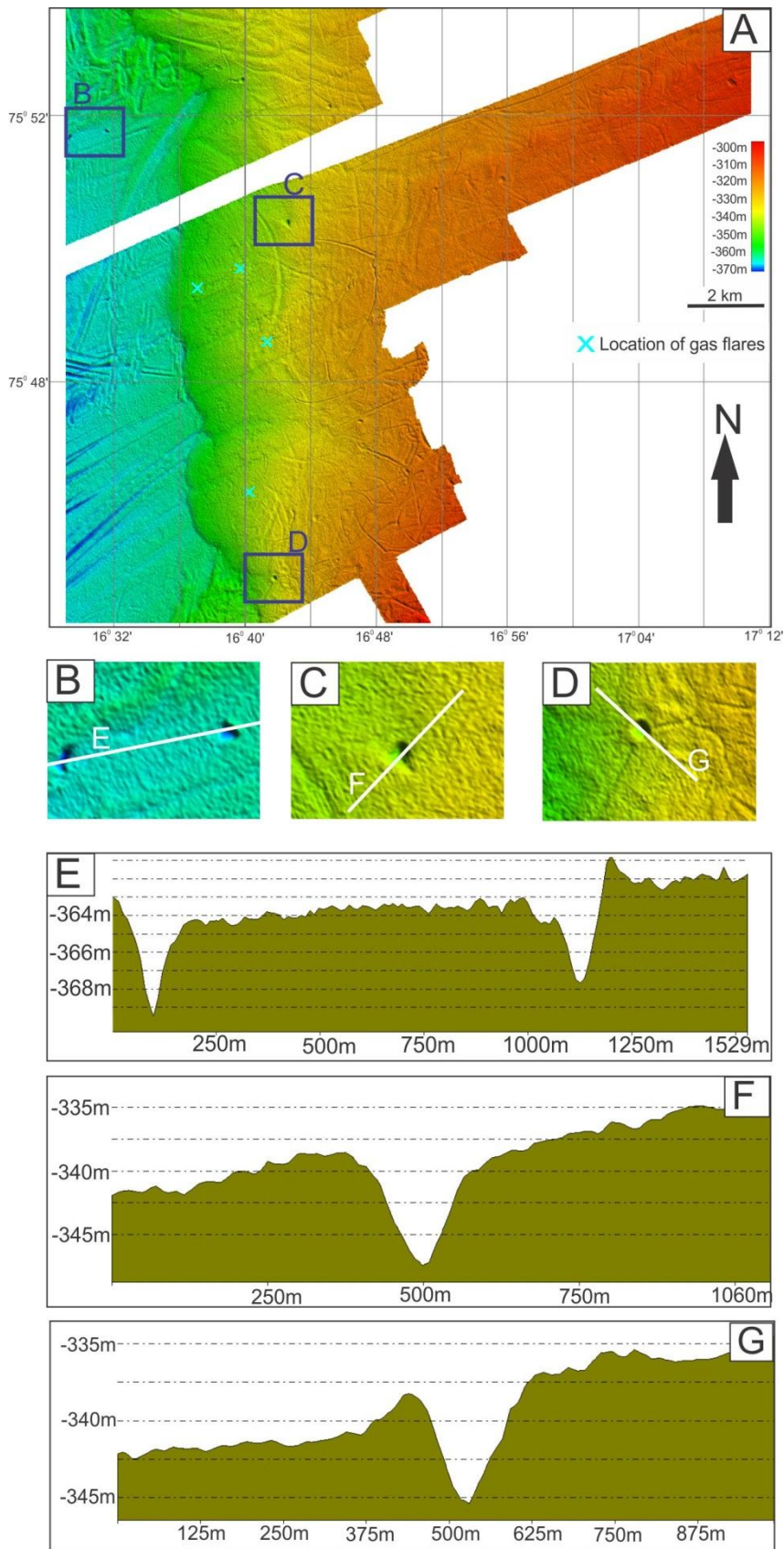


**Figure 4.6.5** A) Pockmarks located in the southern part of Storfjordrenna study area (Fig. 4.6.1). B,C,D) Zoomed in view of pockmarks. E,F,G) Vertical profile across the pockmarks showing the dimensions.

*Discussion*

Presence of pockmarks and gas flares in their vicinity suggests gas seepage as the main mechanism of pockmark formation. These pockmarks may be inactive at present. However, presence of gas in one of the core samples from Storfjordbanken area suggests that some of these pockmarks may still be active. Pockmarks are observed in many parts of the Barents Sea (Chand et al., 2009,2012; Ostanin et al., 2013; Solheim and Elverhøi, 1993; Lammers et al., 1995). Lammers et al. (1995) showed presence of large craters formed from violent release of gas east of Bjørnøya Island. Our study is the first report of pockmark indications in the northern Barents Sea. The location of pockmarks on glacially formed sediment wedges/lobes may suggest glacial activities might have triggered fluid flow and pockmark formation. More data collection, especially deep seismic, is necessary to understand the source of fluids which might have caused formation of these pockmarks. Results from analysis of gas collected from samples collected during this cruise would point toward possible origin of the gas and thus confirm whether the source of gas is located in the shallower or deeper part of the subsurface.

**4.7 Gas Flares (F)**

Evidences of gas seepage in to the water column through the seafloor can manifested as a vertical column of disturbance in a single beam echo sounder. These zones of vertical disturbances are generally termed ‘gas flares’ (e.g., Greinert et al., 2006, Bünz et al., 2012). Such features are observed in many parts of the world (Judd and Hovland, 2007). During our cruise, five locations with such gas flares were observed in the single beam echo sounder (Fig. 4.7.1)

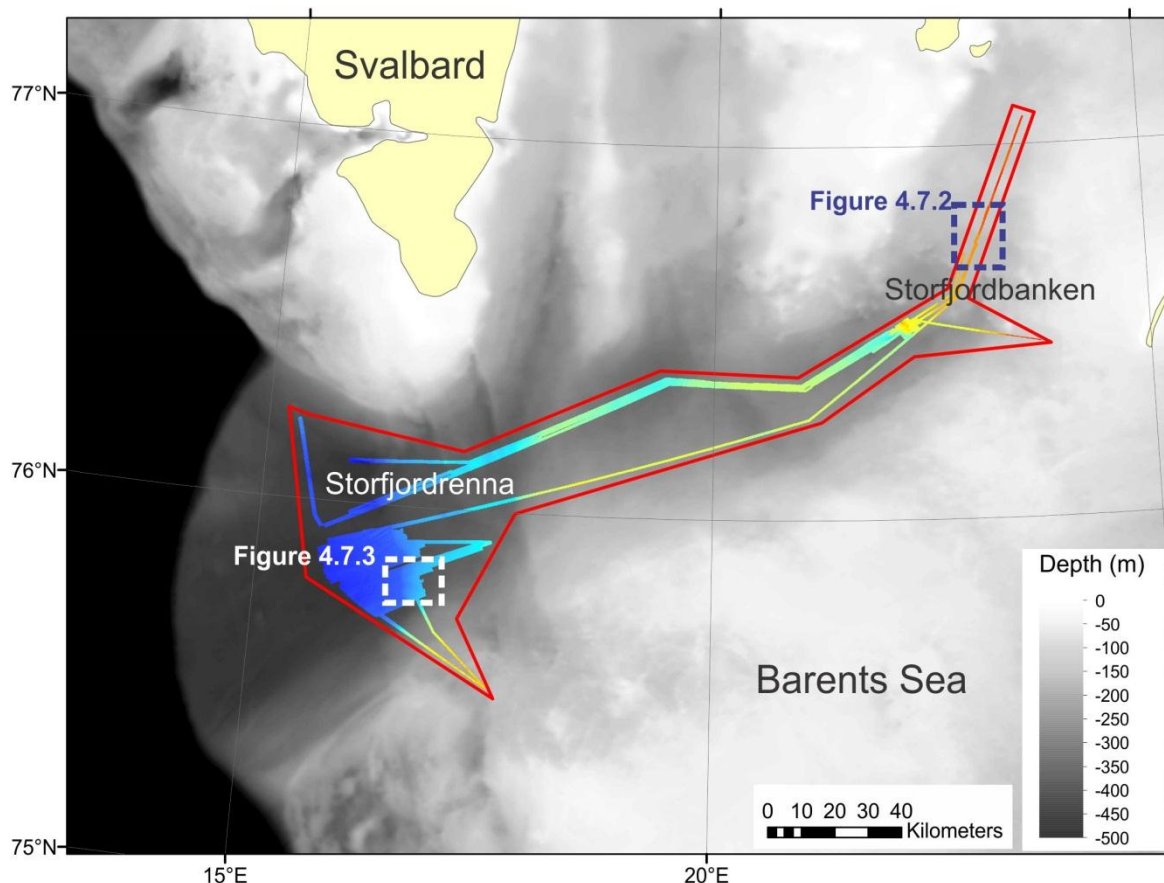


**Figure 4.7.1** Study area (in red) general bathymetry and acquired swath bathymetry. Location of other figures in the chapter is also shown

### *Observations*

We observed the first flare during our cruise in the Storjordbanken area (Fig. 4.7.1, 4.7.2A). It was observed on both 18 KHz and 38 KHz sensors at a water depth of ~206 m and was ~70m high (4.7.2B). The chirp profile across the flare location (Fig.4.7.2A,C) show the flare located at the terminating point of a sedimentary wedge. Also another layer pinches out at the exact location of this flare. There was no indication of any depressions in this location. Pockmarks further up in the sedimentary wedge (Chapter 4.6) may have resulted from such leakage activity.

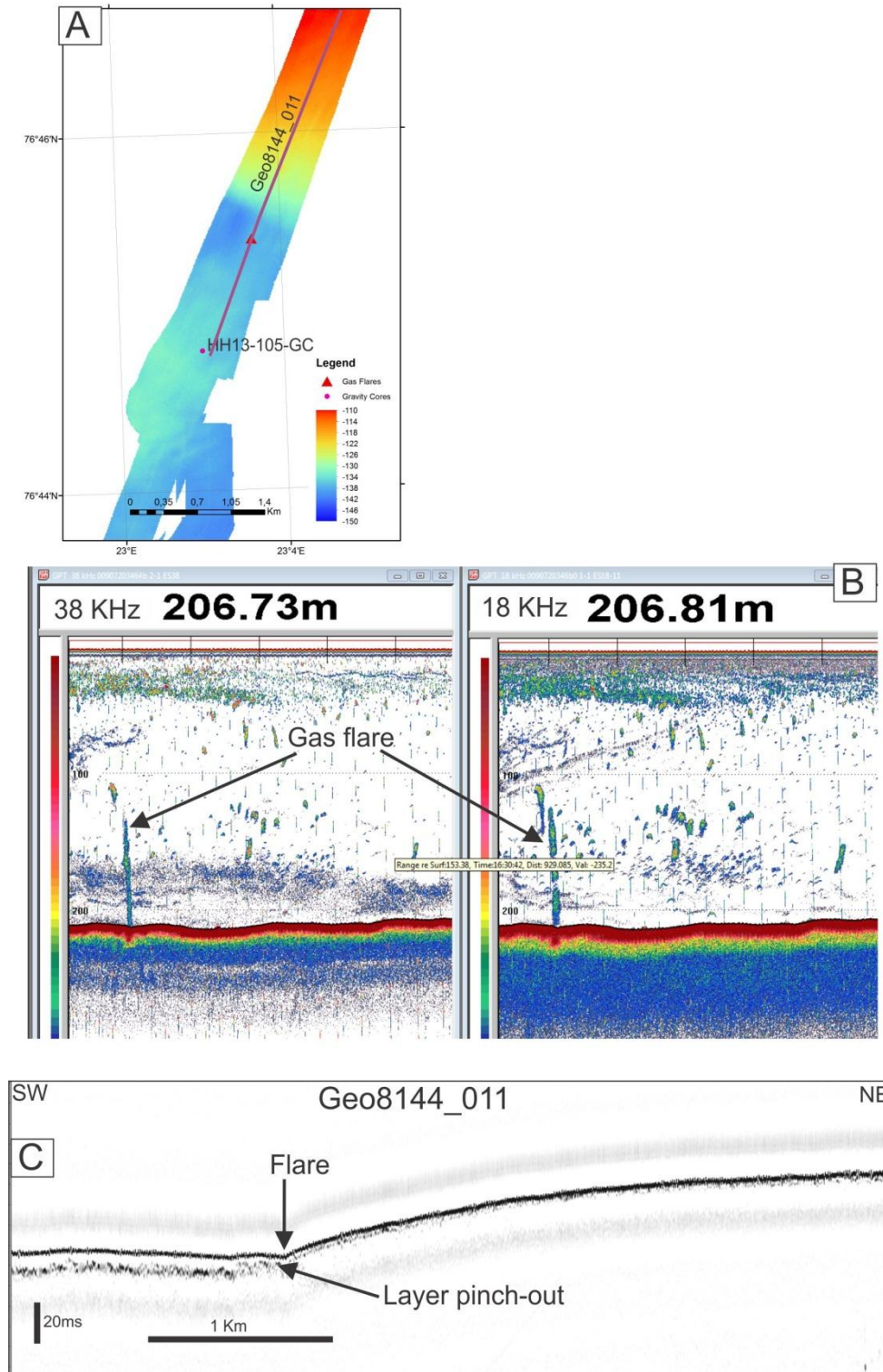


**Figure 4.7.2** A) Location of the flare in the Storfjordbanken area. Swath bathymetry and chirp line location is also shown. B) Screenshot of the flare from Simrad EK60 echo sounder. C) Chirp line showing location of the flare.

In the Storfjordrenna area (Fig.4.7.1), four gas flares were detected (Fig. 4.7.3A). The largest flare observed was flare no.1 which seemed to be highly active (Fig. 4.7.3B). Indication of gas is visible in the seismic section which shows a high-amplitude reflection underneath the flare location (Fig. 4.7.3C). A small depression can be seen at the flare location in both seismic and chirp data (Fig. 4.7.3C, D). Flares no.2 and no.4 were relatively smaller. Flares 1, 2, and 4 reached up to 150m above the seafloor, whereas flare no. 3 was taller reaching up to more than 200m above the seafloor. Indications of other flares were not evident in their respective chirp lines. A gravity core was taken from flare no.1 (See chapter 4.1, Fig4.7.3A) and had a strong smell of hydrogen sulphide when taken out from the core. Gas is sampled for analysis.

### *Discussion*

Very few active gas seepages are discovered in the Barents Sea and adjacent areas. They were located in the west of Svalbard (Westbrook et al., 2009; Bünz et al., 2012) and in the SW Barents Sea (Foucher et al., 2009; Chand et al., 2012). The flares observed during this cruise are the first of such active gas seepage indications in the Barents Sea, north of Bjørnøya and south of Svalbard. This region of the Barents Sea is relatively unexplored. The only previous study indicating past fluid expulsions close to this area is done by Lammers et al. (1995), where large craters thought to be the result of violent fluid expulsions is detailed. If the gas analysis show thermogenic gas signature, it points to the presence of undiscovered petroleum provinces in this area. Flares 2, 3, and 4 were located at approximately equal distances from the edge of the sedimentary lobe/wedge, which indicates that these seepages might have a common origin and probably triggered simultaneously. The relation of these flares to glacial morphology further confirms the effect glaciations had on the petroleum systems of the Barents Sea area (e.g., Henriksen et al., 2011; Vadakkepuliambatta et al., 2013).

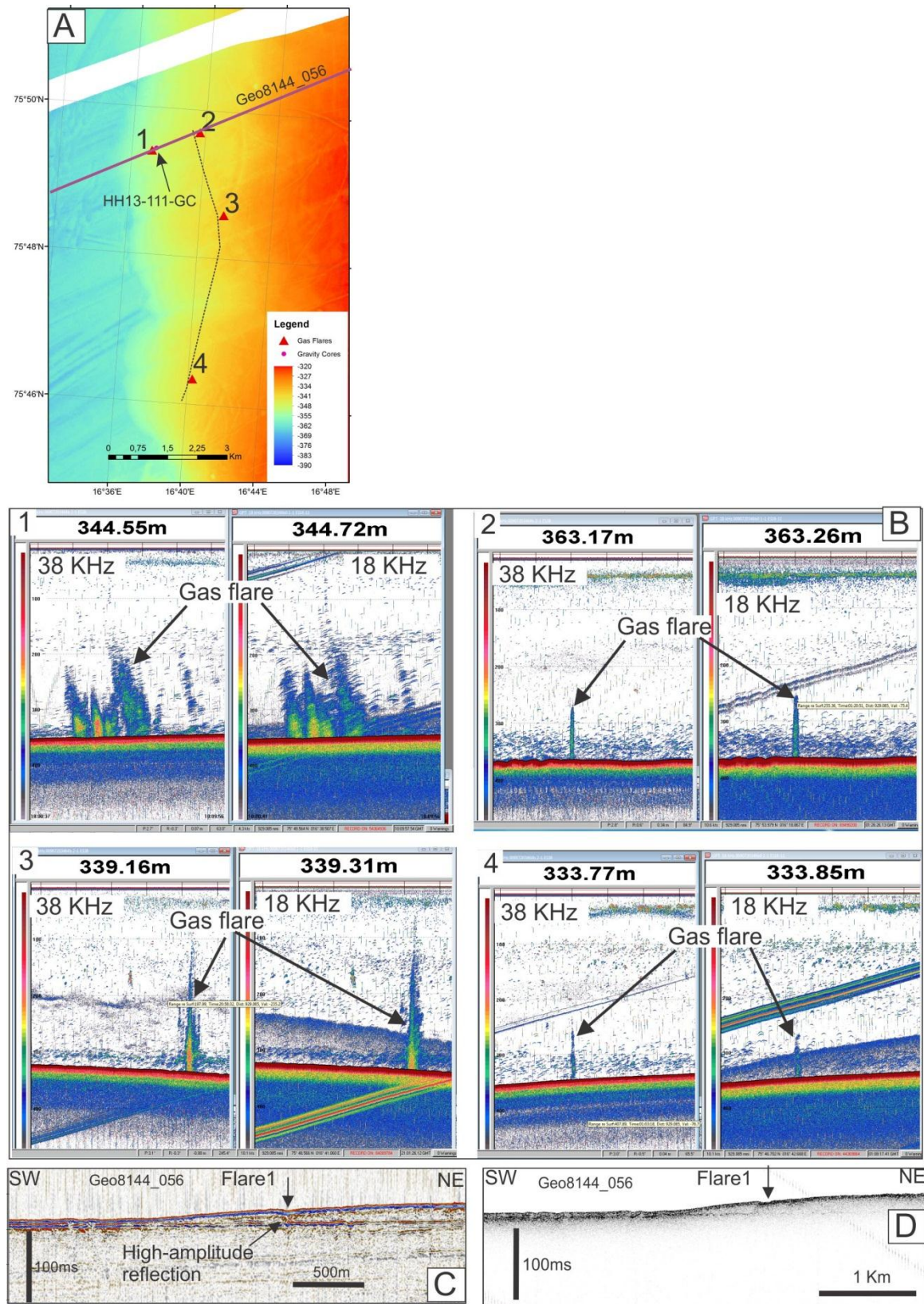


**Figure 4.7.3** A) Location of the flares in the Storfjordrenna area. Swath bathymetry, core and seismic/chirp line location is also shown. B) Screenshots of the flares from Simrad EK60 echo sounder. C) Seismic line with the location of the flare. D) Chirp line showing location of the flare.

## 5. SUMMARY

Results from our cruise provide insight to previously undiscovered glacial geomorphological features which will help in reconstructing the ice sheet history in the area.

Gravity core was used to collect samples of bottom sediments during the cruise HH13KA. Bottom sampling was performed on 9 stations. Sediments collected from 5 stations were cut into 100 cm long sections, packed, labeled, and stored in cool room (5 C°) before transportation to the University of Tromso for further detailed investigations.

Sediments collected from 3 stations were preliminary studied onboard. Each section was split into two halves. One half was used to take photos and for lithological description. The other half of each section was used to collect samples for degassing and more detailed lithological, geochemical and petrophysical investigations. Samples of sediments (40 ml) for further degassing were collected from each 15-20 cm from different lithological units. Obtained gas is transported to Lomonosov Moscow State University for further investigations, using Gas Chromatography (GC) and Isotope Ratio Mass-Spectrometry (IRMS).

A series of lineations were found on the seafloor in Storfjordrenna. These were interpreted to be mega-scale glacial lineations formed at the base of icestreams draining through the trough. Another set of lineations showed a different character (deeper and narrower), and they were interpreted to be mega-multi-keel iceberg ploughmarks. The shallower bank area of the bathymetric survey revealed a third set of lineation (higher wave length, smaller amplitude). These elongated ridges are believed to represent either MSGs or drumlin landforms indicating direction of icestream drainage.

Using a combination of the multibeam and chirp data-sets we are able to identify a complex proglacial system in the lower section of Storfjordrenna. Here we found at least three large multi-keel iceberg ploughmark features. Since these features cross cut each other, we can speculate that there must have been three discharge glacial events. However, the cross cutting of the ploughmarks may indicate that there were several large rerouting events of the ice stream ice and sediment discharge into this area during one or two glacial events instead of the proposed three. Also, the presence of corrugated ridges/washboard ploughmarks, indicates that the ice stream in Storfjordrenna may have been considerably influenced by tidal motions at the ice margins.



Swath bathymetry and IBCAO data, and seismic profiles allow us to identify a series of large ridges in Storfjordrenna and Storfjordbanken. They are interpreted to be grounding zone wedges, formed during episodic retreat of the icestream flowing in this area. The time frame of deposition of the grounding zone wedges needs to be further investigated.

Melt water channels are erosional features of glacier ablation and meltwater flow close to ice-sheet margins, and consequently their distribution and characteristics may be used to decipher patterns of glacial retreat. Melt water channels were identified in the NE part of the study area. Two types of channels can be subdivided. The first type includes large channels, with depth up to 60 m and second – small channels, several meters in depth.

The discovery of gas flares is the first of its kind in the northern Barents Sea. Along with pockmarks it suggests an active fluid plumbing system in the area. The active seepages suggest deeper-lying hydrocarbon accumulations which will help in future hydrocarbon exploration in this relatively under-explored area. The location of flares and pockmarks in association with glacio-morphologic features underlines the impact of glacial cycles on petroleum systems.

## 6. REFERENCES

Aagaard-Sørensen, S., Husum, K., Hald, M. & Knies, J. 2010. Paleoceanographic development in the SW Barents Sea during the Late Weichselian–Early Holocene transition. *Quaternary Science Reviews* 29, 3442–3456.

Andreassen, K., Laberg, J. S., and Vorren, T. O. 2008. Seafloor geomorphology of the SW Barents Sea and its glaci-dynamic implications. *Geomorphology* 97, pp 157-177.

Andreassen, K. & Winsborrow, M. 2009. Signature of ice streaming in Bjørnøyrenna, Polar North Atlantic, through the Pleistocene and implications for ice-stream dynamics. *Annals of Glaciology*, p. 17-26

Butt et al., 2002. Modelling Late Cenozoic isostatic elevation changes in the Barents Sea and their implications for oceanic and climatic regimes: preliminary results, *The Barents Sea Location and sequence stratigraphy* 3-4 pp.

Bünz, S., Polyanov, S., Vadakkepuliambatta, S., Consolaro, C., Mienert, J., 2012. Active gas venting through hydrate-bearing sediments on the Vestnesa Ridge, offshore W-Svalbard. *Marine Geology*.

Chand, S., Rise, L., Ottesen, D., Dolan, M.F.J., Bellec, V., Bøe, R., 2009. Pockmark like depressions near the Goliat hydrocarbon field, Barents Sea: morphology and genesis. *Marine and Petroleum Geology* 26, 1035-1042.

Chand, S., Thorsnes, T., Rise, L., Brunstad, H., Stoddart, D., Bøe, R., Lågstad, P., Svolsbru, T., 2012. Multiple episodes of fluid flow in the SW Barents Sea (Loppa High) evidenced by gas flares, pockmarks and gas hydrate accumulation. *Earth and Planetary Science Letters* 331-332, 305-314.

Dowdeswell, J.A., Evans, J., Ó Cofaigh, C., 2010. Submarine landforms and shallow acoustic stratigraphy of a 40 km-long fjord-shelf-slope transect, Kangerlussuaq margin, East Greenland. *Quaternary Science Reviews*, p. 3359-3369. \*b

Dowdeswell, J.A., Hogan, K.A., Evans, J., Noormets, R., Ó Cofaigh, C., Ottesen, D., 2010. Past ice-sheet flow east of Svalbard inferred from streamlined subglacial landforms. *Geology* 38, 163e166.\*a

Dowdeswell, J.A., Ottesen, D., Evans, J., Ó Cofaigh, C., and Anderson, J.B., 2008, Submarine glacial landforms and rates of ice-stream collapse: *Geology*, v. 36, p. 819–822, doi: 0.1130/G24808A.1.

Faleide, J. I., Vågnes, E. and Gudlaugsson, S. T. 1993 Late Mesozoic-Cenozoic evolution of the southwestern Barents Sea. In Parker, J. R. (ed.) *Petroleum geology of Northwest Europe: Proceedings of the 4th Conference*, 933-950. The Geological Society of London, London, United Kingdom

Foucher et al., 2009. Structure and drivers of cold seep ecosystems. *Oceanography* 22(1)

Gabrielsen et al., 1990. Structural elements of the Norwegian continental shelf, *Structural geology of the Barents Sea*, 5-6 pp.

Graham, A. G. C., Dutrieux, P. Vaughan, D. G., Nitsche, F. O., Gyllencreutz, R., Greenwood, S. L., Larter, R. D., and Jenkins, A. Sea-bed corrugations beneath an Antarctic Ice Shelf revealed by autonomous underwater vehicle survey: origin and implications for the history of Pine Island Glacier. *In Review*.

Greenwood et al., 2006.. Formalising an inversion methodology for reconstructing ice-sheet retreat patterns from meltwater channels: application to the British Ice Sheet. *Journal of Quaternary Science*, 1-4 pp.

Greinert et al., 2006. 1300-m-high rising bubbles from mud volcanoes at 2080m in the Black Sea: Hydroacoustic characteristics and temporal variability. *Earth and Planetary Science Letters* 244, 1-15.

Henriksen, E., Bjørnseth, H.M., Hals, T.K., Heide, T., Kiryukhina, T., Kløvjan, O.S., Larssen, G.B., Ryseth, A.E., Rønning, K., Sollid, K., Stoupakova, A., 2011. Chapter

17 Uplift and erosion of the greater Barents Sea: impact on prospectivity and petroleum systems. In: Geological Society, London, Memoirs, vol. 35, pp. 271-281

Ingólfsson, O., and Landvik, J. Y. The Svalbard-Barents Sea ice sheet – Historical, current and future perspectives. *Quaternary Science reviews* 64, pp 33-60.

Jakobsson, M., Anderson, J.B., Nitsche, F., Dowdeswell, J.A., Gyllencreutz, R., Kirchner, N., Mohammad, R., O'Regan, M., Alley, R.B., Anandkrishnan, S., Eriksson, B., Krishner, A., Fernandes, R., Stollendorf, T., Minzoni, R., Majewski, W. 2010. Geological record of ice shelf break-up and grounding line retreat, Pine Island Bay; West Antarctica. *Geological Society of America*, p. 691-694

Jakobsson, M., Anderson, J.B., Nitsche, F., Gyllencreutz, R., Krishner, A., Kirchner, N., O'Regan, M., Mohammad, R., Eriksson, B. 2012. Ice sheet retreat dynamics inferred from glacial morphology of the central Pine Island Bay Trough, West Antarctica. *Quaternary Science Reviews*, p. 1-10

Jessen, S.P., Rasmussen, T.L., Nielsen, T., Solheim, A., 2010. A new Late Weichselian and Holocene marine chronology for the western Svalbard slope 30,000 cal years BP. *Quaternary Science Reviews* 29, pp 1301-1312.

Judd, A., Hovland, M., 2007. *Seabed Fluid Flow*. Cambridge University Press, Cambridge.

Knies, J., Matthiesen, J., Vogt, C., Laberg, J. S., Hjelstruen, B. O., Smelror, M., Larsen, E., Andreassen, K., Eidving, T., and Vorren, T. O. 2009. The Plio-Pleistocene glaciation of the Barents Sea-Svalbard region: a new model based on revised chronostratigraphy. *Quaternary Science Reviews* 28, pp 812-829.

Knies, J., Nowaczyk, N., Müller, C., Vogt, C., Stein, R., 2000. A multiproxy approach to reconstruct the environmental changes along the Eurasian continental margin over the last 150000 years. *Marine Geology* 163, pp317-344

King, L.H., MacLean, B., 1970. Pockmarks of the Scotian Shelf. *Geol. Soc. Amer. Bull.* 81, 3141– 3148.

Kongsberg EM300 Multibeam echo sounder Product description.

Kristensen, D.K., Rasmussen, T.L., Koç, N. 2012: Palaeoceanographic changes in the northern Barents Sea during the last 16 000 years – new constraints on the last deglaciation of the Svalbard – Barents Sea Ice Sheet. *Boreas*, 10.1111/j.1502-3885.2012.00307.x.

Laberg, J.S., Vorren, T.O., 1995. Late Weichselian submarine debris flow deposits on the Bear Island trough-mouth-fan. *Marine Geology* 127, pp 45-72.

Lammers, S., Suess, E., Hovland, M., 1995. A large methane plume east of Bear Island (Barents Sea): implications for the marine methane cycle. *Geol Rundsch* 84, 59-66.

Landvik, J.Y., Bondevik, S., Elverhøi, A., Fjeldskaar, W., Mangerud, J., Salvigsen, O., Siegert, M.J., Svendsen, J.I., Vorren, T.O., 1998. The last glacial maximum of Svalbard and the Barents Sea area: Ice sheet extent and configuration. *Quaternary Science Reviews* 17, pp 43-75.

Landvik, J. Y., Ingólfsson, Ó., Mienert, J., Lehman, S. J., Solheim, A., Elverhøi, A., and Ottensen, D. 2005. Rethinking Late Weichselian ice-sheet dynamics in coastal NW Svalbard. *Boreas*, Vol 34, pp 7-24.

Larssen et al., 2002. Upper Palaeozoic lithostratigraphy of the southern Norwegian Barents Sea, 5-6 pp.

Mangerud, J., Dokken, T., Hebbeln, D., Heggen, B., Ingólfsson, Ó., Landvik, J.Y., Mejdahl, V., Svendsen, J.I., Vorren, T.O., 1998. Fluctuations of the Svalbard Barents Sea Ice Sheet during the last 150 000 years. *Quaternary Science Reviews* 17, pp 11-42.

Mudelsee, M., and Raymo, M. E. 2005. Slow dynamics of the Northern Hemisphere Glaciation. *Paleoceanography* 20.

Ostanin, I., Anka, Z., di Primio, R., Bernal, A., Hydrocarbon plumbing systems above the Snøhvit gas field: structural control and implications for thermogenic methane leakage in the Hammerfest Basin, SW Barents Sea, *Marine and Petroleum Geology* (2013), doi: 10.1016/j.marpetgeo.2013.02.012.

Ottesen, D., Dowdeswell, J.A., Rise, L., 2005. Submarine landforms and the reconstruction of fast-flowing ice streams within a large Quaternary ice sheet: the 2500 km-long Norwegian-Svalbard margin (57°- 80°N). *Geological Society of America Bulletin* 117, p. 1033-1050.

Piotrowski et al., 1993. Tunnel-valley formation on northwest Germany – geology, mechanisms of formation and subglacial bed conditions for the Bornhoved tunnel valley

Polyak, L., Forman, S.L., Herlihy, F.A., Ivanov, G., Krinitsky, P., 1997. Late Weichselian deglacial history of the Svyataya (Saint) Anna Trough, northern Kara Sea, Arctic Russia. *Marine Geology* 143, pp 169-188

Rasmussen, T. L., Thomsen, E., Słubowska, M. A., Jessen, S., Solheim, A. & Koç, N. 2007: Paleooceanographic evolution of the SW Svalbard margin (76°N) since 20 000 14C yr BP. *Quaternary Research* 67, 100–114.

Rüther, D. C., Mattingsdal, R. Andreassen, K., Forwick, M., and Husum, K. 2011. Seismic architecture and sedimentology of a major grounding zone system deposited by the Bjørnøyrenna Ice Stream during the Late Weichselian deglaciation. *Quaternary Science Reviews* 30, pp 2776-2792.

Saettem, T. Bugge, S. Fanavoll, R.M. Goll, A. Mork, M.B.E. Mork, M. Smelror, J.G. Verdenius, 1994. Cenozoic margin development and erosion of the Barents Sea: Core evidence from southwest of Bjornoya, 1 pp

Saettem, J., Poole, D.A.R., Ellingsen, L., Sejrup, H.P., 1992. Glacial geology of outer Bjørnøyrenna, southwestern Barents Sea. *Marine Geology* 103, pp 15-51.

SBE 9plus CTD-Manual

Sercel Marine Seismic Sources-Manual

Simrad EK60 Echo Sounder-User Manual

Słubowska-Woldengen, M., Koç, N., Rasmussen, T. L., Klitgaard-Kristensen, D., Hald, M. & Jennings, A. E. 2008: Time-slice reconstructions of ocean circulation changes on the

continental shelf in the Nordic and Barents Seas during the last 16 000 cal yr B.P. *Quaternary Science Reviews* 27, 1476–1492.

Solheim, A., Elverhøi, A., 1993. Gas-related sea floor craters in the Barents Sea. *Geo-Marine Letters* 13, 235-243.

Sub-bottom profiler processor software. Technical & user's manual.

Svendsen, J. I., Alexanderson, H., Astakhov, V. I., Demidov, I., Dowdeswell, J. A. et al. 2004. Late Quaternary ice sheet history of northern Eurasia. *Quaternary Science Reviews* 23, pp 1229-1271.

Vadakkepuliambatta, S., Bünz, S., Mienert, J., Chand, S., 2013. Distribution of subsurface fluid-flow systems in the SW Barents Sea. *Marine and Petroleum Geology* 43, 208-221.

Westbrook, G. K., et al., 2009. Escape of methane gas from the seabed along the West Spitsbergen continental margin, *Geophys. Res. Lett.*, 36, L15608, doi:10.1029/2009GL039191.

Winsborrow M.C.M., Andreassen K., Corner G.D. and Laberg J.S. 2010. Deglaciation of a marine-based ice sheet: Late Weichselian palaeo-ice dynamics and retreat in the southern Barents Sea reconstructed from onshore and offshore glacial geomorphology. *Quaternary Science Reviews* 29, 425-426.

**APPENDIX TO THE CRUISE REPORT**

Table 1: Event log Geo3144/8144 cruise 21.07-27.07.2013.

Table 2: Line log Geo3144/8144 cruise 22.07-27.07.2013.

Table 3: Gravity-corer stations Geo3144/8144 cruise 22.07-27.07.2010.



### Eventlog Geo-8144-3144 on RV Helmer Hanssen July 21-28. 2013 Storfjordrenna

Core location numbering starting on HH13-105-GC, following the numbering on the bridge of 'other stations' and CTD station numbering starts at 348, following the CTD numbering on the bridge. Use UTC time (2 hrs after local time)

Date	UTC	Position	Event
21/7	22:05 UTC		Departure from Longyearbyen. Wind ca 8-9 m/s, waveheights 1.5-2 m, temp 5 degrees
22/7	08:13	76°58.360N 014°13.957E	Start Multibeam and Chirp Line Geo8144-001. Transit line from Lyb to study area Storfjorden
22/7	14.25	75°55.862 N 15°41.154E	End multibeam and Chirp Line Geo8144-001
22/7	14.43	75°55.785N 15°41.835 E	CTD station 348
22/7	14.54	75°55.864N 15°43.117E	Start Multibeam 0016 and Chirp Line Geo8144-002. Storfjorden
22/7	20.41	76°22.787N 19°31.534E	End multibeam and Chirp Line Geo8144-002
22/7	20.41	76°22.787N 19°31.534E	Start Multibeam 0029 and Chirp Line Geo8144-003. Storfjorden. Wind 7-8 m/s, temp 5.6 degrees
22/7	22:50	76°20.943N 21°01.668E	End multibeam and Chirp line Geo8144-003. Storfjorden.
22/7	22:50	76°20.943N 21°01.668E	Start Multibeam 0034 and Chirp line Geo8144-004. Storfjorden. Wind 7-8 m/s, temp 5.8, waveheight max 1m
23/7	01:29	76°35.672N 22°45.839E	End Multibeam and Chirp line Geo8144-004, Storfjordrenna.
23/7	01:31	76°36.073N 22°46.441E	Start Multibeam and Chirp line Geo8144-005, Storfjordbanken. Wind 6-7 m/s, temp 5.4
23/7	04:15	77°04.376N 23°37.393E	End Multibeam and Chirp line Geo8144-005, Storfjordbanken.
23/7	04:18	77°04.306N 23°38.070E	Start Multibeam and Chirp line Geo8144-006, Storfjordbanken. Wind 8-9 m/s, temp 4.4
23/7	06:23	76°45.064N 23°03.056E	End Multibeam and Chirp line Geo8144-006, Storfjordbanken. Wind 5 m/s, temp 5
23/7	06:34	76°44.798N 23°02.070E	Chirp Line Geo8144_007. On location HH13-105-GC, CTD 349 and HH13-106
23/7	06:27	76°44.789N 23°02.070E	Start CTD station 349
23/7	06:37	76°44.731N 23°01.769E	Stop CTD station 349

---

23/7	06:50	76°44.785N 23°02.001E	Core station HH13-105-GC Storfjordbanken.
23/7	07:10	76°45.777N 23°08.8051E	Just passed over flares in water. Recording Singlebeam Eccosounder and Er60 18, 38 and 120 kHz .
23/7	07:49	76°45.777N 23°08.8051E	Start Multibeam and chirp line Geo8144_008. Wind 5m/s
23/7	07:49	76°48.608N 23°09.353E	Core station HH13_106_GC Storfjordbanken
23/7	08:05	77°04.397N 23°37.5101E	Stop multibeam and chirp line Geo8144_008, wind 5, temp5
23/7	09:14	76°48.246N 23°08.347E	Core station HH13_107_GC Storfjordbanken at the outskirts of pockmark (did not hit the middle)
23/7	09:17		Start Multibeam and chirp line Geo8144_009 at core location HH13_108GC
23/7	09:49	76°48.269N 23°08.331E	Core station HH13_108-23/7GC Storfjordbanken in pockmark. Wind 5m/s temp 5
23/7	09:54		Stop Multibeam and Chirp line Geo8144_009
23/7	09:55		Start Multibeam and Chirp line Geo8144_010 transit to seismic line Storfjordbanken
23/7	10:51	76°49.887N 23°11.488E	Stop Multibeam and Chirp Line Geo8144_10
23/7	10:51	76°49.887N 23°11.488E	<b>Start Seismic</b> , Multibeam and Chirp Geo8144_11 over wedges and pockmarks and gas flares in Storfjordbanken
23/7	12:07	75°55.928N 18°34.893E	<b>End Seismic</b> , Multibeam and Chirp Line Geo8144_011
23/7	12:15	76°44.313N 23°02.072E	Start Multibeam and Chirp Line Geo8144_012
23/7	12:38	76°43.367N 23°00.385E	End Multibeam and Chirp Line Geo8144_012
23/7	12:38	76°43.367N 23°00.385E	Start Multibeam and Chirp Line Geo8144_013
23/7	13:34	76°35.551N 22°46.760E	End Multibeam and Chirp Line Geo8144_013
23/7	13:34	76°35.551N 22°46.760E	Start Multibeam and Chirp Line Geo8144_014
23/7	16:48	76°16.240N 21°04.456E	End Multibeam and Chirp Line Geo8144_014
23/7	16:48	76°16.240N 21°04.456E	Start Multibeam and Chirp Line Geo8144_015
24/7	00:42	75°53.533N 15°46.043E	End Multibeam and Chirp Line Geo8144_015
24/7	00:42	75°53.533N 15°46.043E	Start Multibeam and Chirp Line Geo8144_016
24/7	01:30	75°54.021N 16°21.670E	Possible flare
24/7	03:16	75°55.151N 17°32.980E	End Multibeam and Chirp Line Geo8144_016

---

---

24/7	03:16	75°55.151N 17°32.980E	Start Multibeam and Chirp Line Geo8144_017
24/7	04:46	75°49.556N 16°37.746E	Possible flare
24/7	04:50	75°49.323N 16°36.196E	Possible flare
24/7	05:49	75°45.672N 16°03.732E	End Multibeam and Chirp Line Geo8144_017
24/7	05:49	75°45.672N 16°03.732E	Start Multibeam and Chirp Line Geo8144_018
24/7	08:18	75°32.061N 17°32.796E	End Multibeam and Chirp Line Geo8144_018
24/7	08:23	75°31.950N 17°34.530E	Start Multibeam 0116 and Chirp Line Geo8144_019, Storfjordrenna. Wind 1 m/s, temp 5 degrees
24/7	09:32	75°40.251N 16°59.554E	End Multibeam and Chirp Line Geo8144_019
24/7	09:32	75°40.251N 16°59.554E	Start Multibeam 0120 and Chirp Line Geo8144_020, Storfjordrenna. Wind 1 m/s, temp 5 degrees
24/7	10:06	75°45.525N 16°47.284E	End Multibeam and Chirp Line Geo8144_020
24/7	10:06	75°45.525N 16°47.284E	Start Multibeam 0122 and Chirp Line Geo8144_021, Storfjordrenna. Wind 3 m/s, temp 6 degrees
24/7	11:12	75°48.773N 16°00.499E	End Multibeam and Chirp Line Geo8144_021
24/7	11:31	75°46.086N 15°59.643E	Start Multibeam 0127 and Chirp Line Geo8144_022, Storfjordrenna. Wind 2 m/s, temp 7 degrees
24/7	13:49	75°54.984N 17°28.228E	End Multibeam and Chirp Line Geo8144_022
24/7	13:54	75°54.127N 17°28.706E	Start Multibeam 0133 and Chirp Line Geo8144_023, Storfjordrenna. Wind 4 m/s, temp 6 degrees
24/7	16:08	75°45.368N 16°05.785E	End Multibeam and Chirp Line Geo8144_023
24/7	16:19	75°46.722N 16°01.198E	Start Multibeam 0133 and Chirp Line Geo8144_024, Storfjordrenna. Wind 3 m/s, temp 7 degrees
24/7	16:59	75°49.080N 16°27.931E	End Multibeam and Chirp Line Geo8144_024
24/7	16:59	75°49.080N 16°27.931E	Start Multibeam 0133 and Chirp Line Geo8144_025, Storfjordrenna.
24/7	17:03	75°49.155N 16°27.468E	CTD Station 350 start. Storfjordrenna.
24/7	17:15	75° 49.155N 16°27.968E	CTD Station 350 stop. Storfjordrenna.
24/7	17:14	75°49.149N 16°27.885E	End Multibeam and Chirp Line Geo8144_025
24/7	17:31	75°49.065N 16°27.964E	Core Station HH13-109-GC Gravity Corer. Storfjordrenna
24/7	17:47	75°49.080N 16°27.931E	Start Multibeam 0143 and Chirp Line Geo8144_026, Storfjordrenna.

---

---

24/7	18:07	75°49.428N 16°37.249E	End Multibeam and Chirp Line Geo8144_026
24/7	18:15	75°49.449N 16°37.349E	Core station HH13-110-GC Storfjordrenna
24/7	18:49	75°49.423N 16°37.160E	Core Station HH13-111-GC Storfjordrenna
24/7	19:38	75°50.646N 16°48.533E	Core Station HH13-112-GC Storfjordrenna
24/7	20:10	75°51.420N 16°56.781E	Core Station HH13-113-GC Storfjordrenna
24/7	20:36	75°50.187N 16°56.426E	Start Multibeam 0145 and Chirp Line Geo8144_027, Storfjordrenna.
24/7	21:03	75°48.597N 16°41.346E	Flare
24/7	21:58	75°44.611N 16°07.413E	End Multibeam and Chirp line Geo8144_027
24/7	22:05	75°44.349N 16°10.696E	Start Multibeam 0151 and Chirp Line Geo8144_028, Storfjordrenna.
24/7	23:09	75°48.664N 16°48.620E	End Multibeam and Chirp line Geo8144_028
24/7	23:15	75°48.109N 16°48.860E	Start Multibeam 0155 and Chirp Line Geo8144_029, Storfjordrenna.
25/7	00:21	75°43.693N 16°11.139E	End Multibeam 0157 and Chirp Line Geo8144_029, Storfjordrenna
25/7	00:25	75°43.419N 16°14.964E	Start Multibeam 0159 and Chirp Line Geo8144_030, Storfjordrenna
25/7	01:10	75°46.348N 16°40.258E	Flare
25/7	01:23	75°47.598N 16°50.286E	End Multibeam 0159 and Chirp Line Geo8144_030, Storfjordrenna
25/7	01:29	75°47.042N 16°50.585E	Start Multibeam 0161 and Chirp Line Geo8144_031, Storfjordrenna
25/7	02:26	75°43.046N 16°17.721E	End Multibeam 0163 and Chirp Line Geo8144_031, Storfjordrenna
25/7	02:31	75°42.621N 16°19.630E	Start Multibeam 0165 and Chirp Line Geo8144_032, Storfjordrenna
25/7	03:25	75°46.761N 16°52.673E	End Multibeam 0167 and Chirp Line Geo8144_032, Storfjordrenna
25/7	03:30	75°46.210N 16°53.153E	Start Multibeam 0168 and Chirp Line Geo8144_033, Storfjordrenna
25/7	04:26	75°42.274N 16°22.012E	End Multibeam and Chirp Line Geo8144_033, Storfjordrenna
25/7	04:26	75°42.274N 16°22.012E	Start Multibeam 0171 and Chirp Line Geo8144_034, Storfjordrenna
25/7	05:10	75°46.261N 15°58.133E	End Multibeam and Chirp Line Geo8144_034, Storfjordrenna
25/7	05:18	75°47.077N 15°58.063E	Start Multibeam 0174 and Chirp Line Geo8144_035, Storfjordrenna

---

---

25/7	06:39	75°52.443N 16°47.874E	End Multibeam and Chirp Line Geo8144_035, Storfjordrenna
25/7	06:45	75°53.063N 16°46.566E	Start Multibeam 0178 and Chirp Line Geo8144_036, Storfjordrenna. Wind 4m/s, temp 7degrees
25/7	08:19	75°46.917N 15°50.167E	End Multibeam and Chirp Line Geo8144_036, Storfjordrenna
25/7	08:24	75°47.385N 15°48.299E	Start Multibeam 0183 and Chirp Line Geo8144_037, Storfjordrenna. Wind 4m/s, temp 7degrees
25/7	10:06	75°54.096N 16°50.160E	End Multibeam and Chirp Line Geo8144_037, Storfjordrenna
25/7	10:11	75°54.774N 16°47.833E	Start Multibeam 0188 and Chirp Line Geo8144_038, Storfjordrenna. Wind 6m/s, temp 7degrees
25/7	11:48	75°47.983N 15°46.992E	End Multibeam and Chirp Line Geo8144_038, Storfjordrenna
25/7	11:53	75°48.495N 15°45.091E	Start Multibeam 0193 and Chirp Line Geo8144_039, Storfjordrenna. Wind 5m/s, temp 7degrees
25/7	13:21	75°54.164N 16°39.116E	End Multibeam and Chirp Line Geo8144_039, Storfjordrenna
25/7	13:28	75°54.594N 16°37.263E	Start Multibeam 0198 and Chirp Line Geo8144_040, Storfjordrenna. Wind 3m/s, temp 7degrees
25/7	14:51	75°49.066N 15°45.131E	End Multibeam and Chirp Line Geo8144_040, Storfjordrenna
25/7	14:58	75°49.745N 15°44.581E	Start Multibeam 0202 and Chirp Line Geo8144_041, Storfjordrenna. Wind 4m/s, temp 7degrees
25/7	16:03	75°53.983N 16°25.283E	End Multibeam and Chirp Line Geo8144_041, Storfjordrenna
25/7	16:08	75°54.340N 16°23.868E	Start Multibeam 0206 and Chirp Line Geo8144_042, Storfjordrenna. Wind 4m/s, temp 7degrees
25/7	17:18	75°50.171N 15°41.497E	End Multibeam and Chirp Line Geo8144_042, Storfjordrenna
25/7	17:23	75°50.772N 15°40.990E	Start Multibeam 0210 and Chirp Line Geo8144_043, Storfjordrenna. Wind 7m/s, temp 6degrees
25/7	18:07	75°53.672N 16°09.598E	End Multibeam and Chirp Line Geo8144_043, Storfjordrenna
25/7	18:10	75°53.914N 16°08.535E	Start Multibeam 0213 and Chirp Line Geo8144_044, Storfjordrenna. Wind 7m/s, temp 6degrees
25/7	18:56	75°51.431N 15°41.227E	End Multibeam and Chirp Line Geo8144_044, Storfjordrenna
25/7	19:01	75°51.960N 15°39.911E	Start Multibeam 0216 and Chirp Line Geo8144_045, Storfjordrenna. Wind 7m/s, temp 6degrees
25/7	19:46	75°54.450N 16°07.757E	End Multibeam and Chirp Line Geo8144_045, Storfjordrenna
25/7	19:46	75°54.450N 16°07.757E	Start Multibeam 0219 and Chirp Line Geo8144_046, Storfjordrenna.
25/7	20:27	75°54.836N 16°36.647E	End Multibeam and Chirp Line Geo8144_046, Storfjordrenna
25/7	20:32	75°55.287N 16°36.065E	Start Multibeam 0222 and Chirp Line Geo8144_047, Storfjordrenna.

---

---

25/7	21:12	75°55.260N 16°09.968E	End Multibeam and Chirp Line Geo8144_047, Storfjordrenna
25/7	21:12	75°55.260N 16°09.968E	Start Multibeam 0225 and Chirp Line Geo8144_048, Storfjordrenna. Wind 6 m/s, temp 6 degrees
25/7	21:22	75°55.729N 16°15.271E	End Multibeam and Chirp Line Geo8144_048, Storfjordrenna
25/7	21:25	75°55.672N 16°15.581E	CTD Station 351 start. Storfjordrenna
25/7	21:42	75°55.656N 16°16.191E	CTD Station 351 stop. Storfjordrenna
25/7	21:48	75°55.632N 16°17.036E	Start Multibeam 0228 and Chirp Line Geo8144_049, Storfjordrenna. Wind 4 m/s, temp 5 degrees. Started using CTD 351 for Multibeam
25/7	22:14	75°55.780N 16°33.718E	End Multibeam and Chirp Line Geo8144_049, Storfjordrenna
25/7	22:18	75°56.309N 16°33.641E	Start Multibeam 0230 and Chirp Line Geo8144_050, Storfjordrenna. Wind 7 m/s, temp 5 degrees
25/7	22:28	75°56.086N 16°27.521E	End Multibeam and Chirp Line Geo8144_050, Storfjordrenna
25/7	22:28	75°56.086N 16°27.521E	Start Multibeam 0232 and Chirp Line Geo8144_051, Storfjordrenna.
25/7	22:37	75°56.855N 16°31.365E	End Multibeam and Chirp Line Geo8144_051, Storfjordrenna
25/7	22:40	75°57.437N 16°31.197E	Start Multibeam 0234 and Chirp Line Geo8144_052, Storfjordrenna. Wind 9 m/s, temp 5 degrees
26/7	00:00	75°53.679N 15°40.222E	End Multibeam and Chirp Line Geo8144_052, Storfjordrenna
26/7	00:05	75°54.189N 15°38.835E	Start Multibeam 0238 and Chirp Line Geo8144_053, Storfjordrenna. Wind 7 m/s, temp 5 degrees
26/7	03:27	76°03.559N 17°45.858E	End Multibeam and Chirp Line Geo8144_053, Storfjordrenna
26/7	03:33	76°04.051N 17°44.121E	Start Multibeam 0246 and Chirp Line Geo8144_054, Storfjordrenna. Wind 7 m/s, temp 5 degrees
26/7	07:01	75°55.045N 15°39.558E	End Multibeam and Chirp Line Geo8144_054, Storfjordrenna
26/7	07:01	75°55.045N 15°39.558E	Start Multibeam 0254 and Chirp Line Geo8144_055, Storfjordrenna. Wind 9 m/s, temp 7 degrees. Transit to the start position of seismic line
26/7	07:47	75°47.897N 15°48.015E	End Multibeam and Chirp Line Geo8144_055, Storfjordrenna
26/7	08:42	75°46.924N 16°13.973E	<b>Start Seismic</b> , Multibeam 0259 and Chirp Line Geo8144_056, Storfjordrenna, Wind 9 m/s, temp 7 degrees.
26/7	15:38	75°58.918N 18°10.457E	End Multibeam 0273 and Chirp line Geo8144_056, Storfjordrenna
26/7	15:44	75°58.786N 18°10.433E	Start Multibeam 0274 and Chirp line Geo8144_057, Storfjordrenna, wind 9 m/s, temp 6.5 deg.

---

---

26/7	22:34	75°44.176N 16°29.370E	End Multibeam 0288 and Chirp line Geo8144_057, Storfjordrenna
26/7	22:46	75°44.167N 16°28.799E	Start Multibeam 0289 and Chirp line Geo8144_058, Storfjordrenna, wind 7 m/s, temp 7 deg.
27/7	02:05	75°35.079N 17°14.909E	<b>End Seismic</b> , Multibeam and Chirp Line Geo8144_058, Storfjordrenna
27/7	02:30	75°34.769N 17°13.108E	Start Multibeam and Chirp Line Geo8144_059, Storfjordrenna, wind 7m/s, temp. 7 degrees
27/7	04:58	75°46.471N 15°46.942E	End Multibeam and Chirp line Geo8144_059, Storfjordrenna
27/7	04:58	75°46.471N 15°46.942E	Start Multibeam and Chirp Line Geo8144_060, Storfjordrenna, wind 6-7m/s, temp. 7 degrees
27/7	05:24	75°50.198N 15°40.599E	End Multibeam and Chirp Line Geo8144_060, Storfjordrenna
27/7	05:24	75°50.198N 15°40.599E	Start Multibeam and Chirp Line Geo8144_061, Storfjordrenna, wind 6m/s, temp. 8 degrees
27/7	05:53	75°55.445N 15°37.333E	End Multibeam and Chirp Line Geo8144_061, Storfjordrenna
27/7	05:53	75°55.445N 15°37.333E	Start Multibeam and Chirp Line Geo8144_062, Storfjordrenna, wind 6m/s, temp. 8 degrees
27/7	07:40	76°00.908N 16°51.422E	End Multibeam and Chirp Line Geo8144_062, Storfjordrenna
27/7	07:40	76°00.908N 16°51.422E	Start Multibeam 0310 and Chirp Line Geo8144_063, Storfjordrenna, wind 7m/s, temp. 7.5 degrees. Transit line from study area Storfjorden to Lyb.

---

### Line log Geo8144\_13 on RV Helmer Hanssen July 21-28. 2013 Storfjordrenna

Airgun: MiniGI (15/15 cu inch), ca 0.5 l, shotrate 3s, towed 35 meters behind vessel at 2m water depth

Subbottom profiler: Edgetech hullmount chirp 4x4 transducer array, freq.range 1.5-9kHz, 4kW, shotrate 1s.

Multibeam: Kongsberg EM300, 32 kHz.

Line name	Date	Location	Start (UTC)	Start Latitude North	Start Longitude East	End (UTC)	End Latitude North	End Longitude East	MB Line Count	Shot rate [sec]	Pulse mode Chirp	Ship's speed [kn]	Comments
Geo8144_001	22/7	Transit Lyb-Storfjordrenna	08:13	76°58.360	014°13.957	14:25	75°55.862	15°41.154	001-0015	1	1.5-9khz,40ms	10	Transit to work area in Storfjorden
Geo8144_002	22/7	Storfjordrenna	14:54	75°55.864	15°43.117	20:41	76°22.787	19°31.534	0016-0028	1	1.5-9khz,40ms	10	Storfjordrenna
Geo8144_003	22/7	Storfjordrenna	20:41	76°22.787	19°31.534	22:50	76°20.943	21°01.668	0029-0033	1	1.5-9khz,40ms	10	Storfjordrenna
Geo8144_004	22/7	Storfjordrenna	22:50	76°20.943	21°01.668	01:29	76°35.672	22°45.839	0034-0040	1	1.5-9khz,40ms	10	Storfjordrenna
Geo8144_005	23/7	Storfjordbanken	01:31	76°36.073	22°46.441	04:15	77°04.376	23°37.393	0041-0046	1	1.5-9khz,40ms	10	line Storfjordrenna
Geo8144_006	23/7	Storfjordbanken	04:18	77°04.376	23°37.393	06:23	76°45.064	23°03.056	0048-0053	1	1.5-9khz,40ms	10	Storfjordbanken
Geo8144_007	23/7	Storfjordbanken	06:34	76°44.744	23°01.831				Not recording MB	1	1.5-9khz,40ms	1	Line on locations GC 105 and 106 Storfjordbanken
Geo8144_008		Storfjordbanken	08:05	76°48.513	23°09.928		76°44.582	23°01.628	0054-056	1	1.5-9khz,40ms	10	Line Storfjordbanken over flares on single bam



Geo8144_009		Storfjordbanken	09:17			09:54			0057-0058	1	1.5-9khz,40ms	1	Line on locations 108GC and 109GC
Geo8144_010	23/7	Storfjordbanken	09:54			10:51	76°49.887	23°11.488	0059-0060	1	1.5-9khz,40ms	10	Line on transit to seismic line 0113 s shot rate Mini GI kammer 15-15 cu in
<b>Geo8144_011 Seismic</b>	23/7	Storfjordbanken	10:51	76°49.887	23°11.488	12:07	75°55.928	18°34.893	0062-0065	1	1.5-9khz,40ms	4-5	<b>Seismic</b> southwards on Storfjordbanken
Geo8144_012	23/7	Storfjordbanken	12:15	76°44.313	23°02.072	12:38	76°43.367	23°00.385	0066-0067	1	1.5-9khz,40ms	2	Taking out seismic equipment
Geo8144_013	23/7	Storfjordbanken	12:38	76°43.367	23°00.385	13:34	76°35.551	22°46.760	0068-0069	1	1.5-9khz,40ms	4-10	Storfjordbanken
Geo8144_014	23/7	Storfjordrenna	13:34	76°35.551	22°46.760	16:48	76°16.240	21°04.456	0070-00?	1	1.5-9khz,40ms	10	Storfjordrenna
Geo8144_015	23/7	Storfjordrenna	16:48	76°16.240	21°04.456	00:42	75°53.533	15°46.043	00?-0095	1	1.5-9khz,40ms	10	Storfjordrenna
Geo8144_016	24/7	Storfjordrenna	00:42	75°53.533	15°46.043	03:16	75°55.151	17°32.980	0096-0101	1	1.5-9khz,40ms	10	Storfjordrenna
Geo8144_017	24/7	Storfjordrenna	03:16	75°55.151	17°32.980	05:49	75°45.672	16°03.732	0103-0108	1	1.5-9khz,40ms	10	Storfjordrenna
Geo8144_018	24/7	Storfjordrenna	05:49	75°45.672	16°03.732	08:18	75°32.061	17°32.796	0110-0115	1	1.5-9khz,40ms	10	Storfjordrenna
Geo8144_019	24/7	Storfjordrenna	08:23	75°31.950	17°34.530	09:32	75°40.251	16°59.554	0116-0119	1	1.5-9khz,40ms	10	Storfjordrenna
Geo8144_020	24/7	Storfjordrenna	09:32	75°40.251	16°59.554	10:06	75°45.525	16°47.284	0120-0121	1	1.5-9khz,40ms	10	Storfjordrenna
Geo8144_021	24/7	Storfjordrenna	10:06	75°45.525	16°47.284	11:12	75°48.773	16°00.499	0122-	1	1.5-	10	Storfjordrenna

		a							0125		9khz,40m s		
Geo8144_022	24/7	Storfjordrenn a	11:31	75°46.086	15°59.643	13:49	75°54.984	17°28.228	0127- 0131	1	1.5- 9khz,40m s	10	Storfjordrenna
Geo8144_023	24/7	Storfjordrenn a	13:54	75°54.127	17°28.706	16:08	75°45.368	16°05.785	0133- 0137	1	1.5- 9khz,40m s	10	Storfjordrenna
Geo8144_024	24/7	Storfjordrenn a	16:19	75°46.722	16°01.198	16:59	75°49.080	16°27.931	0139- 0140	1	1.5- 9khz,40m s	11	Storfjordrenna Transit to Core Locations
Geo8144_025	24/7	Storfjordrenn a	16:59	75°49.08 0	16°27.931	17:14	75°49.149	16°27.885	0141- 0142	1	1.5- 9khz,40m s	8	Core Locations wedge
Geo8144_026	24/7	Storfjordrenn a	17:47	75°49.08 0	16°27.931	18:07	75°49.428	16°37.249	0143- 0144	1	1.5- 9khz,40m s	6-8	Core location flare
Geo8144_027	24/7	Storfjordrenn a	20:36	75°50.18 7	16°56.426	21:58	75°44.611	16°07.413	0145- 0149	1	1.5- 9khz,40m s	10	Storfjordrenna
Geo8144_028	24/7	Storfjordrenn a	22:05	75°44.34 9	16°10.696	23:09	75°48.664	16°48.620	0151- 0153	1	1.5- 9khz,40m s	10	Storfjordrenna
Geo8144_029	24/7	Storfjordrenn a	23:15	75°48.10 9	16°48.860	00:21	75°43.693	16°11.139	0155- 0157	1	1.5- 9khz,40m s	10	Storfjordrenna
Geo8144_030	25/7	Storfjordrenn a	00:25	75°43.41 9	16°14.964	01:23	75°47.598	16°50.286	0159- 0160	1	1.5- 9khz,40m s	10	Storfjordrenna
Geo8144_031	25/7	Storfjordrenn a	01:29	75°47.04 2	16°50.585	02:26	75°43.046	16°17.721	0161- 0163	1	1.5- 9khz,40m s	10	Storfjordrenna 1- 2m/s Calm sea
Geo8144_032	25/7	Storfjordrenn a	02:31	75°42.621	16°19.630	03:25	75°46.761	16°52.673	0165- 0167	1	1.5- 9khz,40m s	10	Storfjordrenna
Geo8144_033	25/7	Storfjordrenn a	03:30	75°46.210	16°53.153	04:26	75°42.274	16°22.012	0168- 0169	1	1.5- 9khz,40m s	10	Storfjordrenna

Geo8144_034	25/7	Storfjordrenna	04:26	75°42.274	16°22.012	05:10	75°46.261	15°58.133	0171-0172	1	1.5-9khz,40ms	9	Storfjordrenna
Geo8144_035	25/7	Storfjordrenna	05:18	75°47.077	15°58.063	06:39	75°52.443	16°47.874	0174-0177	1	1.5-9khz,40ms	9	Storfjordrenna
Geo8144_036	25/7	Storfjordrenna	06:45	75°53.063	16°46.566	08:19	75°46.917	15°50.167	0178-0182	1	1.5-9khz,40ms	10	Storfjordrenna
Geo8144_037	25/7	Storfjordrenna	08:24	75°47.385	15°48.299	10:06	75°54.096	16°50.160	0183-0187	1	1.5-9khz,40ms	10	Storfjordrenna
Geo8144_038	25/7	Storfjordrenna	10:11	75°54.774	16°47.833	11:48	75°47.983	15°46.992	0188-0192	1	1.5-9khz,40ms	10	Storfjordrenna
Geo8144_039	25/7	Storfjordrenna	11:53	75°48.495	15°45.091	13:21	75°54.164	16°39.116	0193-0196	1	1.5-9khz,40ms		Storfjordrenna
Geo8144_040	25/7	Storfjordrenna	13:28	75°54.594	16°37.263	14:51	75°49.066	15°45.131	0198-0200	1	1.5-9khz,40ms	10	Storfjordrenna
Geo8144_041	25/7	Storfjordrenna	14:58	75°49.745	15°44.581	16:03	75°53.983	16°25.283	0202-0204	1	1.5-9khz,40ms	10	Storfjordrenna
Geo8144_042	25/7	Storfjordrenna	16:07	75°54.340	16°23.868	17:18	75°50.171	15°41.497	0206-0208	1	1.5-9khz,40ms	9	Storfjordrenna
Geo8144_043	25/7	Storfjordrenna	17:23	75°50.772	15°40.990	18:07	75°53.672	16°09.598	0210-212	1	1.5-9khz,40ms	9	Storfjordrenna
Geo8144_044	25/7	Storfjordrenna	18:10	75°53.914	16°08.535	18:56	75°51.431	15°41.227	0213-0215	1	1.5-9khz,40ms	9	Storfjordrenna
Geo8144_045	25/7	Storfjordrenna	19:01	75°51.960	15°39.911	19:46	75°54.450	16°07.757	0216-0218	1	1.5-9khz,40ms	9	Storfjordrenna
Geo8144_046	25/7	Storfjordrenna	19:46	75°54.450	16°07.757	20:27	75°54.836	16°36.647	0219-0221	1	1.5-9khz,40ms	9	Storfjordrenna

											s		
Geo8144_047	25/7	Storfjordrenna	20:32	75°55.287	16°36.065	21:12	75°55.260	16°09.968	0222-0224	1	1.5-9khz,40ms	10	Storfjordrenna
Geo8144_048	25/7	Storfjordrenna	21:12	75°55.260	16°09.968	21:22	75°55.729	16°15.271	0225-0227	1	1.5-9khz,40ms	10	Storfjordrenna
Geo8144_049	25/7	Storfjordrenna	21:48	75°55.632	16°17.036	22:14	75°55.780	16°33.718	0228-0229	1	1.5-9khz,40ms	10	Storfjordrenna
Geo8144_050	25/7	Storfjordrenna	22:18	75°56.309	16°33.641	22:28	75°56.086	16°27.521	0230-0231	1	1.5-9khz,40ms	10	Storfjordrenna
Geo8144_051	25/7	Storfjordrenna	22:28	75°56.086	16°27.521	22:37	75°56.855	16°31.365	0232-0233	1	1.5-9khz,40ms	10	Storfjordrenna
Geo8144_052	25/7	Storfjordrenna	22:40	75°57.437	16°31.197	00:00	75°53.679	15°40.222	0234-0237	1	1.5-9khz,40ms	10	Storfjordrenna
Geo8144_053	26/7	Storfjordrenna	00:05	75°54.189	15°38.835	03:27	76°03.559	17°45.858	0238-0244	1	1.5-9khz,40ms	10	Storfjordrenna
Geo8144_054	26/7	Storfjordrenna	03:33	76°04.051	17°44.121	07:01	75°55.045	15°39.558	0246-0253	1	1.5-9khz,40ms	9	Storfjordrenna
Geo8144_055	26/7	Storfjordrenna	07:01	75°55.045	15°39.558	07:47	75°47.897	15°48.015	0254-0256	1	1.5-9khz,40ms	10	Storfjordrenna
Geo8144_056	26/7	Storfjordrenna	08:42	75°46.924	16°13.973	15:38	75°58.918	18°10.457	0259-0273	1	1.5-9khz,40ms	4	Storfjordrenna
Geo8144_057	26/7	Storfjordrenna	15:44	75°58.786	18°10.433	22:34	75°44.176	16°29.370	0274-0288	1	1.5-9khz,40ms	4	Storfjordrenna
Geo8144_058	26/7	Storfjordrenna	22:46	75°44.167	16°28.799	02:05	75°35.079	17°14.909	0289-0295	1	1.5-9khz,40ms	4	Storfjordrenna

Geo8144_059	27/7	Storfjordrenna	02:30	75°34.769	17°13.108	04:58	75°46.471	15°46.942	0297-0301	1	1.5-9khz,40ms	10	Storfjordrenna
Geo8144_060	27/7	Storfjordrenna	04:58	75°46.471	15°46.942	05:24	75°50.198	15°40.599	0302	1	1.5-9khz,40ms	10	Storfjordrenna
Geo8144_061	27/7	Storfjordrenna	05:24	75°50.198	15°40.599	05:53	75°55.445	15°37.333	0303-0304	1	1.5-9khz,40ms	10	Storfjordrenna
Geo8144_062	27/7	Storfjordrenna	05:53	75°55.445	15°37.333	07:40	76°00.908	16°51.422	0305-0309	1	1.5-9khz,40ms	10	Storfjordrenna
Geo8144_063	27/7	Storfjordrenna	07:40	76°00.908	16°51.422				0310-	1	1.5-9khz,40ms	10	Storfjordrenna
	27/7	Storfjordrenna								1	1.5-9khz,40ms	10	Storfjordrenna
	27/7	Storfjordrenna								1	1.5-9khz,40ms	10	Storfjordrenna
	27/7	Storfjordrenna								1	1.5-9khz,40ms	10	Storfjordrenna

**Core Stations Geo-8144-3144 on RV Helmer Hanssen July 21-28. 2013 Storfjordrenna**

Station	Date	Location	Time (UTC)	Position Latitude [N] Longitude [E]	Penetration (GC)	Recovery (GC)	Water depth [m]	Comment
HH13-105-GC	23/7	Storfjordbanken	06:50	76°44.785N 23°02.001E	Full	3.51	131m	Core catcher sampled
HH13-106-GC	23/7	Storfjordbanken	07:49	76°48.608 23°09.353	Ca 3m	2.94	106m	No material in core catcher
HH13-107-GC	23/7	Storfjordbanken	09:14	76°48.246 23°08.347	4.5m	2.56	109	
HH13-108-GC	23/7	Storfjordbanken	09:49	76°48.269 23°08.331	Almost full	2.97	109	Sample from catcher and cutter
HH13-109-GC	24/7	Storfjordrenna	17:31	75°49.065 16°27.964	4.7m	3.78	364	Sample from catcher, 2 from cutter. Ca 1cm of sediment (core top) in a sample bag
HH13-110-GC	24/7	Storfjordrenna	18:15	75°49.449 16°37.349	Full pen	3.40	348	Flare location, sample from catcher and cutter
HH13-111-GC	24/7	Storfjordrenna	18:49	75°49.423 16°37.160	Full	3.72	349	Flare Location 2 (repeat same location)Core opened. Catcher and Cutter acquired
HH13-112- GC	24/7	Storfjordrenna	19:38	75°50.646 16°48.533	Full pen	333	323	Sample from catcher and cutter
HH13-113- GC	24/7	Storfjordrenna	20:10	75°51.420N 16°56.781E	Full pen	396	313	Sample from catcher and cutter

- A. Anastasia Fokina (Master student, MSU)
- B. Andrea Barbolla (PhD student, UiT)
- C. Dina Gillazetdinova (Master student, MSU)
- D. Mariana Esteves (PhD student, UiT)
- E. Robert Virs (Master student, UiT)
- F. Sunil Vadakkepuliambatta (PhD student, UiT)
- G. Trude Hansen (Master student, UiT)